Universidade do Minho
Escola de Ciências

Ana Isabel Rodrigues Alves Antunes Rei

FLUORESCENCE STUDY OF SOL-GEL DERIVED PROTEIN SILICA HYBRIDS FOR OPTICAL BIOSENSOR APPLICATIONS

Agosto de 2009

FLUORESCENCE STUDY OF SOL-GEL DERIVED PROTEIN SILICA HYBRIDS FOR OPTICAL BIOSENSOR APPLICATIONS
Ana Isabel Rodrigues Alves Antunes Rei
UMinho | 2009

Universidade do Minho
Escola de Ciências

Ana Isabel Rodrigues Alves Antunes Rei

FLUORESCENCE STUDY OF SOL-GEL DERIVED PROTEIN SILICA HYBRIDS FOR OPTICAL BIOSENSOR APPLICATIONS

Tese de Doutoramento em Ciências
Área de Conhecimento em Física

Trabalho efectuado sob orientação do
Doutor Graham Hungerford
e da
Professora Doutora M. Isabel C. Ferreira

Agosto de 2009

Dissertação apresentada à Escola de Ciências da Universidade do Minho para obtenção do grau de Doutor em Ciências, Área de Conhecimento em Física.

Este trabalho foi realizado no Departamento de Física da Universidade do Minho, sob a supervisão do Doutor Graham Hungerford e da Professora Doutora M. Isabel C. Ferreira. A sua execução foi financiada pela Fundação para a Ciência e a Tecnologia (FCT) através da Bolsa de Doutoramento SFRH / BD / 27933 / 2006.

ACKNOWLEDGMENTS

I wish to thank both Professor M. Isabel C. Ferreira and Dr Graham Hungerford for their rigorous supervision of this work.

I am grateful to Dr Peter Schellenberg for constructive scientific discussions.

Professor José Luís Figueiredo is acknowledged for having supervised the BET measurements.

FLUORESCENCE STUDY OF SOL-GEL DERIVED PROTEIN SILICA HYBRIDS FOR OPTICAL BIOSENSOR APPLICATIONS

Abstract

The encapsulation of enzymes for optically addressed biosensor applications is an area of great importance. Firstly there is a need to provide a robust, optical quality host in which to incorporate the biomolecule. In principle the host matrix should be "inert" (with minimum interaction with the guest enzyme), protective and should retain the enzyme within its structure, allowing maximum catalytic activity and free passage of the reactants both to and from the enzyme. Materials which are promising in this respect are silica glasses made via the sol-gel technique. They are optically transparent, have a high porosity and they template around the biomolecule providing a protective host. However, the encapsulation process can have adverse effects; the loss of enzymatic catalytic activity can happen and the mass transport through the host is not ideal!

In this work fluorescence techniques were used to monitor the incorporation of an enzyme into a sol-gel derived medium. Several additives were used in tuning the original sol-gel recipe to improve biocompatibility. Complementary measurements of catalytic activity were performed to elucidate the behaviour of the encapsulated protein.

Molecular diffusion was monitored using labelled proteins and unbound fluorescence dye molecules (representative of enzyme substrates) and their interaction with and mobility within the host assessed using time-resolved fluorescence anisotropy and fluorescence recovery after photobleaching observed *via* confocal microscopy.

Viscosity (DASPMI) and polarity (Nile red) sensitive fluorescence probes were employed to monitor the host matrices. Nile red was also used to label two catalytic proteins (cytochrome *c* and subtilisin *Carlsberg*), which were incorporated into different host media and the dye used to ascertain changes in protein conformation.

Overall it was found that the hosts became stable after an aging period approaching twenty days and that the major influence on the catalytic reaction rates is that of host mediated mass transport.

FLUORESCENCE STUDY OF SOL-GEL DERIVED PROTEIN SILICA HYBRIDS FOR OPTICAL BIOSENSOR APPLICATIONS

Resumo

A utilização de enzimas para a construção de biosensores ópticos tem evidenciado um notável desenvolvimento. Neste contexto, a tecnologia sol-gel, cuja versatilidade é a palavra-chave do seu sucesso, tem demonstrado enormes potencialidades. A oclusão de enzimas em matrizes de sílica pela técnica sol-gel permite a obtenção de híbridos com boas qualidades ópticas e considerável robustez física. Para além disso, a sua porosidade permite a difusão dos substratos enzimáticos e produtos de reacção, com retenção da enzima constituindo, simultaneamente, um meio protector contra agentes físicos, químicos e biológicos. Contudo, o processo tem as suas fragilidades, nomeadamente a perda de actividade catalítica devido a desnaturação da enzima, e constrangimentos relativamente ao livre-trânsito dos analitos.

Neste trabalho, foram utilizadas técnicas de fluorescência para seguir a incorporação de proteínas em matrizes de sílica pela técnica sol-gel. A receita original foi adaptada, utilizando-se aditivos (silanos ou polímeros) para melhorar a biocompatibilidade dos híbridos. A difusão molecular foi estudada usando proteínas marcadas com sondas fluorescentes e fluoróforos livres, através das técnicas de anisotropia de fluorescência resolvida no tempo e recuperação de fluorescência após fotobranqueamento, esta última utilizando a microscopia confocal. A polaridade e a viscosidade das matrizes foram estudadas utilizando as sondas *Nile red* e *DASPMI*, através da medição de fluorescência no estado estacionário (fazendo uso da técnica de varrimento síncrono de fluorescência), ou resolvida no tempo. A sonda *Nile red*, por ser hidrofóbica e solvatocrómica, foi escolhida para marcação das proteínas e levar a cabo estudos de conformação enzimática. Estudos complementares de actividade catalítica, foram realizados para caracterizar o comportamento do biocatalisador encapsulado. Concluiu-se que as matrizes produzidas utilizando o nosso método, estabilizam ao fim de um período de aproximadamente 20 dias e que a taxa de transformação substrato-produto das proteínas estudadas, é mais influenciada pelas restrições impostas pela matriz ao livre-trânsito dos analitos, do que pela desnaturação das biomoléculas.

E pur si muove!

(Galileo Galilei)

CONTENTS

LIST OF ACRONYMS

AAF-AMC	Ala-Ala-Phe-7-amido-4-methyl coumarin
AMC	Amido-4-methyl coumarin
APTES	(3-aminopropyl)triethoxysilane
AF	Alexa Fluor 488
BSA	Bovine Serum Albumin
DASPMI	4-(4- (Dimethylamino)styryl)-*N*-methylpyridiniumiodine
FITC	Fluorescein isothyocyanate
FRAP	Fluorescence Recovery After Photobleaching
Fs	Fluorescein
GPTES	(Glycidyloxypropyl)triethoxysilane
GR	Gelrite®
HRP	Horseradish peroxidase
IPN	Interpenetrating Polymer Network
ORMOSIL	Organically Modified Silicates
PEG20k	Poly(ethylene glycol) 20 kD
PEG300D	Poly(ethylene glycol) 300 D
SC	Subtilisin *Carlsberg*
SFS	Synchronous Scan Fluorescence Spectrometry
TCSPC	Time-Correlated Single-Photon Counting
TEOS	Tetraethylortosilane
TICT	Twisted Intramolecular Charge Transfer
TMOS	Tetramethylortosilane
TMPS	Trimethoxypropylsilane

LIST OF MATHEMATICAL TERMS

v_0	Initial velocity
$[S]$	Substrate concentration
v_{max}	Maximum initial velocity that occurs at saturating substrate concentration
K_M	Michaelis constant
E	Energy
h	Plank's constant
v	Frequency of electromagnetic radiation
k_f	Rate of fluorescence emission
k_{ic}	Rate of internal conversion
k_{isc}	Rate of intersystem crossing
k_{nr}	Non-radiative decay rate
k_q	Rate constant for the quenching process
ε	Molar extinction coefficient
Φ_F	Quantum yield
τ	Fluorescence lifetime
$I(t)$	Intensity decay
k_q	Bimolecular quenching constant
[Q]	Quencher concentration
K_D	Stern-Volmer quenching constant
$I_{\parallel}$	Fluorescence intensity parallel to the polarisation of the excitation
$I_{\perp}$	Fluorescence intensity perpendicular to the polarisation of the excitation
$r(t)$	Anisotropy decay
r_0	Fundamental anisotropy in the absence of rotational diffusion
r_∞	Long-time anisotropy in an anisotropy decay
τ_r	Rotational correlation time
k	Boltzmann constant
T	Absolute temperature
η	Viscosity
D_r	Rotational diffusion coefficient

D_t	Translational diffusion coefficient
E_{em}	Excitation function
λ_{exc}	Excitation wavelength
λ_{em}	Emission wavelength
$\Delta\lambda$	Difference between the wavelengths of excitation and emission

Chapter 1

INTRODUCTION

One of the most promising technologies of the 21st century is nanotechnology; the recent breakthroughs in this research area are pushing forward the applications of nanomaterials in several scientific areas such as nanomaterials-based biosensors, which represents the integration of material science, molecular engineering, chemistry and biotechnology [1,2]. A biosensor is a device capable of providing selective quantitative or semi-quantitative analytical information using a biological recognition element, by converting a biochemical event into a detectable signal *via* a transducer and a processor. Biosensors are classified according to the transduction element (e.g., electrochemical, optical, piezoelectrical or thermal) or the biorecognition principle (e.g., enzymatic, immunoaffinity recognition, whole-cell sensor or DNA). The purpose of the biological element is to grant selectivity for the analyte of interest [3-5].

At present, commercial biosensors are still expensive and limited in the number of targets they can test. The future developments of science and technology will permit the fabrication of optical biosensors useful as everyday analytical tools. In the opinion of Ligler "*biological recognition and signal amplification strategies, nanotechnology for geometric control of the biochemistry and signal enhancement, microfluidics for automated reagent delivery and reaction control, and emergence of optical elements amenable to improved systems integration will play a critical role in this evolution*" [6]. The four prerequisites of a competitive biosensor to function in a real-world sample situation are undoubtedly selectivity, sensitivity, detection limits, and robustness. Biosensors have wide applications, including biomarker detection for medical diagnostics, pathogen and toxin detection in food and environmental monitoring. Fibre-

optic biosensors use optical fibres as the transduction element, and rely exclusively on optical transduction mechanisms for detecting target molecules [7,8].

The development of biosensors based on nanostructured sol–gel-derived platforms has attracted increased attention in the last three decades and reports on the successful entrapment of biomolecules such as proteins, enzymes, antibodies or drugs are numerous [9-14]. The term *sol* refers to a colloidal suspension of solid particles (the disperse phase) in a liquid (the continuous phase) that, by condensation, form an irregular, non-crystalline, three-dimensional network that occupies the entire volume of a vessel – the *gel*. The gel network is porous and is filled by an interstitial fluid. In hydrogels, the fluid phase is water or aqueous solution, in alcogels it is alcoholic solution, and in aerogels it is air or other gases [15]. The term colloid was coined by Thomas Graham in the 1860s, to classify substances such as gelatine, albumin and gums, which, in a solution, would not pass a dialysis membrane [16]. Common examples of other types of colloidal dispersions are foam, mayonnaise, fog and mist, and the biological cell [17].

The sol-gel technique is based on the hydrolysis of liquid precursors with the formation of colloidal sols and, after condensation, stable gels. Alkoxides, $M(OR)_z$ (where M^{z+} is a metal/semi-metal ion and R is an alkyl group), are the most widespread precursors. Among these, silicon alkoxides are very popular, as the materials obtained possess good optical properties (transparency), satisfactory mechanical stability, high surface area and porosity, chemical inertness as well as photochemical and thermal stability. Also, they can be obtained in a variety of formats depending on the mould. As the early steps of the sol–gel process occur in liquid phase, it is possible to add almost any substance at this stage, and a uniform distribution of the dopant is obtained merely by mixing. After the gelation, the guest molecules become entrapped within the solid host matrix [18]. The sol-gel immobilisation of biological entities is characterised by physical entrapment without any chemical modification of the biomolecule. The silica nanocage that forms around the dopant molecule protects it and preserves its functionality; the biochemical reaction is basically the same as in aqueous solution, except for the fact that it is generally slower, most probably because of mass transport limitations [19].

The potential applications of sol-gel technology are not restricted to sensing devices, they also have been studied in the context of drug delivery, drug targeting, tissue engineering, gene transfection, and cell tracking [20-23]. Applications in the

medical field such as bone implant rely on the fact that sol-gel derived media are biocompatible, bioactive and inert [24,25]. The enormous versatility of the sol-gel chemistry enables the production of robust hybrids at low temperatures with remarkable new material properties that can be used to enhance the stability of a certain biomolecule. Chemically engineered surfaces, modification by additives and alcohol-free routes are some of the strategies that have been reported aiming to produce amenable sol-gel hosts [8,26-30]. However, before commercialisation, problems inherent to the sol-gel process like stability, response time or repeatability have to be resolved [31].

The sensor area has grown considerably through the design of sol–gel materials with enhanced biorecognition. A great effort has been made to understand short and long-term interactions between the biorecognition elements and the evolving sol–gel matrix. These interactions are essential because they govern the function of the entrapped biomolecule [10,32,33]. Also, in the particular case of enzymes, ensuring that the substrate and the products of reaction are not sterically hindered from diffusing to or from the active site, is fundamental [34,35]. Similarly, the local environment of the entrapped biomolecules and the ability of analytes to diffuse through the matrix are two basic issues when developing sol–gel-based biosensors [10].

The fact that sol-gel hybrids can be transparent, therefore light addressable, enables the study of the embedded biomolecule via spectroscopic methods and the application of the technology to optical biosensors. The investigation in this area is intense, ranging from simple one-enzyme devices to multi-enzyme systems [36-39]. Fluorescence spectroscopy has been widely used to monitor the sol-gel process, the conformation/interactions of proteins in aqueous solution and to determine enzymatic activity [40-47]. The use of fluorescence techniques to monitor sol-gel hybrid systems seems ideal as it can address both the host matrix and the guest biomolecule, and enables the visualisation of molecular diffusion down to single-molecule level [48]. Moreover, the use of fluorescent probes with different sensitivities allows the discrimination between diverse physical and chemical properties within these micro-heterogeneous systems. In fact, the information obtained by experiments depends on the attributes of the probe, therefore a careful scrutiny of the fluorophore must be done before setting up any experiment [49]. For example, the strong solvent-dependency of electronic bands (solvatochromism) which is exhibited in particular by molecules having large dipole moments can be used to extract information about the solvent

polarity, out of simple fluorescence measurements [50,51]. This property can further be exploited by synchronous fluorescence spectrometry (SFS), a technique that enables resolving the broad-band overlapping of conventional fluorescence spectra, which arise from their similar molecular structures. Like this, it is possible to discriminate a probe within several environments or, conversely, several compounds in a mixture [52].

The advantages of fluorescence include extreme sensitivity, specificity, and the ability to measure both intensity and lifetime. Time-resolved measurements give additional information besides steady-state data and they are especially relevant to *in vivo* sensing because they can be chosen so that light scattering and concentration effects become negligible [53]. Supplementary information is given by time-dependant anisotropy measurements. From here it is possible to extract information on size, shape, flexibility and rotation of molecules, and also information about the properties of the medium like viscosity [49]. The dynamics of a system can also be monitored by exploiting a phenomenon related to the properties of the fluorophores – photobleaching. Although in certain circumstances it can represent a drawback, it can also be an advantage for studying the movements of molecules when combined with imaging techniques. Fluorescence recovery after photobleaching (FRAP) was initially employed to study the dynamics of lipids and proteins in living cells but its applications have expanded greatly with the development of confocal microscopy [54].

This thesis demonstrates how fluorescence can be successfully employed to monitor the production of a sol-gel derived biosensor. Our investigation followed the behaviour of biomolecules in the host, namely protein stability, mobility, and microenvironment characteristics, making use of both steady-state and time-resolved fluorescence techniques. Taking advantage of the flexibility of sol-gel chemistry, optimisation of the sol-gel "recipe" was made in order to make the hosts more amenable to the guest biomolecules. Protein-compatible monoliths were produced using the polymers polyethylene glycol (PEG 300 D and PEG 20 KD) and Gelrite®, to tune the resulting sol-gel composite dipolarity and pore templating, and thus control the flow of materials through the matrix [55-57]. The silanes (3-Aminopropyl)triethoxysilane (APTES), trimethoxypropylsilane (TMPS) or (glycidyloxypropyl)triethoxysilane (GPTES), were added to prepare organically modified silica gels with differing hydrophobycities and, like that, promote the protein stability [58-61]. The proteins horseradish peroxidise (HRP), bovine serum albumin (BSA), subtilisin *Carlsberg* and

cytochrome c were encapsulated in inorganic and modified sol-gel derived media, acting as model systems of protein-doped sol-gel glasses, as their mechanistic behaviour is well documented in literature. Both HRP and cytochrome c are haem containing proteins and, although not strictly an enzyme, cytochrome c exhibits catalytic activity and was selected as it could be the forerunner for the inclusion of other cytochromes and even be part of the building blocks for incorporating an enzyme reaction chain within sol-gel derived media.

The host manufacturing process was observed making use of viscosity (DASPMI) and polarity (Nile red) sensitive fluorescent probes, by monitoring their emission via steady state and time-resolved fluorescence techniques. In addition, combining FRAP of FITC-labelled proteins of different sizes (HRP and BSA) in sol-gel monoliths with time-resolved fluorescence anisotropy measurements (also using Alexa Fluor 488), it was shown that lateral and rotational diffusion could be measured. Like that, it was possible to relate the molecules' retention with the size and connectivity of the pores in the sol-gel matrix.

Nile red was also used to label two catalytically active proteins (cytochrome *c* and subtilisin *Carlsberg*), which were incorporated into the different host media. Motivated by the fact that Nile red's SFS was previously successfully used to ascertain the probe's distribution between lipoproteins and albumin in blood [62], we used a similar approach to ascertain changes in protein conformation, both upon incorporation and throughout the sol-gel aging period. Catalytic activity measurements were performed in order to correlate the fluorescence data with the embedded proteins' biological activity.

Measurement of cytochrome *c* activity was obtained from the oxidation of 2,2-Azino-bis(3-ethylbenzothiazoline-6-sulfonic acid) diammonium salt (ABTS), by hydrogen peroxide (H_2O_2). The formation of the $ABTS^{\bullet+}$ radical cation was monitored at 414 nm with time, using absorption spectroscopy. A similar procedure was employed in the case of the subtilisin *Carlsberg* hybrid matrices. However, in this case, the catalytic activity was monitored against a substrate of Ala-Ala-Phe-7-amido-4-methyl coumarin (AAF-AMC) and the product formation was monitored at 370 nm. This strategy also allowed the influence of choice of substrate to be elucidated, as $ABTS^{\bullet+}$ radical is charged and can revert to its uncharged form. Conversely, AAF-AMC and the reaction product AMC (7-amido-4-methyl coumarin) are neutral and formed irreversibly. These complementary studies (Nile red SFS and catalytic activity)

provided an estimation of the influence of protein denaturing (and/or conformational change) as well as host mediated effects (diffusional access) on the observed catalytic activity.

In this work fluorescence is employed to monitor the fabrication of a sol-gel hybrid protein-containing silica-based biosensor. Although this thesis does not encompass the manufacture of a complete sensor (device), it addresses important features of any biosensor system: how the biomolecule interacts with its host. Therefore, it is believed that the information obtained is relevant in advancing this field of study.

References

[1] Ernest, H. S., Rahul. *Impact of Nanotechnology on Biomedical Sciences: Review of Current Concepts on Convergence of Nanotechnology With Biology* Journal of Nanotechnology Online 2005.

[2] Zhang, X. Q.; Guo, Q.; Cui, D. X. *Recent Advances in Nanotechnology Applied to Biosensors* Sensors 2009, *9*, 1033.

[3] Wingard, L. B. F., J. P. Concepts, Biological Components, and Scope of Biosensors. In *Biosensors with Fiberoptics (Contemporary Instrumentation and Analysis)*; Wingard, L. B. W., D. L., Ed.; The Humana Press inc.: Clifton, 1991.

[4] Farre, M.; Kantiani, L.; Perez, S.; Barcelo, D. *Sensors and biosensors in support of EU Directives* Trac-Trends in Analytical Chemistry 2009, *28*, 170.

[5] Forano, C.; Vial, S.; Mousty, C. *Nanohybrid enzymes - Layered double hydroxides: Potential applications* Current Nanoscience 2006, *2*, 283.

[6] Ligler, F. S. *Perspective on Optical Biosensors and Integrated Sensor Systems* Analytical Chemistry 2009, *81*, 519.

[7] Luong, J. H. T.; Male, K. B.; Glennon, J. D. *Biosensor technology: Technology push versus market pull* Biotechnology Advances 2008, *26*, 492.

[8] Mansur, H. S.; Orefice, R. L.; Vasconcelos, W. L.; Lobato, Z. P.; Machado, L. J. C. *Biomaterial with chemically engineered surface for protein immobilization* Journal of Materials Science-Materials in Medicine 2005, *16*, 333.

[9] Diaz, A. N.; Sanchez, F. G.; Ramos, M. C.; Torijas, M. C. *Horseradish peroxidase sol-gel immobilized for chemiluminescence measurements of alkaline-phosphatase activity* Sensors and Actuators B-Chemical 2002, *82*, 176.

[10] Gupta, R.; Chaudhury, N. K. *Entrapment of biomolecules in sol-gel matrix for applications in biosensors: Problems and future prospects* Biosensors & Bioelectronics 2007, *22*, 2387.

[11] Kim, J.; Grate, J. W.; Wang, P. *Nanostructures for enzyme stabilization* Chemical Engineering Science 2006, *61*, 1017.

[12] Lan, D.; Li, B. X.; Zhang, Z. J. *Chemiluminescence flow biosensor for glucose based on gold nano particle-enhanced activities of glucose oxidase and horseradish peroxidase* Biosensors & Bioelectronics 2008, *24*, 934.

[13] Lai, Y. C.; Lin, S. C. *Application of immobilized horseradish peroxidase for the removal of p-chlorophenol from aqueous solution* Process Biochemistry 2005, *40*, 1167.

[14] Wallace, J. M.; Stroud, R. M.; Pietron, J. J.; Long, J. W.; Rolison, D. R. *The effect of particle size and protein content on nanoparticle-gold-nucleated cytochrome c superstructures encapsulated in silica nanoarchitectures* Journal of Non-Crystalline Solids 2004, *350*, 31.

[15] John, F. C.; Mary, E. P.; Pamela, M. N. *Applications for Sol-Gel-Derived Materials in Medicine and Biology* 2000, *5*, 52.

[16] van Duijneveldt, J. S. Colloids. In *Encyclopedia of Chemical Physics and Physical Chemistry*; Moore, J. H. S., N. D., Ed.; Institute of Physics; Vol. Volume I.

[17] Vincent, B. Introduction to colloidal dispersions. In *Colloid science: Principles Methods and Applications*
Cosgrove, T., Ed.; Willey-Blackwell, 2005.

[18] Lukowiak, A.; Strek, W. *Sensing abilities of materials prepared by sol-gel technology* Journal of Sol-Gel Science and Technology 2009, *50*, 201.

[19] Lan, E. H.; Dave, B. C.; Fukuto, J. M.; Dunn, B.; Zink, J. I.; Valentine, J. S. *Synthesis of sol-gel encapsulated heme proteins with chemical sensing properties* Journal of Materials Chemistry 1999, *9*, 45.

[20] Yun, H. S.; Kim, S. E.; Hyun, Y. T.; Heo, S. J.; Shin, J. W. *Hierarchically Mesoporous-Macroporous Bioactive Glasses Scaffolds for Bone Tissue Regeneration* Journal of Biomedical Materials Research Part B-Applied Biomaterials 2008, *87B*, 374.

[21] Hudson, S. P.; Padera, R. F.; Langer, R.; Kohane, D. S. *The biocompatibility of mesoporous silicates* Biomaterials 2008, *29*, 4045.

[22] Wang, G. H.; Zhang, L. M. *Manipulating formation and drug-release behavior of new sol-gel silica matrix by hydroxypropyl guar gum* Journal of Physical Chemistry B 2007, *111*, 10665.

[23] Radin, S.; Chen, T.; Ducheyne, P. *The controlled release of drugs from emulsified, sol gel processed silica microspheres* Biomaterials 2009, *30*, 850.

[24] Choi, A. H.; Ben-Nissan, B. *Sol-gel production of bioactive nanocoatings for medical applications. Part II: current research and development* Nanomedicine 2007, *2*, 51.

[25] Ben-Nissan, B.; Choi, A. H. *Sol-gel production of bioactive nanocoatings for medical applications. Part 1: an introduction* Nanomedicine 2006, *1*, 311.

[26] Chen, J. P.; Lin, W. S. *Sol-gel powders and supported sol-gel polymers for immobilization of lipase in ester synthesis* Enzyme and Microbial Technology 2003, *32*, 801.

[27] Sangeetha, K.; Morris, V. B.; Abraham, T. E. *Stability and catalytic properties of encapsulated subtilisin in xerogels of alkoxisilanes* Applied Catalysis a-General 2008, *341*, 168.

[28] Trewyn, B. G.; Slowing, II; Giri, S.; Chen, H. T.; Lin, V. S. Y. *Synthesis and functionalization of a mesoporous silica nanoparticle based on the sol-gel process and applications in controlled release* Accounts of Chemical Research 2007, *40*, 846.

[29] Ren, L.; Tsuru, K.; Hayakawa, S.; Osaka, A. *Synthesis and characterization of gelatin-siloxane hybrids derived through sol-gel procedure* Journal of Sol-Gel Science and Technology 2001, *21*, 115.

[30] Liu, Y.; Wang, M. J.; Li, J.; Li, Z. Y.; He, P.; Liu, H. T.; Li, J. H. *Highly active horseradish peroxidase immobilized in 1-butyl-3-methylimidazolium tetrafluoroborate room-temperature ionic liquid based sol-gel host materials* Chemical Communications 2005, 1778.

[31] MacCraith, B. D.; McDonagh, C.; McEvoy, A. K.; Butler, T.; Okeeffe, G.; Murphy, V. *Optical chemical sensors based on sol-gel materials: Recent advances and critical issues* Journal of Sol-Gel Science and Technology 1997, *8*, 1053.

[32] Badjic, J. D.; Kostic, N. M. *Effects of encapsulation in sol-gel silica glass on esterase activity, conformational stability, and unfolding of bovine carbonic anhydrase II* Chemistry of Materials 1999, *11*, 3671.

[33] Fang, J.; Zhou, J. C.; Lan, E. H.; Dunn, B.; Zink, J. I. *Bio-hybrid materials for immunoassay-based sensing of cortisol* Journal of Sol-Gel Science and Technology 2009, *50*, 176.

[34] Chaplin, M. B. C. *Enzyme Technology*; Cambridge University Press, 1990.

[35] Kanungo, M.; Collinson, M. M. *Controlling diffusion in sol-gel derived monoliths* Langmuir 2005, *21*, 827.

[36] Ferrer, M. L.; Del Monte, F.; Mateo, C. R.; Gomez, J.; Levy, D. *Denaturation and leaching study of horseradish peroxidase encapsulated in sol-gel matrices* Journal of Sol-Gel Science and Technology 2003, *26*, 1169.

[37] Salinas-Castillo, A.; Pastor, I.; Mallavia, R.; Mateo, C. R. *Immobilization of a trienzymatic system in a sol-gel matrix: A new fluorescent biosensor for xanthine* Biosensors & Bioelectronics 2008, *24*, 1053.

[38] Yi, Y. Y.; Kermasha, S.; Neufeld, R. *Characterization of sol-gel entrapped chlorophyllase* Biotechnology and Bioengineering 2006, *95*, 840.

[39] Jurgen-Lohmann, D. L.; Legge, R. L. *Immobilization of bovine catalase in sol-gels* Enzyme and Microbial Technology 2006, *39*, 626.

[40] Zhuang, X. W.; Ha, T.; Kim, H. D.; Centner, T.; Labeit, S.; Chu, S. *Fluorescence quenching: A tool for single-molecule protein-folding study* Proceedings of the National Academy of Sciences of the United States of America 2000, *97*, 14241.

[41] Birch, D. J. S.; Geddes, C. D.; Karolin, J.; Leishman, R.; Rolinski, O. J. *Fluorescence nanometrology in sol-gels* Fluorescence Spectroscopy, Imaging and Probes - New Tools in Chemical, Physical and Life Sciences 2002, *2*, 69.

[42] Karolin, J.; Geddes, C. D.; Wynne, K.; Birch, D. J. S. *Nanoparticle metrology in sol-gels using multiphoton excited fluorescence* Measurement Science & Technology 2002, *13*, 21.

[43] Suhling, K.; Hungerford, G.; Airey, R. W.; Morgan, B. L. *A position-sensitive photon event counting detector applied to fluorescence imaging of dyes in sol-gel matrices* Measurement Science & Technology 2001, *12*, 131.

[44] Lasagna, M.; Gratton, E.; Jameson, D. M.; Brunet, J. E. *Apohorseradish peroxidase unfolding and refolding: Intrinsic tryptophan fluorescence studies* Biophysical Journal 1999, *76*, 443.

[45] Geoghegan, K. F.; Rosner, P. J.; Hoth, L. R. *Dye-pair reporter systems for protein-peptide molecular interactions* Bioconjugate Chemistry 2000, *11*, 71.

[46] Palmier, M. O.; Van Doren, S. R. *Rapid determination of enzyme kinetics from fluorescence: Overcoming the inner filter effect* Analytical Biochemistry 2007, *371*, 43.

[47] Toutchkine, A.; Kraynov, V.; Hahn, K. *Solvent-sensitive dyes to report protein conformational changes in living cells* Journal of the American Chemical Society 2003, *125*, 4132.

[48] Zurner, A.; Kirstein, J.; Doblinger, M.; Brauchle, C.; Bein, T. *Visualizing single-molecule diffusion in mesoporous materials* Nature 2007, *450*, 705.

[49] Lakowicz, J. R. *Principles of Fluorescence Spectroscopy*, Third edition ed.; Springer, 2006.

[50] Liptay, W. *Electrochromism and Solvatochromism* Angewandte Chemie-International Edition 1969, *8*, 177.

[51] Boldrini, B.; Cavalli, E.; Painelli, A.; Terenziani, F. *Polar dyes in solution: A joint experimental and theoretical study of absorption and emission band shapes* Journal of Physical Chemistry A 2002, *106*, 6286.

[52] Yang, H. M.; Wang, Y. S.; Li, J. H.; Li, G. R.; Wang, Y.; Tan, X.; Xue, J. H.; Mao, X. L.; Kang, R. H. *Synchronous fluorescence determination of urinary 1-hydroxypyrene, beta-naphthol and 9-hydroxyphenanthrene based on the sensitizing effect of beta-cyclodextrin* Analytica Chimica Acta 2009, *636*, 51.

[53] Pickup, J. C.; Zhi, Z. L.; Khan, F.; Saxl, T.; Birch, D. J. S. *Nanomedicine and its potential in diabetes research and practice* Diabetes-Metabolism Research and Reviews 2008, *24*, 604.

[54] Parson, W. W. *Modern Optical Spectroscopy*; Springer: Heidelberg, 2007.

[55] Shchipunov, Y. A.; Karpenko, T. Y. *Hybrid polysaccharide-silica nanocomposites prepared by the sol-gel technique* Langmuir 2004, *20*, 3882.

[56] Brook, M. A.; Chen, Y.; Guo, K.; Zhang, Z.; Brennan, J. D. *Sugar-modified silanes: precursors for silica monoliths* Journal of Materials Chemistry 2004, *14*, 1469.

[57] Baker, G. A.; Jordan, J. D.; Bright, F. V. *Effects of poly(ethylene glycol) doping on the behavior of pyrene, rhodamine 6G, and acrylodan-labeled bovine serum albumin sequestered within tetramethylorthosilane-derived sol-gel-processed composites* Journal of Sol-Gel Science and Technology 1998, *11*, 43.

[58] Rocha, V. A.; Eggers, D. K. *Hydrophobic, organically-modified silica gels enhance the secondary structure of encapsulated apomyoglobin* Chemical Communications 2007, 1266.

[59] Bottini, M.; De Venere, A.; Lugli, P.; Rosato, N. *Conformation and stability of myoglobin in dilute and crowded organically modified media* Journal of Non-Crystalline Solids 2004, *343*, 101.

[60] Bottini, M.; Di Venere, A.; Tautz, L.; Desideri, A.; Lugli, P.; Avigliano, L.; Rosato, N. *Structural stability of azurin encapsulated in sol-gel glasses: A fluorometric study* Journal of Sol-Gel Science and Technology 2004, *30*, 205.

[61] Ide, A.; Scholz, G.; Thomas, A. *Tunable Porosity in Bridged Organosilicas Using Self-Organizing Precursors* Langmuir 2008, *24*, 12539.

[62] Ivanov, A. I.; Gavrilov, V. B.; Furmanchuk, D. A.; Aleinikova, O.; Konev, S. V.; Kaler, G. V. *Fluorescent probing of the ligand-binding ability of blood plasma in the acute-phase response* Clinical and Experimental Medicine 2002, *2*, 147.

Chapter 2

THE SOL-GEL METHOD

2.1. Introduction

The initial steps of the sol-gel science go back to the mid-1800, when M. Ebelman and T. J. Graham tried to manufacture inorganic ceramic and glass materials using tetraethylorthosilane (TEOS). However, to prevent silica gels to break into pieces, a long drying period was required (up to one year!). This, of course, reduced the interest on the method. For the next hundred years only academic chemists would give attention to the sol-gel process, gathering a reasonable amount of descriptive literature, but sparse understanding on the physical and chemical principles. Interest in the sol-gel process re-emerged given the great optimism towards its ability to manufacture glass components such as fibres, lenses and mirrors, by direct low-temperature production. Besides this very important advantage, others commonly mentioned are the high homogeneity and purity of resulting materials and the possibility of greater control of the "glass" forming reaction. This allows the formation of materials of high porosity with a large internal surface area [1,2]. The word "tailor-made" is often employed to address these special features of the sol-gel process, and it is also the key to the success (present and future) of this technology. The recent revival of sol-gel method and the growing number of laboratories investigating this field during the last few decades is related to the requirement to produce new materials to be used in electronics, communication, energy, and other high technology fields [3-5]. In the 1990's Avnir and co-workers succeeded in encapsulate biomolecules within silica sol-gel matrices, inaugurating a new era in

biotechnology-related materials [6,7]. This achievement motivated several other groups towards combining advanced materials with biology, producing applications in medicine, environmental science, biotechnology, sensors and photonics [8-12].

2.2. The sol-gel chemistry

The name *sol* refers to a suspension of solid (colloidal) particles ranging in size from 1 nm to 100 nm, in a liquid. The predominant interaction between these particles originates from their surface charge and Van der Waals attractions. The *sol* comprises the *precursors*, or initial components of the sol-gel reaction. The most common class are the silicon alkoxides, with tetraethylorthosilane (TEOS) and tetramethylorthosilane (TMOS) the most thoroughly studied. Some studies make use of TEOS as it is less toxic than TMOS. Alkoxides readily react with water – *hydrolysis* and two partially hydrolysed molecules can bind to each other releasing an alcohol. This reaction is called *condensation*, and if it continues, can form a long random branched *polymeric* molecule. Consequently, the process by which it forms is called *polymerisation*. When the molecule reaches macroscopic proportions and extends to the whole colloidal solution, it is said to have achieved the *gelation* point, signalling the moment when the system consists of a combination of solid and fluid phases. The gel point is easy to observe and measure qualitatively, but it is difficult to measure analytically, as it depends on the temperature, solvent and pH [1,13,14].

Most alkoxides and water are not miscible leading to the use of a co-solvent such as ethanol. Both hydrolysis and condensation can happen under acidic or basic conditions. Acid catalysis favours a relatively slower rate of hydrolysis; the linear polymerisation produces long molecules that can entwine resulting in gelation. Base catalysis favours a faster rate of hydrolysis giving rise to clusters of polymer chains, which behave as discrete species. Gelation occurs by linking of these clusters. With silicon alkoxides the pH above which condensation becomes faster than hydrolysis is around three [15,16]. Figure 2.1 illustrates the hydrolysis and condensation reaction of TEOS precursor molecules in an acid catalysed reaction.

Hydrolysis

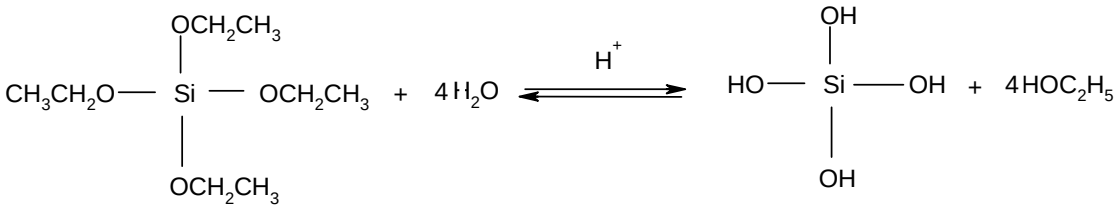

Water condensation

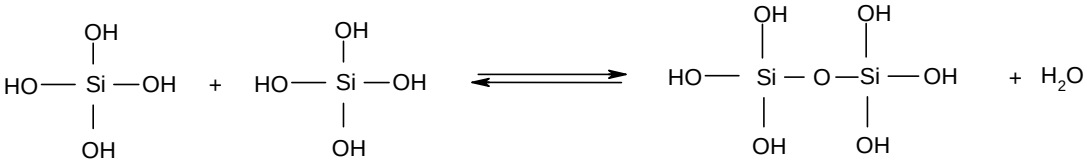

Alcohol condensation

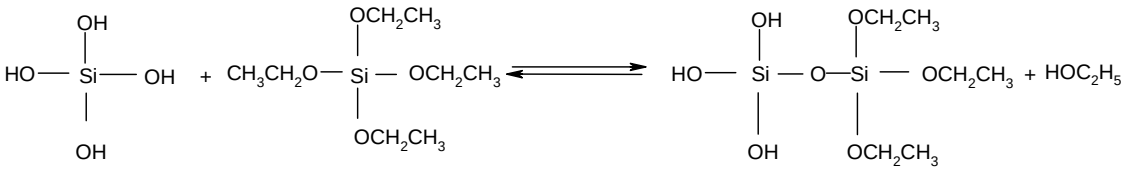

Silica matrix

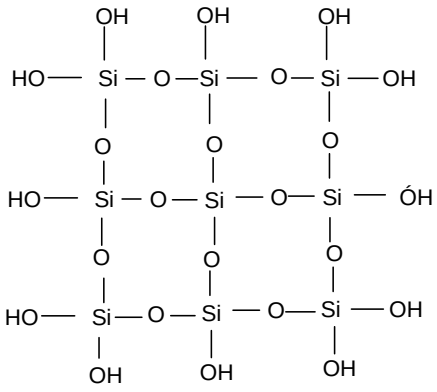

Figure 2.1. Hydrolysis and polycondensation of TEOS molecules (alkoxide precursor) in an acid catalysed sol-gel reaction. The condensation reactions release water and ethanol into the solution as the SiO_2 matrix forms.

After gelation, the reaction continues, as the polymer network is flexible enough to move, allowing supplementary condensation. Also, there is still sol present inside the pores. As a result, monomers or small polymers can bind to the network, producing further changes in its structure and properties. This process is termed *aging* and is the reason why the gel shrinks in the early stages subsequent to gelation. Further shrinkage during the *drying* phase can occur, which involves the deformation of the network and transport of liquid through the pores, part of which can evaporate. This forms a product called a *xerogel*. Additional processing to remove further residual solvent may be performed and can result in a dense ceramic under conditions of an oxygen atmosphere and heat, or even an *aerogel* if supercritical extraction (using CO_2, for example) is done. Aerogels are an interesting class of materials with exceedingly large porosities (up to 99%!) and good thermal insulation properties [13,17].

The versatility of the sol-gel method enables the manufacture of materials with a great variety of forms (films, fibres, monoliths, and powders) as shown in figure 2.2. Moreover, it allows the incorporation of doping species (proteins, antibodies, drugs, particles, dyes, etc) by addition to the sol prior to gelation (figure 2.3).

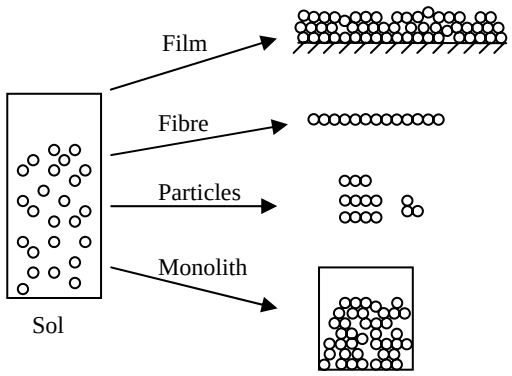

Figure 2.2. Material flexibility of the sol-gel reaction. Thin-films, thick-films, fibres, monoliths and particles can be produced using the appropriated technique.

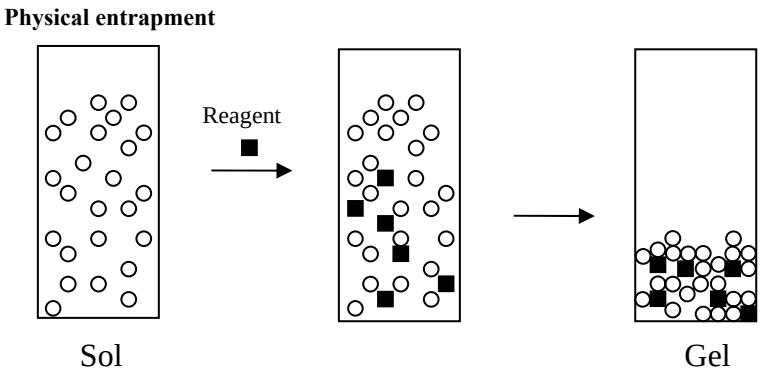

Figure 2.3. The sol-gel reaction with physical entrapment of a doping species.

The resultant materials can be chemically, photochemically and electrochemically stable. In addition, their transparency (in the visible spectral region) allows their optical characterisation and application in optoelectronic devices [18-28]. The combination of inorganic precursors with organoalkoxysilanes is very attractive in the sense that the new material can exhibit unique chemical and physical properties, which can be tuned for a multiplicity of purposes. This is the field of "organically modified silicates" – ORMOSILS with the general formula R-Si-(OR')$_3$, where R represents the functionality and OR' represents the reactive alkoxide group [18]. The organic modification reduces the cross-linking during the polymerisation stage and densification is attenuated through the creation of numerous and/or large pores within the sol-gel network. Figure 2.4 depicts the organic modification of a silicon alkoxide and the ORMOSIL connectivity [17,18,29]. Hybrid materials can also be produced by interpenetrating polymer networks and formation of two concurrent organic and inorganic phases (possibly chemically bonded to each other). For example, the mixture of a silica sol with a solution of a water soluble polymer, such as agar, can produce an interpenetrating polymer network (or IPN) composite sol-gel matrix. Finally, organic compounds can be simply trapped within the host matrix. Blending more than one organic phase has been extensively used, such as combination of biopolymers with silica, for incorporation of biomolecules [30-36].

Organic modification

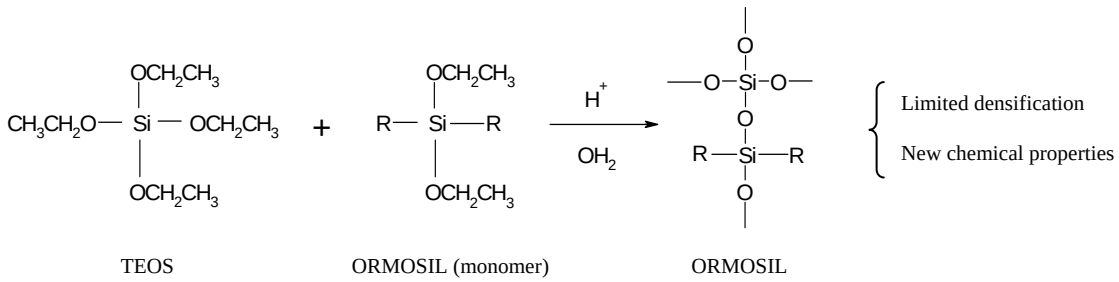

Figure 2.4. Organic modification of a silicon alkoxide, in the present case, TEOS. Two alkoxide groups were substituted by an organic functionality (R). The substituent group creates a specific free volume around it, reducing the densification during drying.

In this work, an adaptation of the acid catalysed production method proposed by Hench and West [1] with a TEOS precursor was used. The hydrolysis and polycondensation of this alkoxide precursor followed by aging under ambient temperature and pressure results in a "sponge-like" network of hydrated amorphous silica, with pores ranging from 1 to 10nm in diameter [1]. As previously mentioned, as water and silicon alkoxides are immiscible, a co-solvent (*e.g.* alcohol) is normally used. The objective here is the incorporation of biomolecules and alcohol is well known to deactivate them [15]. It is therefore important to limit the exposure of any biomolecule to ethanol. With this in mind, instead of using a co-solvent, sonication of the initial two-phase system was performed to promote mixing of the two phases. The release of alcohol as a by-product of the hydrolysis is sufficient to promote further homogenisation [13]. The use of an acid catalysis was also preferred as the monoliths produced possess excellent optical properties. This is obviously desirable if the material is intended for application as an optical addressable biosensor. To avoid any adverse effects caused by an acidic environment, the biomolecules were added to the sol in a second step, in a neutral buffered solution and the concentration of acid kept low (<0.01M). Finally, a set of ORMOSIL and IPN matrices were produced to encapsulate selected biomolecules. The silane modifiers were (3-Aminopropyl)triethoxysilane (APTES), trimethoxypropylsilane (TMPS) and (glycidyloxypropyl)triethoxysilane (GPTES). The chosen polymers were PEG 300 D, PEG 20 KD and Gelrite®.

2.3. Protein-doped sol-gel systems

The mid-1950's witnessed the first successful entrapment of enzymes into silica sol-gel derived media, with partial retention of their catalytic activity. The importance of this achievement was not immediately grasped but, three decades later, Avnir and Zink's research groups restarted investigation on the application of a biological moiety into sol-gel derived media. In this framework, the central question is how to stabilise the biological component in the artificial environment, while preserving its properties, activity and function? Approaches used to immobilise biomolecules, like adsorption onto a surface and covalent attachment [37-39], can cause partial loss of activity because of steric hindrance as a result of the proximity between neighbouring molecules and orientational considerations. Moreover, adsorbed molecules can be easily degraded and covalent linkage techniques are often tedious and require several chemical steps. Sol-gel encapsulation, given the versatility, inertness and biocompatibility of the material, can reduce these problems [40,41]. The term *encapsulation* means the embedding of biomolecules into a sol-gel network — the silica condensation occurs surrounding each macromolecule, which can also act as a template. The pores formed in this way are in harmony with the molecule they host. If the biomolecule is an enzyme, it can retain its catalytic activity, which means that the active site is allowed to adjust its conformation inside the "nanocage". For the system to fulfil its function it is also crucial that the enzyme substrates reach the enzyme and that the reaction products are able to leave the host. It is also important that the pores are big enough to permit the subtle changes in protein structure as it undergoes catalysis. Thus, it is desirable that the enzyme is not adsorbed or covalently bonded to the matrix, although some of these interactions may occur resulting in diminished catalytic efficiency [15].

The unique reactivity of enzymes is well suited for application in the discovery of new compounds, for example in the synthesis of molecules and molecular architectures that are difficult to achieve by traditional synthetic routes. Avnir and Frenkel-Mullerand have recently suggested, that confinement within the pore, rather than just physically prevent detrimental conformational change can also provide chemical protection preserving enzymatic activity, even under extreme pH conditions [42].

Molecular confinement within silica nanopores can produce high volumetric catalyst loadings with an enhancement in the enzymes thermal stability. This fact supports the idea that sol-gel encapsulation can mimic the effects of molecular crowding and confinement in living cells [43-46]. Moreover, the entrapment of proteins in transparent sol-gel silica matrices has enabled the analysis of the longer timescale folding intermediates of cytochrome c to be elucidated and thus, redefine the folding pathways [47]. This study suggests that the same methodology can be applied to study other proteins.

As previously stressed, silica gels can be produced with a large range of porous textures and network structures under different processing conditions, depending on the objective of the hybrid material [15,48,49]. Bioencapsulation in mineral/hybrid sol-gel hosts has been successfully attempted with a great variety of biological entities including numerous proteins, enzymes, antibodies, DNA, phospholipids and even whole cells [50]. This helps to explain the reason why investigation into sol-gel hybrid systems has progressed dramatically over the past two decades.

2.4. Enzyme-based optical biosensors

A biosensor is a sensing device in which the outcome of a biochemical process provides a measurable response. In other words, a biological transducer undergoes a specific biochemical reaction rendering a measurable analyte concentration [51]. In the case of optical biosensors after interacting with the analyte a change in the optical properties occurs. This information can be transmitted by means of an optical fibre or another light propagation process. Bio-optrodes are constructed by immobilising biological recognition components into optical fibres and are divided into two main categories based on their bioactivity; biocatalysts (enzymes and cells) and bioaffinity molecules (antibodies, receptors, and nucleic acids) [52].

The use of enzymes as the chemical transducer has enabled notable progress in the research of optical biosensors and has become indispensable. Many enzymatic reactions involve the use of coloured or luminescent substances, either as a substrate or

product of reaction, which enables their direct detection. Changes in absorbance and fluorescence for instance can be directly detected using an optical biosensor. If the enzymatic reaction does not involve such substances, optochemical transduction is obligatory and indirect detection required [53]. Several enzyme-based optical fibre biosensors have been reported, with applications in environmental, clinical, industrial, food, pharmaceutical and biotechnological sectors [54,55].

Enzymes are the most efficient catalysts known. In the living cell, they control all metabolic pathways by simply lowering the activation energy necessary for reactions, which would otherwise proceed at an exceedingly slow rate. The well-known mechanism describing the reversible single-substrate enzyme reaction, proposed in 1913 by Michaelis and Menten, is described by the scheme [56]:

$$\mathbf{E + S \leftrightarrow ES \leftrightarrow E+P}$$

Figure 2.5. Scheme of the Michaelis-Menten model, valid for one-substrate reversible reactions. In the equilibrium expression (E) signifies enzyme, (S) substrate, (ES) Complex enzyme-substrate, and (P) products of reaction.

From an analytical point of view, the enzyme's *efficiency* is a key feature, as are its reaction *specificity* and substrate *selectivity*. In fact, an enzyme chooses its substrate, selects the precise part of the molecule where to bind and can even differentiate optical isomers. All of these attributes allow straightforward catalysis to proceed, without side-reactions or by-products and with increasing efficiency [57]. Thus, an accurate analysis is possible as the enzyme's substrates (analytes) are selectively converted into species that are easy to detect. However, it is known that the use of enzymes in large scale technological processes has some drawbacks. Procedures for enzyme recovery are usually expensive and, although not consumed by the reaction, they denature with time with an associated loss in activity. If used in solution, purification is needed to obtain the enzymes after the reaction and, if disposable, environmental consequences have to be taken into account. For routine or on-site analysis, the immobilisation of enzymes is essential. The main benefit of immobilisation is the ability to separate the enzymes from the reaction products, permitting the catalyst to be reused. This leads to greater

efficiency as the number of reactions can be increased, along with the possibility to employ higher substrate concentrations [53,58].

One major advantage of optical biosensors is that they are very sensitive to low analyte concentrations, sometimes reaching the single molecule level if fluorescence is used. Some enzymes already contain in their structure chromophoric or fluorescent groups that can report on the reaction mechanism. There is however, the possibility of labelling the enzyme with chromophoric or fluorescent dyes prior to its incorporation in the supportive matrix [59]. Sol-gel glasses are promising materials for optical biosensors. Their porosity, robustness, transparency in the UV and visible part of the spectrum along with the inherent flexibility of the sol-gel method has allowed the encapsulation of a wide range of enzymes. Nevertheless, major fundamental questions relating to this method remain to be optimised, thus explaining why it is still an intense area of investigation [52]. In the present work some of those questions will be addressed, namely:

1. Kinetics in confining media

The temporal resolution achieved by the sensor is connected with the kinetics of the enzymatic process. More precisely, the efficiency of the binding and transduction events, determine how fast a measurement can be done. The Michaelis-Menten mechanism has been used to compare the kinetics of encapsulated enzymes with the kinetics in aqueous solution. The interpretation of the kinetic parameters is not straightforward, because the accessibility of the analytes to the entrapped enzyme (largely determined by the pore size and electrostatics) can be limited. Furthermore, the silanol content, pH conditions and the hydrophobicity of the matrix can influence the enzyme integrity [15,59]. Therefore, the kinetic measurements only do not discern between partitioning of the substrate and enzyme activity effects [60].

2. Microenvironment within the pores

The composition of the solution inside the pores of a sol-gel matrix is different from the bulk solution where the kinetic studies are usually performed, and it varies with aging time. Differences in the pH, for example, may affect the enzyme kinetics and the reaction mechanism. The external solution's pH, however, is not necessarily the same as inside the pores [42]. Fluorescent probes have been successfully used to

monitor the sol-gel process, providing valuable information about the polarity of the solvent entrapped within the pores [61-64]. However, these probes report only on their local environment.

3. Molecular mobility of the encapsulate

A variety of techniques have been used to address molecular mobility in both bulk and sol-gel films, including fluorescence anisotropy, fluorescence correlation spectroscopy and single molecule tracking [65-67]. These studies have unravelled a number of environments within the sol-gel media, with different microviscosities. It was suggested that the mobility of the molecule is inherent to its size, sol-gel preparation method and aging time [67].

4. Stability of the encapsulate

Several studies have reported the enhanced stability of enzymes in sol-gel derived media [68-71]. The understanding of enzyme-host interactions seems to be a priority in order to improve the reactivity of these biomaterials [72]. Attempts to make the sol-gel process more amenable for the encapsulation of biological molecules are plenty; they include alcohol-free, IPN and ORMOSIL manufacturing routes, addition of glycerol, sugars and other osmolites to alter the protein hydration [73,74].

2.5. References

[1] Hench, L. L.; West, J. K. *The Sol-Gel Process* Chemical Reviews 1990, *90*, 33.

[2] Zarzycki, J. *Past and present of sol-gel science and technology* Journal of Sol-Gel Science and Technology 1997, *8*, 17.

[3] Dislich, H. *Glassy and Crystalline Systems from Gels - Chemical Basis and Technical Application* Journal of Non-Crystalline Solids 1983, *57*, 371.

[4] Dislich, H. *Sol-Gel 1984- 2004* Journal of Non-Crystalline Solids 1985, *73*, 599.

[5] Sakka, S. *Sol-Gel Synthesis of Glasses - Present and Future* American Ceramic Society Bulletin 1985, *64*, 1463.

[6] Avnir, D.; Braun, S.; Lev, O.; Ottolenghi, M. *Enzymes and Other Proteins Entrapped in Sol-Gel Materials* Chemistry of Materials 1994, *6*, 1605.

[7] Avnir, D. *Organic-Chemistry within Ceramic Matrices - Doped Sol-Gel Materials* Accounts of Chemical Research 1995, *28*, 328.

[8] Dunn, B.; Miller, J. M.; Dave, B. C.; Valentine, J. S.; Zink, J. I. *Strategies for encapsulating biomolecules in sol-gel matrices* Acta Materialia 1998, *46*, 737.

[9] Gill, I.; Ballesteros, A. *Encapsulation of biologicals within silicate, siloxane, and hybrid sol-gel polymers: An efficient and generic approach* Journal of the American Chemical Society 1998, *120*, 8587.

[10] Flora, K.; Brennan, J. D. *Comparison of formats for the development of fiber-optic biosensors utilizing sol-gel derived materials entrapping fluorescently-labelled protein* Analyst 1999, *124*, 1455.

[11] Livage, J.; Coradin, T.; Roux, C. *Encapsulation of biomolecules in silica gels* Journal of Physics-Condensed Matter 2001, *13*, R673.

[12] Stevens, M. M. *Biomaterials for bone tissue engineering* Materials Today 2008, *11*, 18.

[13] Brinker, C. J. S., George W. *Sol-Gel Science - The Physics and the Chemistry of Sol-Gel Processing*; Academic Press, 1990.

[14] Wen, J.; Wilkes, G. L. *Organic/Inorganic Hybrid Network Materials by the Sol-Gel Approach* Chemistry of Materials 1996, *8*, 1667.

[15] Pierre, A. C. *The sol-gel encapsulation of enzymes* Biocatalysis and Biotransformation 2004, *22*, 145.

[16] Buckley, A. M.; Greenblatt, M. *The Sol-Gel Preparation of Silica-Gels* Journal of Chemical Education 1994, *71*, 599.

[17] Zarzycki, J. *Glasses and Amorphous Materials*; Wiley-VCH, 1991; Vol. 9.

[18] Collinson, M. M. *Recent trends in analytical applications of organically modified silicate materials* Trac-Trends in Analytical Chemistry 2002, *21*, 30.

[19] Zhan, S. H.; Chen, D. R.; Jiao, M. L. *Co-electrospun SiO2 hollow nanostructured fibers with hierarchical walls* Journal of Colloid and Interface Science 2008, *318*, 331.

[20] Mezza, P.; Phalippou, J.; Sempere, R. *Sol-gel derived porous silica films* Journal of Non-Crystalline Solids 1999, *243*, 75.

[21] Patel, A. C.; Li, S. X.; Yuan, J. M.; Wei, Y. *In situ encapsulation of horseradish peroxidase in electrospun porous silica fibers for potential biosensor applications* Nano Letters 2006, *6*, 1042.

[22] Numata, M.; Li, C.; Bae, A. H.; Kaneko, K.; Kazuo, S. C.; Shinkai, S. *beta-1,3-Glucan polysaccharide can act as a one-dimensional host to create novel silica nanofiber structures* Chemical Communications 2005, 4655.

[23] Cavallaro, G.; Pierro, P.; Palumbo, F. S.; Testa, F.; Pasqua, L.; Aiello, R. *Drug delivery devices based on mesoporous silicate* Drug Delivery 2004, *11*, 41.

[24] Hudson, S. P.; Padera, R. F.; Langer, R.; Kohane, D. S. *The biocompatibility of mesoporous silicates* Biomaterials 2008, *29*, 4045.

[25] Kaufman, V. R.; Levy, D.; Avnir, D. *A Photophysical Study of the Sol-Gel Transition in Silica - Structural Dynamics and Oscillations, Room-Temperature Phosphorescence and Photochromic Gel Glasses* Journal of Non-Crystalline Solids 1986, *82*, 103.

[26] Nakazumi, H.; Tarao, T.; Taniguchi, S.; Nanto, H. *Fluorescent thin gel films using organic dyes and pigments* Sol-Gel Optics Iv 1997, *3136*, 159.

[27] Choi, S. S.; Chu, B.; Lee, S. G.; Lee, S. W.; Im, S. S.; Kim, S. H.; Park, J. K. *Titania-doped silica fibers prepared by electrospinning and sol-gel process* Journal of Sol-Gel Science and Technology 2004, *30*, 215.

[28] Sertchook, H.; Elimelech, H.; Avnir, D. *Composite particles of silica/poly(dimethylsiloxane)* Chemistry of Materials 2005, *17*, 4711.

[29] Hoebbel, D.; Nacken, M.; Schmidt, H. *The effect of nanoscaled metal oxide sols on the structure and properties of glycidoxypropyltrimethoxysilane derived sols and gels* Journal of Sol-Gel Science and Technology 2000, *19*, 305.

[30] Gill, I. *Bio-doped nanocomposite polymers: Sol-gel bioencapsulates* Chemistry of Materials 2001, *13*, 3404.

[31] Gill, I.; Ballesteros, A. *Bioencapsulation within synthetic polymers (Part 1): sol-gel encapsulated biologicals* Trends in Biotechnology 2000, *18*, 282.

[32] Gutierrez, M. C.; Jobbagy, M.; Rapun, N.; Ferrer, M. L.; del Monte, F. *A biocompatible bottom-up route for the preparation of hierarchical biohybrid materials* Advanced Materials 2006, *18*, 1137.

[33] Coradin, T.; Allouche, J.; Boissiere, M.; Livage, J. *Sol-gel biopolymer/silica nanocomposites in biotechnology* Current Nanoscience 2006, *2*, 219.

[34] Shchipunov, Y. A.; Burtseva, Y. V.; Karpenko, T. Y.; Shevchenko, N. M.; Zvyagintseva, T. N. *Highly efficient immobilization of endo-1,3-beta-D-glucanases (laminarinases) from marine mollusks in novel hybrid polysaccharide-silica nanocomposites with regulated composition* Journal of Molecular Catalysis B-Enzymatic 2006, *40*, 16.

[35] Li, B.; Takahashi, H. *New immobilization method for enzyme stabilization involving a mesoporous material and an organic/inorganic hybrid gel* Biotechnology Letters 2000, *22*, 1953.

[36] Reetz, M. T. *Entrapment of biocatalysts in hydrophobic sol-gel materials for use in organic chemistry* Advanced Materials 1997, *9*, 943.

[37] Hudson, S.; Cooney, J.; Magner, E. *Proteins in Mesoporous Silicates* Angewandte Chemie-International Edition 2008, *47*, 8582.

[38] Jones, J. R. *Observing cell response to biomaterials* Materials Today 2006, *9*, 34.

[39] Cao, L. Q. *Immobilised enzymes: science or art?* Current Opinion in Chemical Biology 2005, *9*, 217.

[40] Kandimalla, V. B.; Tripathi, V. S.; Ju, H. X. *Immobilization of biomolecules in sol-gels: Biological and analytical applications* Critical Reviews in Analytical Chemistry 2006, *36*, 73.

[41] Gupta, R.; Chaudhury, N. K. *Entrapment of biomolecules in sol-gel matrix for applications in biosensors: Problems and future prospects* Biosensors & Bioelectronics 2007, *22*, 2387.

[42] Frenkel-Mullerad, H.; Avnir, D. *Sol-gel materials as efficient enzyme protectors: Preserving the activity of phosphatases under extreme pH conditions* Journal of the American Chemical Society 2005, *127*, 8077.

[43] Eggers, D. K.; Valentine, J. S. *Molecular confinement influences protein structure and enhances thermal protein stability* Protein Science 2001, *10*, 250.

[44] Dordick, J. S.; Freeman, A. *Biocatalysis as a discovery tool: from nanoscale to high-throughput and beyond* Current Opinion in Biotechnology 2006, *17*, 559.

[45] Eggers, D. K.; Valentine, J. S. *Crowding and hydration effects on protein conformation: A study with sol-gel encapsulated proteins* Journal of Molecular Biology 2001, *314*, 911.

[46] Bottini, M.; De Venere, A.; Lugli, P.; Rosato, N. *Conformation and stability of myoglobin in dilute and crowded organically modified media* Journal of Non-Crystalline Solids 2004, *343*, 101.

[47] Shibayama, N. *Slow motion analysis of protein folding intermediates within wet silica gels* Biochemistry 2008, *47*, 5784.

[48] Holowacz, I.; Podbielska, H.; Bauer, J.; Ulatowska-Jarza, A. *Viscosity, surface tension and refractive index of tetraethylorthosilicate-based sol-gel materials depending on ethanol content* Optica Applicata 2005, *35*, 691.

[49] Ariga, K. *Silica-supported biomimetic membranes (vol 3, pg 297, 2004)* Chemical Record 2004, *4*, 59.

[50] Avnir, D.; Coradin, T.; Lev, O.; Livage, J. *Recent bio-applications of sol-gel materials* Journal of Materials Chemistry 2006, *16*, 1013.

[51] Alfaya, A. A. S.; Kubota, L. T. *The utilization of materials obtained by the sol-gel process in biosensors construction* Quimica Nova 2002, *25*, 835.

[52] Jenna L. Rickus, B. D., Jeffrey I. Zink. Optically Based Sol-Gel Biosensor Materials. In *Optical Biosensors:Present and Future*; Ligler, F. S., Taitt, C. A. R., Eds.; Elsevier Science B.V., 2002; pp 427

[53] Kuswandi, B.; Andres, R.; Narayanaswamy, R. *Optical fibre biosensors based on immobilised enzymes* Analyst 2001, *126*, 1469.

[54] Mehrvar, M.; Bis, C.; Scharer, J. M.; Moo-Young, M.; Luong, J. H. *Fiber-optic biosensors - Trends and advances* Analytical Sciences 2000, *16*, 677.

[55] Wolfbeis, O. S. *Fiber-optic chemical sensors and biosensors* Analytical Chemistry 2004, *76*, 3269.

[56] Fersht, A. *Enzyme Structure and Mechanism*, second edition ed.; W.H. Freeman and Company: New York, 1985.

[57] Cornish-Bowden, A. *Fundamentals of Enzyme Kinetics*; Portland Press, 1995.

[58] El-Essi, F. A.; Zuhri, A. Z. A.; Al-Khalil, S. I.; Abdel-Latif, M. S. *Spectrophotometric determination of enzymatically generated hydrogen peroxide using Sol-Gel immobilized horseradish peroxidase* Talanta 1997, *44*, 2051.

[59] Jin, W.; Brennan, J. D. *Properties and applications of proteins encapsulated within sol-gel derived materials* Analytica Chimica Acta 2002, *461*, 1.

[60] Menaa, B.; Herrero, M.; Rives, V.; Lavrenko, M.; Eggers, D. K. *Favourable influence of hydrophobic surfaces on protein structure in porous organically-modified silica glasses* Biomaterials 2008, *29*, 2710.

[61] Gupta, R.; Mozumdar, S.; Chaudhury, N. K. *Fluorescence spectroscopic studies to characterize the internal environment of tetraethyl-orthosilicate derived sol-gel bulk and thin films with aging* Biosensors & Bioelectronics 2005, *20*, 1358.

[62] Dunn, B.; Zink, J. I. *Probes of pore environment and molecule-matrix interactions in sol-gel materials* Chemistry of Materials 1997, *9*, 2280.

[63] Goring, G. L. G.; Brennan, J. D. *Fluorescence and physical characterization of sol-gel-derived nanocomposite films suitable for the entrapment of biomolecules* Journal of Materials Chemistry 2002, *12*, 3400.

[64] Lobnik, A.; Wolfbeis, O. S. *Characterization of sol-gel and ormosils via polarity sensitive probes* Sol-Gel Optics Iv 1997, *3136*, 284.

[65] Ye, F. M.; Collinson, M. M.; Higgins, D. A. *What can be learned from single molecule spectroscopy? Applications to sol-gel-derived silica materials* Physical Chemistry Chemical Physics 2009, *11*, 66.

[66] Zurner, A.; Kirstein, J.; Doblinger, M.; Brauchle, C.; Bein, T. *Visualizing single-molecule diffusion in mesoporous materials* Nature 2007, *450*, 705.

[67] Gottfried, D. S.; Kagan, A.; Hoffman, B. M.; Friedman, J. M. *Impeded rotation of a protein in a sol-gel matrix* Journal of Physical Chemistry B 1999, *103*, 2803.

[68] Vidinha, P.; Barreiros, S.; Cabral, J. M. S.; Nunes, T. G.; Fidalgo, A.; Ilharco, L. M. *Enhanced biocatalytic activity of ORMOSIL-encapsulated cutinase: The matrix structural perspective* Journal of Physical Chemistry C 2008, *112*, 2008.

[69] Macario, A.; Moliner, M.; Corma, A.; Giordano, G. *Increasing stability and productivity of lipase enzyme by encapsulation in a porous organic-inorganic system* Microporous and Mesoporous Materials 2009, *118*, 334.

[70] Jurgen-Lohmann, D. L.; Legge, R. L. *Immobilization of bovine catalase in sol-gels* Enzyme and Microbial Technology 2006, *39*, 626.

[71] Liu, Y.; Wang, M. J.; Li, J.; Li, Z. Y.; He, P.; Liu, H. T.; Li, J. H. *Highly active horseradish peroxidase immobilized in 1-butyl-3-methylimidazolium tetrafluoroborate room-temperature ionic liquid based sol-gel host materials* Chemical Communications 2005, 1778.

[72] Braun, S.; Rappoport, S.; Zusman, R.; Avnir, D.; Ottolenghi, M. *Biochemically active sol-gel glasses: The trapping of enzymes (Reprinted from Materials Letters, vol 10, pg 1, 1990)* Materials Letters 2007, *61*, 2843.

[73] Ferrer, M. L.; del Monte, F.; Levy, D. *A novel and simple alcohol-free sol-gel route for encapsulation of labile proteins* Chemistry of Materials 2002, *14*, 3619.

[74] Brennan, J. D. *Biofriendly sol-gel processing for the entrapment of soluble and membrane-bound proteins: Toward novel solid-phase assays for high-throughput screening* Accounts of Chemical Research 2007, *40*, 827.

Chapter 3

FLUORESCENCE AND MEASUREMENT TECHNIQUES

3.1. Introduction

Fluorescence is the most sensitive and versatile technique to investigate molecular interactions within matter and it is used by scientists from different disciplines. The past 20 years have witnessed an extraordinary increase in the application of fluorescence in several fields of the biological sciences and it is presently the leading research tool in biotechnology [1]. Fluorescence techniques have boosted new discoveries in biomedical sciences and, reciprocally, these achievements have pushed forward fluorescence measurement systems. An example is the sequencing of DNA by fluorescence (known since 1987), which enabled the completion of the human genome sequence in 2001 [2,3]. This was decisive in the development of new methods and applications of fluorescence. Other emerging applications (e.g. analytical chemistry) are the result of advances in laser, detector and computer technology. These have made it possible, for example, to create lifetime images of samples taking advantage of sophisticated microscopy techniques [1,4]. Furthermore, the numerous publications on the use fluorescence to study the sol-gel process confirm the adequacy of this technique on monitoring sol-gel derived material [5].

Fluorescent molecules report on their specific microenvironment (polarity, pH, hydrogen bonding, electric potential, etc) and their fluorescence properties quite frequently show up differences between the bulk and nanoscale local environments within each material. Fluorescence is strongly influenced by interfacial interactions, providing additional information, for example, on the local structure, confinement or microviscosity. The information obtained also depends on the techniques employed to measure fluorescence. Furthermore, progress in technology is reducing the cost of equipment, thus allowing measurements that would have been considered exotic or impractical [1,4].

3.2. Fluorescence

The absorption of ultra-violet or visible light by a molecule can result in the formation states of higher energy. Such excited states are very unstable and the molecule returns rapidly to the ground state. This can occur with or without the emission of light. In the former the energy loss is called radiative and can give rise to the phenomenon of luminescence. The latter produces a non-radiative de-excitation. The phenomenon of luminescence is formally divided into fluorescence, if the transition is between states of the same spin multiplicity, or phosphorescence if the transition is between states of different multiplicity. These processes are appropriately illustrated by the Jablonski energy diagram, which is depicted in figure 3.1. The absorption of light or excitation of a fluorophore is represented by the straight upward arrow from the ground electronic single state (S_0) to the excited states (S_1, S_2 etc) [1]. The subscripts 0, 1, 2, 3 … refer to the energy ranking of the state relative to the ground state (S_0). Superimposed on these electronic energy levels are a number of vibrational energy levels. Triplet states (designated T) are populated via the first excited singlet state and involve a change (flip) of spin. The first triplet level located energetically above S_0 is T_1, where the subscript 1 indicates the energy ranking among triplets [6]. As these electronic states are quantised the excitation energy, E has to match the energy difference between the ground state and the higher energy electronic state. According to quantum mechanics,

$$E = h\nu = h\frac{c}{\lambda} = hc\bar{\nu} \tag{3.1}$$

where E is the energy, h is Planck's constant, c the speed of light, and v the frequency of the incoming photon, and λ the photon wavelength.

The absorption of a photon occurs on the femtosecond (10^{-15} seconds) timescale and can bring a molecule to high vibrational levels of S_1, S_2 ... Subsequently this is followed by vibrational relaxation of electrons from high energy excited state levels to the lowest excited state energy level. This type of de-excitation process usually takes place on the sub-picosecond ($<10^{-12}$ seconds) timescale. Emission of photons from the lowest vibrational level of the first excited singlet state back to the ground state, called fluorescence, proceeds on the picosecond to nanosecond (10^{-9} seconds) time range. Molecules in S_1, after undergoing spin conversion to the triplet state T_1 (intersystem crossing) emit radiation on a longer time scale (10^{-6} – 1 second) commonly called phosphorescence. There are distinctive rate constants for each process, usually denoted as follows: fluorescence emission (k_f), internal conversion $S_1 \rightarrow S_0$ (k_{ic}) and intersystem crossing (k_{isc}).

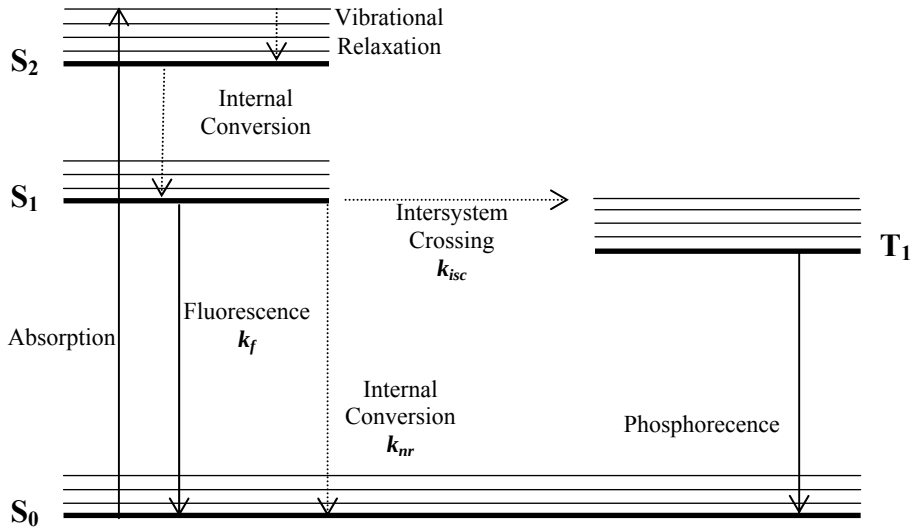

Figure 3.1. Jablonski Energy Diagram illustrating the singlet ground state (S_0), the first exited singlet state (S_1), the second exited singlet state (S_2) and the first triplet state (T_1). The thick lines correspond to electronic energy levels and the thin ones represent their respective vibrational energy levels. Absorption is represented as straight upward arrow. Fluorescence and phosphorescence are represented as downward arrows. All non-radiative processes are represented by the dotted arrows.

The decay to the ground state, when observed in molecular species, is normally measured as a band (fluorescence spectrum) rather than a sharp line, upon steady state excitation. This is due to the numerous vibrational energy levels that occur in each electronic state, thus producing a wide range of photon emissions. Compared with the absorption spectrum, fluorescence emission is an approximate "mirror image" shifted to longer wavelengths as result of energy loss in excited state interactions. The shift (figure 3.2) is known as the Stokes' shift, in honour of George Stokes, who is credited with the first description of the phenomenon of fluorescence in 1852.

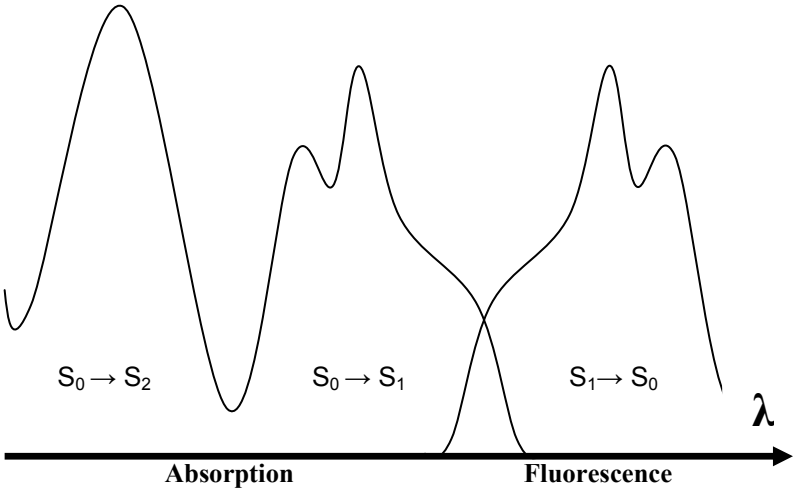

Figure 3.2. Relative positions of absorption and fluorescence spectra.

There are three fundamental parameters used in fluorescence spectroscopy: the fluorescence spectrum e.g. the emission intensity measured upon steady state excitation; the quantum yield (Φ_F), ranging from zero to one, is the ratio between emitted photons and absorbed photons (equation 3.2).

$$\Phi_F = \frac{k_f}{k_f + k_{nr}} \tag{3.2}$$

In equation 3.2, k_f is the rate constant for radiative deactivation $S_1 \rightarrow S_0$ with emission of fluorescence, k_{nr} is the rate constant for the overall non-radiative pathways of

deactivation $S_1 \rightarrow S_0$. k_{nr} is defined such $k_{nr} = k_{ic} + k_{isc}$; finally, fluorescence lifetime (τ) gives the characteristic time that a molecule stays in the excited state S_1 before returning to the ground state and is given by the time that it takes for the intensity to drop to *1/e* of its initial value. It is commonly written:

$$\tau = \frac{1}{k_f + k_{nr}} \tag{3.3}$$

The fluorescence decay with time is described by the function (3.4) where I is the fluorescence intensity measured at time t, I_0 is the initial intensity observed immediately after pulsed excitation and τ is the fluorescence lifetime.

$$I(t) = I_0 e^{-t/\tau} \tag{3.4}$$

For an ensemble of fluorophores, some will emit soon after the excitation pulse, others will emit at times longer than the molecules characteristic lifetime, according to statistical physics. The time distribution of emitted photons is the intensity decay (figure 3.3).

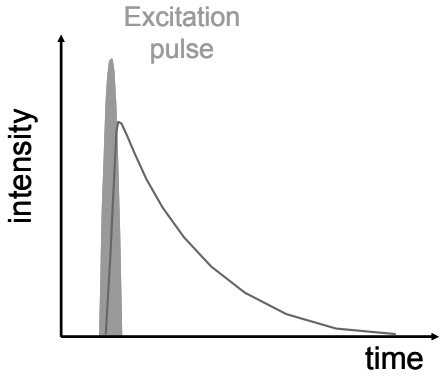

Figure 3.3. The fluorescence intensity is proportional to the number of molecules in the excited singlet state.

3.3. Excited state-host interactions

Whenever immersed in a medium, the photophysics of a fluorescent probe, inevitably reports on the medium's characteristics through its interaction with the surroundings. It is well-known that probe-host interactions are, in most cases, the result of: (a) electronic and/ or dipolar relaxation events, expressed as solvatochromic shifts in the emission spectra; (b) hydrodynamic factors that arise from the probe mobility (translational and/or rotational), expressed by the influence of the viscosity of the host medium on the photophysics of the probe, particularly on the nonradiative decay processes; and (c) other specific interactions, largely dependent upon the nature of the probe and the host medium.

Solvatochromism is caused by differential solvation of the ground-state and first excited-state of the molecule (Franck-Condon excited state with the solvation pattern of the ground state). If, with increasing solvent polarity, the ground-state of the molecule is better stabilised by the surrounding solvent molecules than the excited-sate, a hypsochromic (or blue) shift of the absorption band is observed. If, the excited molecule is better stabilised by solvation than the relaxed molecule, a bathochromic (or red) shift of the absorption band is observed. The difference between these two states is also responsible for the solvent influence on the fluorescence emission. Since the time for the excitation event ($\sim 10^{-15}$ s) is much shorter than the time required for rotational or vibrational motions ($\sim 10^{-12} - 10^{-10}$ s), the nuclei (of the fluorophore plus the solvation shell) do not alter their position during the electronic transition. However, if the lifetime of the excitation is long enough, the solvent molecules around the fluorophore reorient their dipole moments accordingly, and solvent relaxation takes place. It is from this equilibrium excited state that fluorescence occurs. Solvent relaxation has the effect of reducing the energy gap between ground and excited states, resulting in a red shift of the fluorescence emission. Conversely, there is now a Franck-Condon ground state with a solvation pattern of the excited state that slowly (10 to 100 picoseconds) reorganises to the equilibrium ground state. It is easily understandable that solvatochromism depends on the physico-chemical properties of the fluorophore and solvent molecules. In general, dye molecules with a large change in their permanent dipole moments upon excitation, display stronger solvatochromic shifts. If after excitation the dipole moment increases a positive solvatochromism results. However, a decrease in the solute dipole

moment upon excitation results in a negative solvatochromism. Furthermore, the ability for the solute to create hydrogen bonds with the solvent (either in the ground or excited Franck-Condon states) enhances the extent of the solvatochromic shift. Solutes with intramolecular charge transfer absorptions are an example of molecules that display this particular solvatochromic behaviour and the dye Nile red is among them. Positive fluorescence solvatochromism is illustrated by figure 3.4.

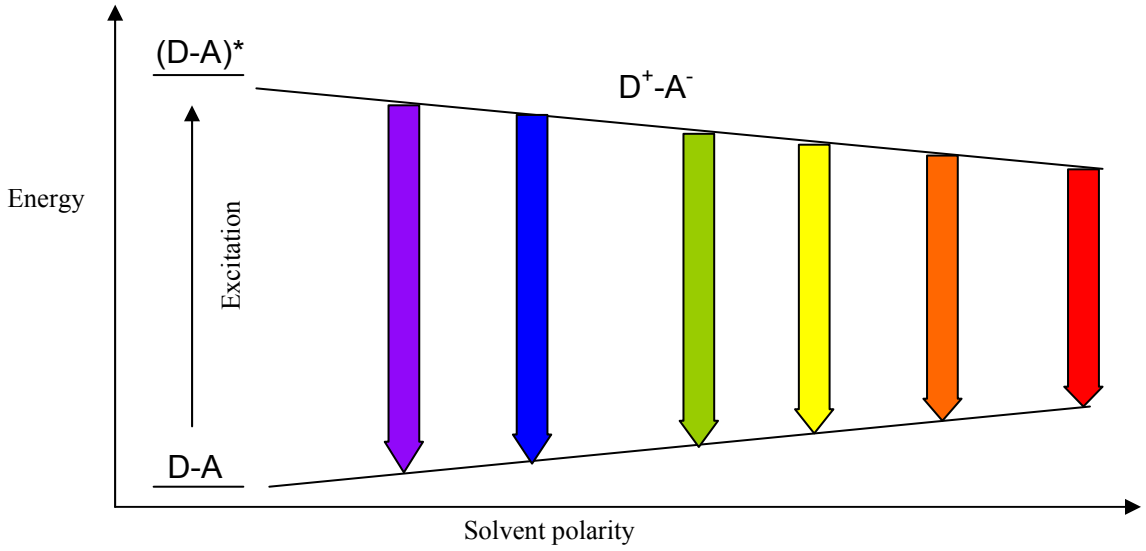

Figure 3.4. Schematic representation of positive fluorescence solvatochromism. The non-polar ground state D-A absorbs a photon and reaches the locally excited state (D-A)*, which subsequently decays into a charge separated state. The solvent will stabilise this charge separated state by aligning its dipoles. The more polar the solvent, the greater the stabilising effect will be and the more the excited state will be lowered in energy. At the same time the ground state, which is non-polar, will be destabilised. The net result of these interactions is a decrease in the energy gap between the ground state and the excited state and thus a red shift in emission [7].

Several authors have established that the spectral shifts in the emission spectra (by reference to the vapour phase spectrum, E_F^0), caused by local effects produced by electronic and dipolar relaxation are adequately described by the following equations [8,9]:

$$\Delta E_F = E_F - E_F^0 = C_1 \frac{n^2 - 1}{2n^2 + 1} + C_2 \left(\frac{\varepsilon - 1}{\varepsilon + 2} - \frac{n^2 - 1}{n^2 + 2} \right) \tag{3.5}$$

or

$$\Delta \overline{\nu}_{abs} - \Delta \overline{\nu}_{flu} = \frac{1}{4\pi\varepsilon_0}\frac{2}{hc}\frac{\Delta\mu^2}{R^3}\left(\frac{\varepsilon-1}{\varepsilon+2} - \frac{n^2-1}{n^2+2}\right) \qquad (3.6)$$

In expression 3.5, $\frac{n^2-1}{n^2+2} = f(n^2)$ refers to the redistribution of electrons, and the term $f(\varepsilon, n^2)$ refers to the orientation of dipoles. Like this, it is possible to measure spectral shifts in the emission produced by a general solvatochromic effect. In equation 3.6, so called Mataga-Lippert equation, $\Delta\mu$ is the difference in the dipole moment of the molecule between ground and excited states, *R* is the cavity radius considering the molecule a point dipole at the centre of a spherical cavity, ε is the static dielectric costant of the host medium and *n* its refractive index. A well characterised solvatochromic effect has been observed for the dye Nile red in homogeneous media [10]. According to these authors the following data were found:

E_F^0 = 2.649 eV (487 nm)

C_1= -1.128 eV

C_2= -0.556 eV

$\Delta\mu$ = 6.1 D

Hydrodynamic effects are generally expressed through viscosity. However, when examining molecular interactions, frequently the size of the probe is comparable to the size of the surrounding medium molecules. Thus, the molecule under study probes the medium as discontinuous. In this case, macroscopic viscosity becomes inaccurate to describe any observed effects. In the absence of a proper theory, phenomenological approaches have been employed by several authors [4,11]. This effect has been addressed in the present work as described in chapter 4 by adopting the concept of an "effective viscosity" when studying the fluorescence of 4-(4- (dimethylamino)styryl)-*N*-methylpyridiniumiodine (DASPMI).

Finally, regarding specific interactions an important illustration of this type of interaction is the hydrogen bond, also addressed during the course of this work.

3.4. The quenching of fluorescence

Quenching effects have been studied at the fundamental level, but also as a source of information about biochemical systems [12,13]. The term quenching refers to any process that can result in effective reduction in fluorescence intensity. This can happen simply by boosting the non-radiative relaxation pathways from the excited state electrons to the ground state. Quenching processes may be either intramolecular or intermolecular and can reduce the excited state lifetime as well as the quantum yield of the fluorophore. Examples include excited-state reactions, molecular rearrangements, energy transfer, ground-state complex formation, and collisional quenching. Dynamic quenchers (e.g. O_2, acrylamide, I^-) reduce fluorescence intensity by collision, due to diffusive encounters between the fluorophore and quencher during the lifetime of the excited state. Quenchers are usually termed static (e.g. nicotinamide and heavy metals) if the fluorophore and quencher form a non-fluorescent complex in the ground state, thus reducing the population of excitable molecules [1].

Collisional quenching is described using the relation 3.7, called the Stern-Volmer equation where I_o and I are, respectively, the steady-state fluorescence intensities in the absence and presence of quencher, $[Q]$ is the quencher concentration and k_q is the bimolecular quenching constant, τ_0 is the lifetime of the fluorophore in the absence of quencher, and $K_D = k_q\,\tau_0$ is the Stern-Volmer quenching constant [4]. In the simplest cases the Stern-Volmer plot (where the ratio I_o/I is plotted against the quencher concentration) gives a straight line with slope equal to K_D

$$\frac{I_0}{I} = 1 + k_q \tau_0 [Q] = 1 + K_D [Q] \tag{3.7}$$

The bimolecular quenching constant, k_q, reflects the efficiency of quenching or the accessibility of the fluorophore to the quencher. An important characteristic of collisional quenching is that the ratio I_o/I is proportional to τ_o/τ. This happens because quenching is an additional competing process that depopulates the excited state [1]. Sometimes both collisional and static quenching phenomena can occur simultaneously for the same fluorophores. If so, a characteristic upward deviation from linearity is observed in the Stern-Volmer plot [1,4].

3.5. Time-resolved fluorescence

Time-resolved fluorescence is used to measure the excited state lifetime of a fluorophore. The knowledge of decay times can add precious information about rates and hence kinetics, where a simple steady-state measurement is insufficient. An example is discrimination between dynamic and static quenching; dynamic quenching is a rate process acting on the entire excited state population, decreasing the mean decay time of the entire population [1,14].

There are several methods available for time-resolved fluorescence measurements such as: streak camera measurements, fluorescence upconversion, time-correlated single-photon counting (TCSPC), among others. In this work, the chosen method was the most widely used, TCSPC, which presents several advantages namely, high sensitivity with possibility of detecting very low fluorescence intensities (down to the single molecule level), large dynamic range, well defined statistics (Poisson) and intuitive data representation in the time domain [15].

The underlying principle of TCSPC relies on the concept that the emission probability of a single photon after the excitation event is equal to the intensity of emission of the ensemble of molecules over time. TCSPC allows measuring the arrival time of a fluorescent photon after excitation. After a large number of excitation cycles, a histogram of photon arrival times is built up [16,17].

Unless otherwise stated, in the work presented in this thesis, time-resolved measurements used a single-photon counting apparatus equipped with a NanoLED excitation source emitting at 490 nm (HORIBA, Jobin Yvon, IBH Ltd. Glasgow, Scotland). In order to minimise deadtime effects in the electronics, the equipment operated in "reverse mode", *i.e.* the pulse from the detector providing the START pulse and that from the source, providing the STOP pulse. This was necessary because of the high repetition rate of the LED used to excite the sample (800 KHz). The fluorescence emission was wavelength-selected using a 550 nm cut-off filter and detected with a Hamamatsu R2949 photomultiplier. The equipment layout is shown in figure 3.5.

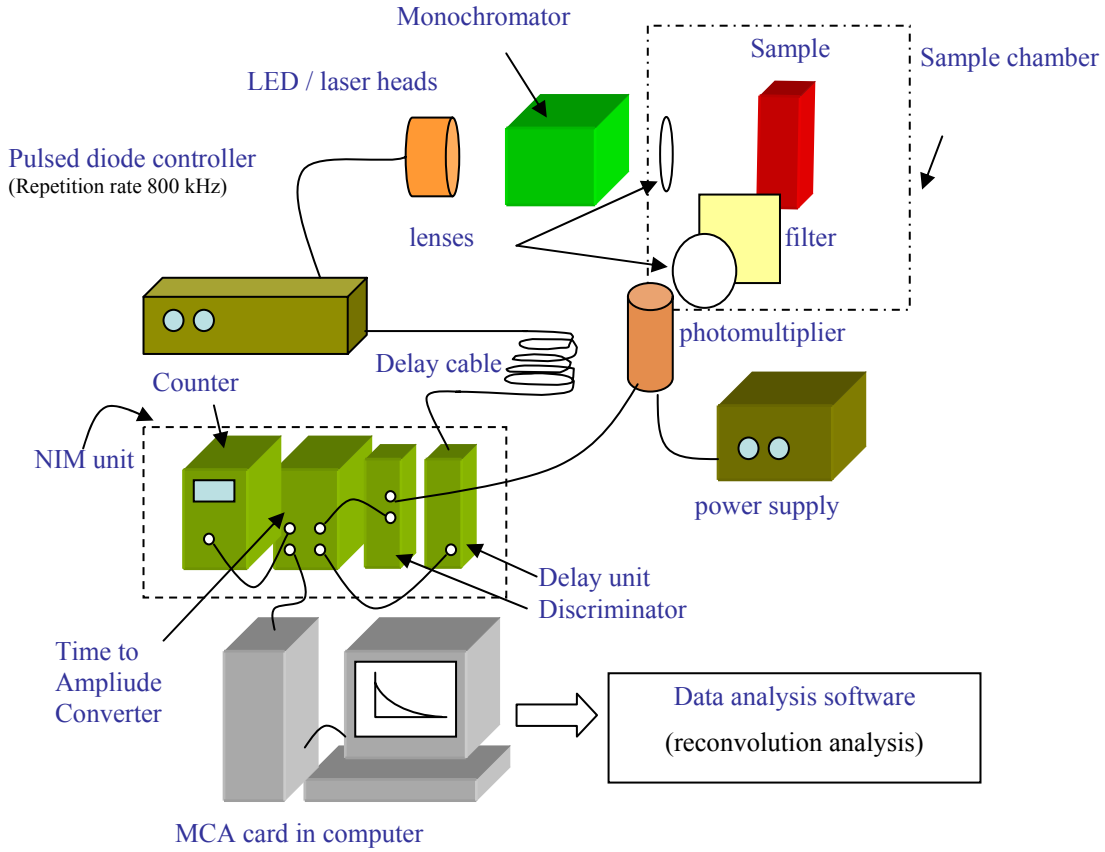

Figure 3.5. Schematic diagram of the equipment layout used in this work.

The signal from the PMT was fed via an Ortec 265 constant fraction discriminator to an Ortec 567 TAC, housed in an Ortec 4001A NIM bin. The TAC output was built into a histogram using an Oxford Instruments PCA3 MCA card in a Pentium III (800 MHz) computer running Windows 2000, and data acquisition controlled using DataStation software from HORIBA Jobin Yvon IBH Ltd.

Very seldom the measured decays can be fitted to a single exponential. But most decays are, in fact, multiexponential, as found in the present work. Data analysis was performed with IBH DAS6 software and the goodness of fit judged in terms of a χ^2 value and weighted residuals. The decay time data were analysed by using a sum of exponentials, employing a nonlinear least-squares reconvolution analysis of the form [14]

$$I(t) = \sum_{i=1}^{n} \alpha_i \exp\left(\frac{-t}{\tau_i}\right) \tag{3.8}$$

The preexponential factors (α_i) are given normalized to unity and errors given as three standard deviations. Average lifetimes, $\langle\tau\rangle$, were calculated as [18]

$$\langle\tau\rangle = \sum_i \alpha_i \tau_i \tag{3.9}$$

3.6. Time-resolved fluorescence anisotropy

Fluorescence anisotropy has been used since the early 1970's for monitoring molecular reorientation in solution. Improved experimental techniques and scientific advances e.g. in life sciences have increased the interest in these studies [16]. Fluorescence anisotropy describes the level of polarised emission of a fluorophore when excited with plane-polarised light. Following an instantaneous pulse of light, the total fluorescence intensity at time t is $I(t) = I_{\parallel}(t) + 2I_{\perp}(t)$, where $I_{\parallel}$ and $I_{\perp}$ are the fluorescence intensities parallel and perpendicular to the polarisation of the excitation, respectively. The instantaneous emission anisotropy, $r(t)$, at that time is [4]

$$r(t) = \frac{I_{\parallel}(t) - I_{\perp}(t)}{I_{\parallel}(t) + 2I_{\perp}(t)} = \frac{I_{\parallel}(t) - I_{\perp}(t)}{I(t)} \tag{3.10}$$

In practice, time-resolved fluorescence anisotropy measurements are performed by using linearly polarized light as the excitation source and measuring the fluorescence emission decays at polarizations parallel, $I_{\parallel}(t)$, and perpendicular, $I_{\perp}(t)$, to that of the excitation and include a G factor so that

$$r(t) = \frac{I_{\parallel}(t) - GI_{\perp}(t)}{I_{\parallel}(t) + 2GI_{\perp}(t)} \tag{3.11}$$

G corrects for the instrumental response and is the ratio of the sensitivities of the detection system for vertically (S_V) and horizontally (S_H) polarised light $G = S_V/S_H$ [16].

With the equipment used in the experiments described in this thesis, G was 1. Furthermore, the fluorescence anisotropy decay can be related to the rotational mobility of a spherical molecule using the expression

$$r(t) = r_0 \exp\left(-\frac{t}{\tau_r}\right) \tag{3.12}$$

where r_0 is the anisotropy observed at $t = 0$ and τ_r is the rotational correlation time of the sphere. The rotational correlation time is associated to the solvent viscosity, η, and the volume of the rotating molecule, V, according to the well-known equation [19,20]

$$\tau_r = \frac{\eta V}{kT} \tag{3.13}$$

where k is the Boltzmann constant and T is the absolute temperature. Using the Stokes-Einstein equation it is now possible to calculate the rotational diffusion coefficient, D_r

$$D_r = \frac{kT}{6\eta V} \tag{3.14}$$

In the case that the angular range of the rotational motion is limited (hindered rotation), the anisotropy will never decay to zero and a residual anisotropy will be observed at times comparatively longer than the fluorescence lifetime. The anisotropy is than described by

$$r(t) = (r_0 - r_\infty) \exp\left(-\frac{t}{\tau_r}\right) + r_\infty \tag{3.15}$$

where r_0 is the initial anisotropy and r_∞ the limiting anisotropy. However, in the "wobble-in-cone" model [4,21] the rotations in anisotropic media of a rod-like fluorophore are restricted to a cone. The rotational motions are described by the rotational diffusion around an axis perpendicular to the long molecular axis and an ordered parameter which is the half–angle of a cone, θ. Rotation beyond this angle is

assumed to be energetically impossible. The angle θ can be determined from the ratio r_∞/r_0

$$2\left(\frac{r_\infty}{r_0}\right)^{1/2} = \cos^2\theta + \cos\theta \tag{3.16}$$

3.7. Fluorescence Recovery After Photobleaching (FRAP)

Photobleaching is the light-induced irreversible conversion of a fluorescent molecule into a non-fluorescent entity. The exact mechanism of photobleaching of organic dyes is complex and/or mostly unknown. In many cases, the excited triplet state and several intermediates are involved. A common cause of photodamage is the oxidation of the dye by singlet oxygen or even water if the experiments are done in aqueous solution. Most fluorophores can repeat the excitation and emission cycle many hundreds to thousands of times before the highly reactive excited state molecule is photobleached. This ability is dependent upon the molecular structure and the local environment. For instance, photobleaching increases with temperature because more reaction pathways become activated [22-24].

Experiments with Fluorescence Recovery After Photobleaching (FRAP) started almost 40 years ago to observe the lateral mobility of proteins and lipids in living cells [25]. Since then many studies have been successfully done employing the technique as a valuable tool to study diffusion in other environments than biological, namely polymer solutions and gels [26-28]. In FRAP experiments fluorescent molecules are photobleached by a high-power laser beam focused in the region of interest of the sample. Immediately after photobleaching an attenuated light beam measures the diffusion of fluorescent molecules back into the bleached area from outside the irradiation zone. The intensity increases as the number of unbleached probes reaches the bleached area and a plot of intensity versus time is then obtained. Figure 3.6 shows a typical FRAP curve. FRAP measurements require a microscope to image the sample.

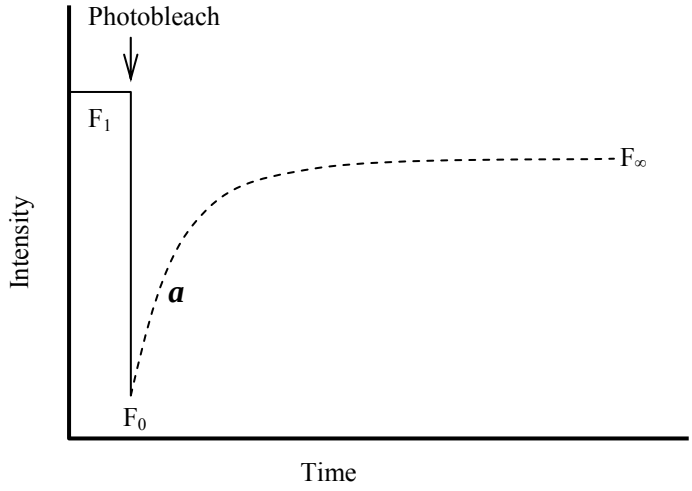

Figure 3.6. Scheme showing a typical FRAP curve. F_1 is the initial fluorescence intensity. F_0 is the intensity just after bleaching. Region ***a*** shows the fluorescence recovery. The stabilisation in the recovery gives a final intensity of F_∞.

Two parameters can be deduced from the graph:

a) The intensity of fluorescence after recovery in relation to the initial intensity. This is known as the mobile fraction, R, and is defined as

$$R = (F_\infty - F_0) / (F_1 - F_0) \times 100 \qquad (3.17)$$

where F_1 is the intensity before bleaching, F_0 the intensity just after bleaching and F_∞ the intensity after full recovery. These regions are shown in figure 3.6.

b) The rate of mobility or how quickly the molecules diffuse back into the bleached area. If a steep curve is found, there is a fast recovery. The mobility is expressed as D_t, the diffusion coefficient, which is related to the diffusion time, τ_D.

The diffusion time, τ_D can be calculated by finding the time it takes for the fluorescence to recover to half of its final value, $\tau_{1/2}$. The half time can be established by fitting the recovery data to a curve of the form [29]

$$I(t) = A(1 - e^{-kt}) + C \qquad (3.18)$$

Where I is the fluorescence intensity, A is the final plateau intensity after recovery minus the initial intensity after bleaching i.e. (F_∞ - F_0), C is F_0 and k is a time constant ($\tau_{1/2}$= ln 2/k). The half time, $\tau_{1/2}$ is related to τ_D by a factor γ_D which takes into account the recovery during the bleaching process. In the case of a circular beam γ_D = 0.88 such that [25]

$$D_t = \frac{0.88\omega^2}{4\tau_{1/2}} \tag{3.19}$$

Where D_t is the translational diffusion coefficient which is related to the viscosity via the Stokes-Einstein formula.

$$D_t = \frac{kT}{6\pi\eta r} \tag{3.20}$$

where r is the hydrodynamic radius of the sphere.

As is evident, FRAP provides complementary information to time-resolved anisotropy measurements, used to calculate viscosity where rotational diffusion is probed instead of translational diffusion.

3.8. Synchronous Scan Fluorescence Spectroscopy

Synchronous Scan Fluorescence Spectroscopy (SFS) is a methodology developed for multicomponent analysis and simple routine based applications by Tuan Vo-Dinh, although the idea of synchronous excitation luminescence is attributed to Lloyd, 1971 [30]. The applications of the method include the determination of polynuclear aromatic hydrocarbons, qualitative and quantitative analysis (for environmental monitoring or drugs screening)[31-37].

The synchronous fluorescence signal can be understood either as an emission spectrum with synchronously scanned excitation wavelength or as an excitation spectrum with synchronously scanned emission wavelength [30,38]. The SFS implies simultaneously varying both the excitation wavelength (λ_{exc}) and the emission wavelength (λ_{em}) while keeping a constant interval ($\Delta\lambda$) between them. The synchronous fluorescence intensity, I_s is given by the expression [30]

$$I_s = KcdE_x(\lambda_{exc})E_m(\lambda_{ex} + \Delta\lambda) \tag{3.21}$$

where E_x is the excitation function at the wavelength λ_{exc}, E_{em} is the emission intensity at the wavelength λ_{em} (normal emission spectrum), c is the analyte concentration, d is the thickness of the sample and k an experimental constant factor. The maximum intensity with the narrowest half-width is obtained when $\Delta\lambda$ corresponds to the difference between the wavelengths of absorption and emission maxima. SFS presents three major advantages over conventional fluorescence spectrometry: narrowing of spectral bands, simplification of emission spectra and reduction of the spectral range (figure 3.7) [30].

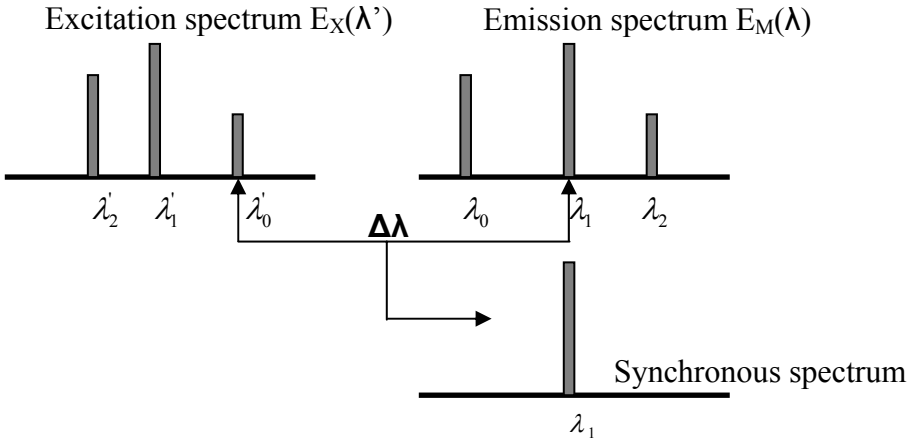

Figure 3.7. Spectral simplification effect. $E_M(\lambda)$=emission spectrum; $E_X(\lambda')$ excitation spectrum.

Concerning the instrumentation utilised in this work, all the absorption spectra were measured on a Shimadzu UV- 3101 PC and steady-state fluorescence emission, excitation and synchronous spectra were recorded on a Fluorolog 3, from HORIBA Jobin Yvon.

Unless otherwise stated, the equipment utilised to perform the measurements described in this thesis, belongs to Centro de Física da Universidade do Minho (CFUM).

3.9. References

[1] Lakowicz, J. R. *Principles of Fluorescence Spectroscopy*, Third edition ed.; Springer, 2006.

[2] Smith, L. M.; Sanders, J. Z.; Kaiser, R. J.; Hughes, P.; Dodd, C.; Connell, C. R.; Heiner, C.; Kent, S. B. H.; Hood, L. E. *Fluorescence Detection in Automated DNA-Sequence Analysis* Nature 1986, *321*, 674.

[3] Venter, J. C. *The sequence of the human genome (vol 292, pg 1304, 2001)* Science 2001, *292*, 1838.

[4] Valeur, B. *Molecular Fluorescence - Principles and applications*; Wiley-VHC: Weinheim, 2002.

[5] Birch, D. J. S. G., C. D.; Karolin J.; Leishman R.; Rolinski O. J. Fluorescence Nanometrology in Sol-Gels. In *Fluorescence Spectroscopy, Imaging and Probes*; Kraayenhof, R. V., A. J. W. G. ; Gerritsen, H. C., Ed.; Springer.

[6] Turro, N. J. *Modern Molecular Photochmistry*; University Science books: Sausalito, 1991.

[7] Zoon, P. D. Fluorescent Probe Molecules with Individual Detection Capability. PhD, University of Amsterdam, 2009.

[8] Kubota, N. M. T. *Molecular Interactions and molecular spectra*; Marcell Dekker: New York, 1970.

[9] Renge, I. *Mechanisms of solvent shifts, pressure shifts, and inhomogeneous broadening of the optical spectra of dyes in liquids and low-temperature glasses* Journal of Physical Chemistry A 2000, *104*, 7452.

[10] Viseu, T. M. R.; Hungerford, G.; Coelho, A. F.; Ferreira, M. I. C. *Dye-host interactions for local effects recognition in homogeneous and nanostructured media* Journal of Physical Chemistry B 2003, *107*, 13300.

[11] Doolittle, A. K.; Doolittle, D. B. *Studies in Newtonian Flow .5. Further Verification of the Free-Space Viscosity Equation* Journal of Applied Physics 1957, *28*, 901.

[12] Somogyi, B.; Lakos, Z. *Protein Dynamics and Fluorescence Quenching* Journal of Photochemistry and Photobiology B-Biology 1993, *18*, 3.

[13] Costa, S. M. B.; Lopes, J.; Martins, M. J. T. *Steady-State Fluorescence Quenching Kinetics of Water-Soluble Zinc Porphyrins in Reversed Micelles* Journal of the Chemical Society-Faraday Transactions Ii 1986, *82*, 2371.

[14] Birch, D. J. S. I., R. E. Time-Domain Fluorescence Spectroscopy Using Time-Correlated Single-Photon Counting. In *Topics in Fluorescence Spectroscopy*; Lakowicz, J. R., Ed.; Plenum Press: New York, 1991; Vol. Volume 1: techniques.

[15] Bohmer, M.; Pampaloni, F.; Wahl, M.; Rahn, H. J.; Erdmann, R.; Enderlein, J. *Time-resolved confocal scanning device for ultrasensitive fluorescence detection* Review of Scientific Instruments 2001, *72*, 4145.

[16] O'Connor, D. V. P., D. *Time Correlated Single Photon Counting*; Academic Press: London, 1984.

[17] Becker, W. *Advanced Time-Correlated Single Photon Counting Techniques*; Springer: Berlin, 2005.

[18] Sillen, A.; Engelborghs, Y. *The correct use of "average" fluorescence parameters* Photochemistry and Photobiology 1998, *67*, 475.

[19] Valeur, B.; Keh, E. *Determination of the Hydrodynamic Volume of Inverted Micelles Containing Water by the Fluorescence Polarization Technique* Journal of Physical Chemistry 1979, *83*, 3305.

[20] Suwaiyan, A. A.; Jamjoom, F.; Aljuwair, H.; Stuff, R.; Klein, U. K. A. *Nondestructive Laser Technique for the Measurement of Viscosities in Fluid-Flows - Application to a Newtonian Fluid* Journal of the Chemical Society-Faraday Transactions 1992, *88*, 1531.

[21] Kinosita, K.; Ikegami, A.; Kawato, S. *On the Wobbling-in-Cone Analysis of Fluorescence Anisotropy Decay* Biophysical Journal 1982, *37*, 461.

[22] Zondervan, R.; Kulzer, F.; Kol'chenko, M. A.; Orrit, M. *Photobleaching of rhodamine 6G in poly(vinyl alcohol) at the ensemble and single-molecule levels* Journal of Physical Chemistry A 2004, *108*, 1657.

[23] van Dijk, M. A.; Kapitein, L. C.; van Mameren, J.; Schmidt, C. F.; Peterman, E. J. G. *Combining optical trapping and single-molecule fluorescence spectroscopy: Enhanced photobleaching of fluorophores* Journal of Physical Chemistry B 2004, *108*, 6479.

[24] Dittrich, P. S.; Schwille, P. *Photobleaching and stabilization of fluorophores used for single-molecule analysis with one- and two-photon excitation* Applied Physics B-Lasers and Optics 2001, *73*, 829.

[25] Axelrod, D.; Koppel, D. E.; Schlessinger, J.; Elson, E.; Webb, W. W. *Mobility Measurement by Analysis of Fluorescence Photobleaching Recovery Kinetics* Biophysical Journal 1976, *16*, 1055.

[26] Meyvis, T. K. L.; De Smedt, S. C.; Van Oostveldt, P.; Demeester, J. *Fluorescence recovery after photobleaching: A versatile tool for mobility and interaction measurements in pharmaceutical research* Pharmaceutical Research 1999, *16*, 1153.

[27] Houtsmuller, A. B.; Rademakers, S.; Nigg, A. L.; Hoogstraten, D.; Hoeijmakers, J. H. J.; Vermeulen, W. *Action of DNA repair endonuclease ERCC1/XPF in living cells* Science 1999, *284*, 958.

[28] Reits, E. A. J.; Neefjes, J. J. *From fixed to FRAP: measuring protein mobility and activity in living cells* Nature Cell Biology 2001, *3*, E145.

[29] Klonis, N.; Rug, M.; Harper, I.; Wickham, M.; Cowman, A.; Tilley, L. *Fluorescence photobleaching analysis for the study of cellular dynamics* European Biophysics Journal with Biophysics Letters 2002, *31*, 36.

[30] Vodinh, T. *Multicomponent Analysis by Synchronous Luminescence Spectrometry* Analytical Chemistry 1978, *50*, 396.

[31] Yang, X. J.; Chou, J.; Sun, G. Q.; Yang, H.; Lu, T. H. *Synchronous fluorescence spectra of hemoglobin: A study of aggregation states in aqueous solutions* Microchemical Journal 1998, *60*, 210.

[32] Poulli, K. I.; Mousdis, G. A.; Georgiou, C. A. *Synchronous fluorescence spectroscopy for quantitative determination of virgin olive oil adulteration with sunflower oil* Analytical and Bioanalytical Chemistry 2006, *386*, 1571.

[33] Xia, T. T.; Wang, L.; Bian, G. R.; Dong, L.; Hong, S. *Synchronous fluorescence determination of protein with functional organic nanoparticles* Microchimica Acta 2006, *154*, 309.

[34] Sikorska, E.; Gorecki, T.; Khmelinskii, I. V.; Sikorski, M.; De Keukeleire, D. *Fluorescence spectroscopy for characterization and differentiation of beers* Journal of the Institute of Brewing 2004, *110*, 267.

[35] Nevin, A.; Comelli, D.; Valentini, G.; Cubeddu, R. *Total Synchronous Fluorescence Spectroscopy Combined with Multivariate Analysis: Method for*

the Classification of Selected Resins, Oils, and Protein-Based Media Used in Paintings Analytical Chemistry 2009, *81*, 1784.

[36] Ivanov, A. I.; Gavrilov, V. B.; Furmanchuk, D. A.; Aleinikova, O.; Konev, S. V.; Kaler, G. V. *Fluorescent probing of the ligand-binding ability of blood plasma in the acute-phase response* Clinical and Experimental Medicine 2002, *2*, 147.

[37] Perez-Ruiz, T.; Lozano, C. M.; Tomas, V.; Carpena, J. *Sensitive synchronous spectrofluorimetric methods for the determination of naproxen and diflunisal in serum* Fresenius Journal of Analytical Chemistry 1998, *361*, 492.

[38] Rubio, S.; Gomezhens, A.; Valcarcel, M. *Analytical Applications of Synchronous Fluorescence Spectroscopy* Talanta 1986, *33*, 633.

Chapter 4

FLUORESCENT PROBES USED IN THIS STUDY

4.1. Introduction

Fluorescent dyes have an immense range of applications as reporters for structural changes in proteins and other molecules, measuring different parameters in micro-heterogeneous systems or just as tags for analysis and sorting [1]. Choosing the appropriate fluorescent probe depends on the system to be monitored as well as techniques to be employed. Sensitivity, selectivity, calibration method, labelling technique and the fluorescence spectral properties, are certainly important criteria when choosing a fluorescent indicator [2]. Biological material is itself fluorescent. In proteins, the intrinsic fluorescence is mainly due to the aromatic amino acid residues of tryptophan, tyrosine, and phenylalanine. The green fluorescent protein (GFP) from the jellyfish *Aequorea victoria* contains a built-in chromophore formed by the cyclization and oxidation of a sequence of amino acids (Serine – Tyrosine – Glycine). Today, GFP is one of the most widely studied and exploited proteins in biochemistry and cell biology [3].

There are, however, some adversities which make extrinsic labelling preferable to the amino acid fluorescence study. First, in terms of time-resolved measurements, the photophysics of tryptophan is complicated and the origin of its fluorescence decay is

ambiguous. Second, most proteins have more than one tryptophan residue, further complicating this scenario [4,5]. Also, the fluorescence quantum yield of phenylalanine is very low (0.022 in aqueous solution) and, in the case of tyrosine, its fluorescence is often quenched by the neighbouring tryptophan residues [1]. In this work, extrinsic labelling was preferred, not only because of the mentioned reasons, but also because the proteins were monitored encapsulated within sol-gel media where scattered excitation light may be problematic.

This chapter focuses on the fluorescent probes utilised, which were chosen on the basis of their particular properties to monitor the sol-gel reaction (the *sol* to *gel* transition and the aging process), to assess interactions between the host and guest molecules, and to elucidate conformational changes of the encapsulated proteins. Characterisation of both the host environment and guest conformation is important, as the matrix is intended to be protective to the enzyme and simultaneously allow access to substrate molecules. Only if these conditions are fulfilled can the entrapped biomolecule exercise its catalytic function. With this in mind, the probe 7-diethylamino-3,4-benzophenoxazine-2-one (Nile red) was selected to monitor both the host polarity and changes in protein conformation [6-8]. The dye 4-(4- (dimethylamino)styryl)-*N*-methylpyridiniumiodine (DASPMI), was chosen to assess the internal host viscosity [9-12]. A preliminary study was performed to examine the photophysics of these two probes in homogeneous solution. The outcome is discussed in this chapter after a brief introduction to the mechanism by which they unravel the dynamics of the hybrid sol-gel systems.

Fluorescein was chosen to perform fluorescence recovery after photobleaching (FRAP) measurements, and Alexafluor 488 was selected to make a complementary study, because of its resistance to photobleaching. The derivative of fluorescein, fluorescein isothyocyanate (FITC) and Alexafluor 488 are both well used dyes for protein labelling [13-18]. Their photophysical properties are well characterised in the supplier's manual [19] and both of them were utilised according to the protocol provided by the manufacturer.

4.2. DASPMI

Stilbenoid dyes are promising in that their photophysical properties are very sensitive to solvent viscosity [33]. The dye 4-(4- (dimethylamino)styryl)-*N*-methylpyridiniumiodine (DASPMI) has been commonly used to study cellular processes [34,35] and its decay time found to be dependent on viscosity with its multiple fluorescence ascribed to intramolecular charge transfer [9,11]. Its properties were also exploited to provide an insight into the changes that occur in the *sol* to *gel* transition [10,36].

The fluorescence of DASPMI is complex and has been related to the formation of charge transfer states and associated conformational change with possibility of reaching the Twisted Intramolecular Charge Transfer (TICT) state. The "TICT" model was suggested by Lyppert et al. and later pushed forward by Grabowski and co-workers to explain the dual fluorescence of the probe 4N,N-dimethylaminobenzonitrile (DMABN) in polar solvents. The model is included in the area of adiabatic photoreactions which occur on the hypersurface of the lowest (singlet or triplet) exited state. When this state is energetically very close to the ground state, the molecule can twist providing an efficient and fast non radiative transition to the ground state [23]. Depending on the motion, these molecules require a specific reaction volume in order to take place; the smaller the volume required, more easily the reaction occurs (figure 4.1).

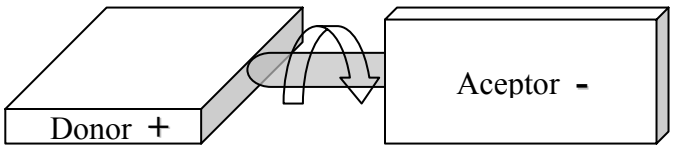

Figure 4.1. Molecular rotor consisting of two different moieties (donor and acceptor) in a TICT (twisted intramolecular charge transfer) sate. The typical TICT probe starts from a planar state geometry in the Franck-Condon excited state, with partial charge separation. As solvent relaxation occurs, the acceptor moiety assists rotating towards a perpendicular conformation with full charge separation between the donor and the acceptor. Adapted from [24].

The surrounding medium strongly influences the degree of the intramolecular motion enabling molecular rotors to be employed as fluorescent probes to characterise it in terms of micropolarity and microviscosity [25-28]. The twisting motion in the TICT mechanism can be easily hindered at very high viscosity conditions and rotors with various rotating moieties can be used as free-volume probes. Free volume effects derive from the discontinuous nature of matter which is composed by molecules of diverse sizes and shapes. The free space between these molecules provides an extra possibility for movement, especially in biological membranes and solvents, which are highly dynamic systems. Sometimes, it happens that the *microviscosity* or *effective viscosity* probed by a molecular rotor is inferior to the *bulk viscosity* because of free volume effects [24].

The emission of DASPMI (figure 4.2), in general, consists of three distinct decay times with emission from the planar form (state *A* in scheme II) and the possible consecutive population of other states (*B* and *C*) via charge transfer and bond twisting:

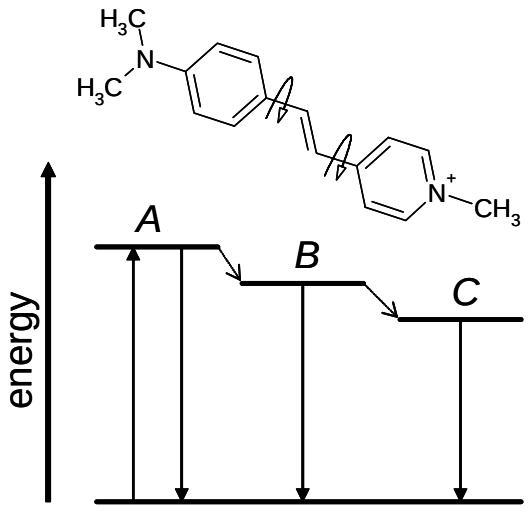

Figure 4.2 The fluorescent probe DASPMI and its fluorescent states.

This bond twisting (as the origin of the observed fluorescence) is restricted to single bonds, as the energy for a double bond mechanism is prohibitive under normal conditions [11] and work investigating the role of twisting in this class of molecule, showing the effect of inhibiting certain rotations, has confirmed single bond twisting as the dominant

mechanism with a lack of isomerism [9]. As solvent viscosity increases the ability to rotate is reduced causing a reduction in the non radiative pathways, hence producing an increase in the observed fluorescence lifetime.

4.2.1. Experimental characterisation of DASPMI

4.2.1.1. Materials and methods

The dye *p*-DASPMI was purchased from Molecular Probes (Invitogen SA) and glycerol from Riedel-de Haën. Fluorescence quantum yields, Φ_F, in solution were determined relative to *p*-DASPMI in ethanol, reported to be 0.008 by Rettig and Strehmel [9]. The optically dilute method was adopted [37], and correction for the spectral response of the equipment was also made. Time-resolved measurements were performed as described in sections 3.5. and 3.6. The rotational correlation time, τ_r, was calculated using equation 3.13.

4.2.1.2. Results and discussion

The photophysics of DASPMI was studied in water-glycerol mixtures, containing different percentages of glycerol. Such mixtures were considered appropriate models because glycerol possesses several OH groups and water is a relevant species in the synthesis of the sol-gel hybrids. All emission spectra, obtained upon excitation at 490 nm, showed one broad maximum centred at 600 nm and no structure. All decays were found to be multiexponential, in agreement with previous work [9,11,33]. Table 4.1 shows the results from the analysis of the time-resolved fluorescence data.

Sample Composition (wt % Gly)	τ_1 (ns)	τ_2 (ns)	τ_3 (ns)	α_1	α_2	α_3	χ^2	$\langle\tau\rangle$ (ns)
80	0.15±0.11	0.37±0.02	-	0.52	0.48	-	1.04	0.26
84	0.17±0.10	0.46±0.01	-	0.45	0.55	-	1.06	0.33
88	0.16±0.17	0.57±0.01	-	0.33	0.67	-	1.12	0.44
92	0.22±0.08	0.75±0.02	2.22±0.40	0.29	0.70	0.01	1.20	0.60
96	0.27±0.18	0.91±0.04	1.77±0.19	0.25	0.73	0.03	1.12	0.77
100	0.40±0.06	1.25±0.04	2.68±0.58	0.28	0.71	0.01	1.10	1.03

Table 4.1. Time-resolved fluorescence decay parameters of DASPMI in glycerol-water mixtures.

According to Rettig *et al.* [11], the multiple fluorescence emission is related to different states: a planar excited state, originating directly from the $S_0 \rightarrow S_1$ transition, to which the lowest lifetime is ascribed (τ_1); a second emitting state, planar and most probably with a significant charge-transfer character (τ_2); and a third, a twisted intramolecular charge-transfer excited state (TICT sate), associated with the longest lifetime component (τ_3). Under the experimental conditions of this study, components τ_1 and τ_2 dominate the observed decays. Only minute contributions ascribed to τ_3 could be found, with negligible physical significance. These results indicate that, most probably, the solvent cage surrounding the excited dye molecule may hinder the twisting of the molecule, thus precluding the formation of the TICT state. The "rigidity" of the solvent cage is a consequence of the hydrogen bonds that occur between the glycerol molecules and glycerol-water molecules [38]. This hypothesis is supported by arguments further presented in this section, when discussing the time-resolved fluorescence anisotropy data. The average emission lifetime for each sample was obtained from the analysis of the respective fluorescence decay, according to equation 3.9. The radiative (k_f) and nonradiative (k_{nr}) rate constants for DASPMI were then obtained from the well-known equations

$$k_f = \frac{\Phi_F}{\tau_f} \tag{4.1}$$

$$k_{nr} = \frac{\left(1 - \Phi_F\right)}{\tau_f} \tag{4.2}$$

Since the emission decays were found to be multiexponential, the average emission lifetime was taken as τ_f in the previous equations. All results are shown in table 4.2, where the refractive index (n) and the macroscopic viscosity (η) of each water-glycerol mixture are also indicated.

Sample Composition (wt % Gly)	Refractive index [a]	Relative viscosity [a] (cP)	Quantum yield [b]	Average life-time (ns)	k_f (s^{-1}) [c]	k_{nr} (s^{-1}) [d]
80	1.4431	59.78	0.034	0.26	1.52×10^8	3.85×10^9
84	1.4492	84.17	0.043	0.33	1.49×10^8	2.91×10^9
88	1.4553	147.2	0.055	0.44	1.42×10^8	2.14×10^9
92	1.4613	383.7	0.074	0.60	1.42×10^8	1.52×10^9
96	1.4674	778.9	0.086	0.77	1.29×10^8	1.16×10^9
100	1.4735	1759.6	0.206	1.03	2.34×10^8	7.37×10^8

Table 4.2. Photophysical parameters of DASPMI in glycerol-water mixtures. *a)* From reference [39] Viscosity data are relative to the viscosity of water at 20 °C (η_0 = 1.002 cP). *b)* Measured relative to DASPMI in ethanol (Φ_FDASPMI in ethanol = 0.008). *c)* k_r= radiative rate constant. *d)* k_{nr} = nonradiative rate constant.

These data show that a significant decrease of k_{nr} is observed with the increase in the medium viscosity, in agreement with previous results obtained for *o*-DASPMI in several *n*-alcohols [9]. Also, it is of importance to examine the correlation between the medium's viscosity and k_{nr}, through the phenomenological (empirical) relationship [40].

$$k_{nr} = \frac{A}{\eta^x} \tag{4.3}$$

where A and x are parameters depending on the system. The logarithmic representation, shown in figure 4.3 gives $x = 0.45$.

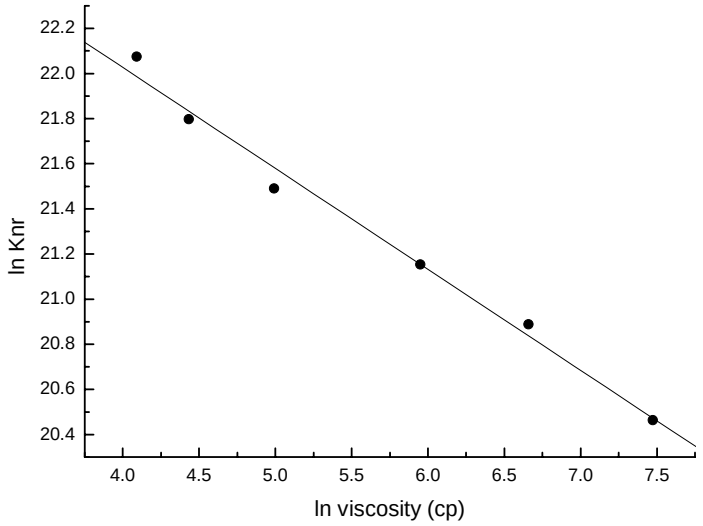

Figure 4.3. Correlation between the non-radiative constant of P-DASPMI emission and the host medium viscosity. Linear fit with a gradient of -0.45 ± 0.02. The goodness of fit (R) was 0.994.

This result indicates that the macroscopic viscosity is not appropriate to describe the microenvironment probed by DASPMI. In fact the free volume of the solvent mixture becomes a relevant parameter and thus the probe senses the solvent as a discontinuous medium [40]. This behaviour is understandable since the characteristic dimensions of the probe are most probably comparable to the mean free path in the host media. The approximate volume of DASPMI, as calculated using Hyperchem 7 software, is estimated to be on the order of 240 $Å^3$. A realistic approach to the hydrodynamics of DASPMI was obtained from time-resolved anisotropy measurements, performed as described in the previous chapter (section 3.4).

Table 4.3 shows the measured rotational correlation times (τ_r) and the initial anisotropy (r_0). The limiting anisotropy (r_∞) was assumed to be zero throughout. The values found for r_0 indicate that a significant part of the initial decay is observed. However, the fact that the values of τ_r are somewhat longer than the fluorescence lifetimes (τ_f) precluded the measurement of the complete $r(t)$ decay function.

Sample Composition (wt % Gly)	τ_r (ns)	r_0	χ^2	η_{eff} (cP)	V_H (Å^3)	R_H (Å)
84	3.2 ± 0.3	0.294	1.23	7.35	1791	7.5
88	5.7 ± 0.9	0.280	1.25	9.45	2481	8.4
92	16.0 ± 1.8	0.338	1.11	14.55	4525	10.3
96	15.6 ± 1.4	0.231	1.20	20.01	3208	9.1
100	38.9 ± 6.8	0.274	1.05	28.87	5544	11.0

Table 4.3. Time-resolved anisotropy data of DASPMI in glycerol-water mixtures and hydrodynamic parameters. Limiting anisotropy, r_∞, fixed as 0.

Table 4.3 also includes the values for the hydrodynamic volume (V_H) and radius (R_H) of DASPMI in each solution. These values were obtained through equation 3.13 assuming the effective viscosity (η_{eff}),

$$\eta_{\text{eff}} = (\eta_{\text{bulk}})^{0.45} \tag{4.4}$$

and are thought to be more suitable to describe the local environment probed by DASPMI in each solution. All values found for V_H were substantially higher than the approximate volume of DASPMI (~240 Å3). These values show that the probe is associated with solvent molecules (either glycerol or water). The positive charge of the dye molecule facilitates its interaction with the solvent molecules, thus promoting the "binding of a solvent cage" to each DASPMI molecule, which rotates along with the dye.

4.3. Nile red

The term *solvatochromism* was introduced by Hantzsch (1857-1935) in the beginning of the last century to express the phenomenon by which, UV/visible/near-IR absorption spectra of molecules were influenced by the surrounding medium, in terms of position, intensity, and shape of the absorption bands. The suggestion that solvatochromic dyes could be used as visual indicators for solvent polarity was initially made by Brooker et al. (from Eastman Kodak Company) in 1951 [20]. Nonetheless, examples of their practical use can be found prior to that date. For example, dyes of the Nile Blue group were utilised as indicator standards to the detection and semi-quantitative estimation of acids in airplane motor fuels and lubricants [21]. Spectroscopic probes, however, can measure not only the polarity of liquids, but also that of solids, glasses and surfaces.

Nile red (figure 4.4) is a neutral, hydrophobic, and highly solvatochromic dye which has been extensively applied to examine the structure, environment, and dynamics of biological samples and micro-heterogeneous media. Although nearly insoluble and non-fluorescent in water, it has a very high partition coefficient from water to hydrophobic solvents, where it fluoresces strongly [8,41-48].

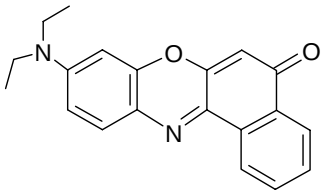

Figure 4.4. Structure of the fluorescent probe Nile red.

Nile red shows a positive solvatochromism, meaning that it undergoes a bathochromic shift both in absorption and in fluorescence spectrum with increasing solvent polarity. The dramatic solvatochromic effect is attributed to the high dipole moment of the molecule in the ground state, which is even higher during the excited state. The large shift has been explained through charge separation between the

diethylamino group which acts as a donor, and the quinoid system which acts as acceptor, with the possibility of the formation of a twisted intramolecular charge transfer state (TICT) [6,49-51]. Still, two different groups have published theoretical and experimental work where the TICT hypothesis is negated; one referring as an evidence the negligible effect of viscosity on the photophysical properties of the probe, the other a low value for the difference between excited-state and ground-state dipole moments, reported as being incompatible with the formation of a TICT sate [52,53]. The fluorescence spectra of Nile red in organic solvents, is also suggestive of hydrogen bonding effects. This property is visible when probing biphasic or biological systems [53-58].

Nile red has previously been used to monitor the conformation of horseradish peroxidase upon incorporation into a silica *sol-gel* derived host [59]. This was achieved by spectral decomposition of the fluorescence, showing that the probe experienced different environments within the enzyme, each with a different critical Förster distance for energy transfer [60]. This thesis will concentrate on the fact that synchronous scan fluorescence spectroscopy (SFS) can be used to differentiate between different probes, or the same probe in different environments, and employ it with Nile red. In solution the band position was found to depend on the polarity and influenced by the effect of hydrogen bonding. The combination of Nile red and SFS will be employed to elucidate changes in protein conformation, as well as changes within the host during the aging process.

4.3.1. Experimental characterisation of Nile red

4.3.1.1. Materials and methods

Nile red was from Molecular Probes and the solvents were either from Sigma, Aldrich or Fluka. The equipment used to measure Nile red spectra was described in chapter 3. The solvatochromic properties were observed by SFS in homogeneous solution.

4.3.1.2. Results and discussion

In this study, Nile red solvatochromic properties are reported for a large range of solvents, from hexane to THF. Initially three different wavelength offsets were employed, as shown in figure 4.4 for three solvents. In a solvent of low polarity, such as hexane, the greater offset spectrum is more structured, because of the vibrational features present in both the normal absorption and emission spectra [61]. This structure decreases with a reduction of the offset between the excitation and emission wavelengths and is lost when an offset of 10 nm is used. In higher polarity media, all the spectra at the three different offsets exhibit a Gaussian band shape. This is not surprising as the normal absorption and emission spectra do not exhibit vibrational structure. It should be noted that the feature (small band) situated at 650 nm is present throughout and hence may relate to an artefact and thus will be ignored for the purpose of this work.

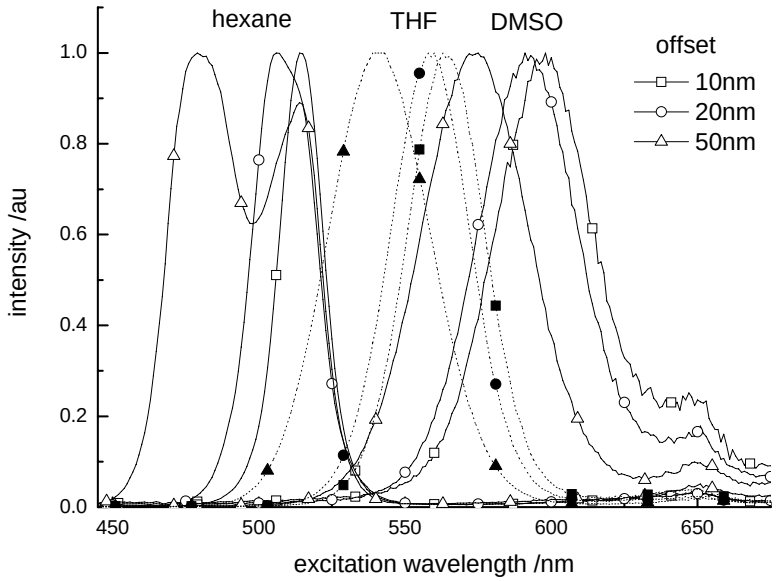

Figure 4.5. Effect of wavelength offset (10 nm squares, 20 nm circles, 50 nm triangles) on synchronous scan spectrum of Nile red in a solvent of low (hexane), moderate (THF – dotted lines) and high (DMSO) dielectric constant. The spectra are shown normalised.

A compromise offset of 20 nm was chosen for a larger study as it indicates whether the spectra possess any vibrational structure, while producing an easily identifiable peak. Figure 4.6 shows the spectra of Nile red in various solvents and figure 4.7 is a plot of the respective peak wavelength against the solvent dielectric constant. The observed trend is in accordance with studies using the Nile red fluorescence emission [62,63]. Therefore, in adopting SFS of Nile red with the 20 nm offset, it is possible to obtain an "easy to use local polarity sensor". Figure 4.7 clearly shows a relationship between the peak position of the synchronous scan spectrum and the dielectric constant of the solvent used. As expected, the behaviour in alcohols (shown by open symbols) is different [53] and a red shift is observed for this class of solvents in comparison to the others of similar dielectric constant. It is notable that using this technique, small changes in relatively low values of dielectric constant produce a relatively large change in spectral position. However, it should be noted that a constant wavelength offset is used, as the apparatus does not allow the use of a constant energy offset set up. At higher values of dielectric constant (greater than 10) smaller peak shifts are observed. In summary, these data provide an expedient means by which to detect changes in dielectric constant and to assess the contribution of hydrogen bonding in the measured spectral shifts, over a range of polarities pertinent to the present system.

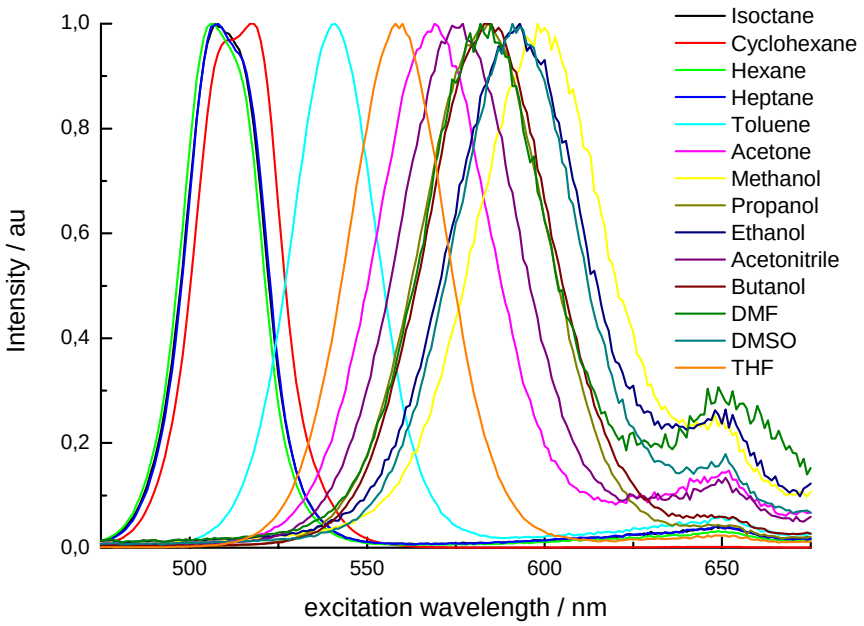

Figure 4.6. SFS of Nile red in various solvents with a 20 nm offset. Spectra shown normalised.

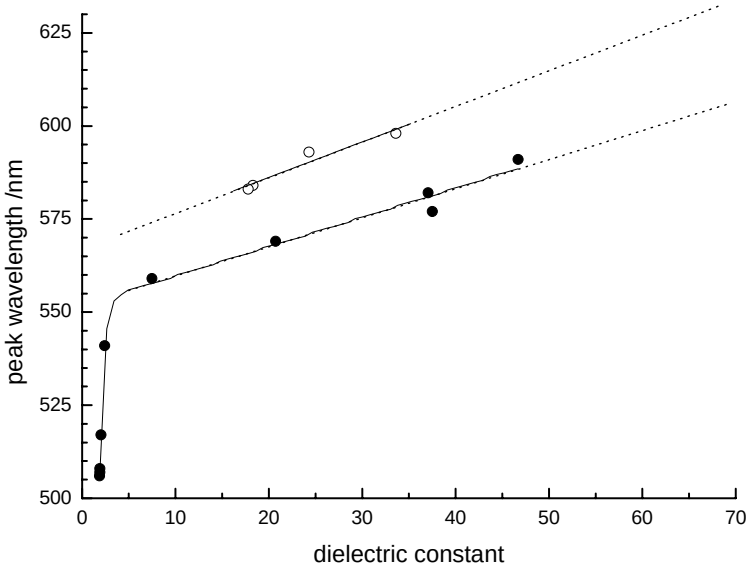

Figure 4.7. Peak wavelength obtained from the synchronous scan spectra of Nile red in various solvents of differing dielectric constants. The data for alcohols are shown by open symbols. Lines are for guidance (solid lines fitted to data, dotted lines show trends only).

In summary, these results show that SFS applied to Nile red solvatochromism is a promising strategy to study changes in local polarity, when examining sol-gel derived media, as will be shown later.

4.4. Fluorescein, FITC and Alexa Fluor 488

Fluorescein is the most widely used green fluorescent dye. This is because of its large molar absorptivity at the wavelength of the commonly used Argon ion laser (488 nm spectral line) and its high fluorescence quantum yield. Fluorescein is commercially available in many derivatives, such as fluorescein isothyocyanate (FITC). It is also susceptible to photobleaching which makes it a good probe for carrying out fluorescence recovery after photobleaching (FRAP) measurements. Alexa Fluor 488 is a similar probe in its fluorescence properties and it is also efficiently excited by the 488 laser line of the

Argon ion laser. It is made by the sulfonation of dyes like rhodamine or fluorescein to become charged and hydrophilic. It also has a high quantum yield when coupled to proteins [29-32]. The structure of fluorescein, FITC and Alexa Fluor 488 can be seen in figure 4.8.

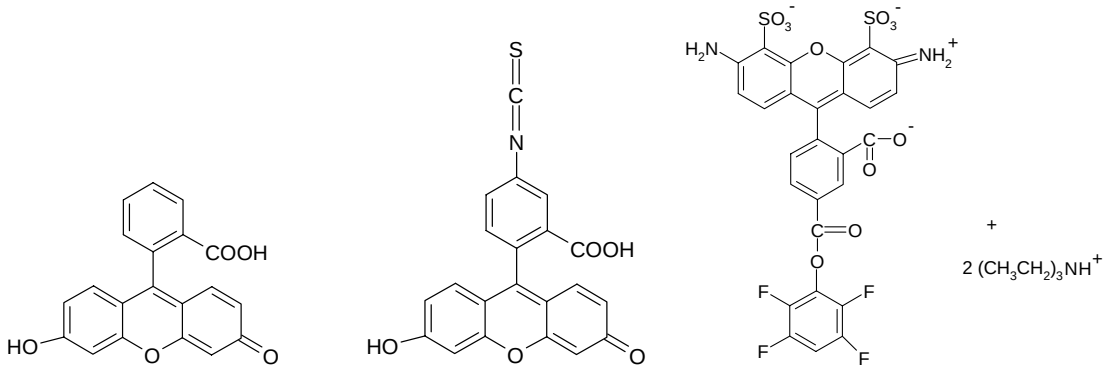

Figure 4.8. The fluorescent probes (from left to the right) fluorescein, FITC and Alexa Fluor 488.

4.5. References

[1] Parson, W. W. *Modern Optical Spectroscopy*; Springer: Heidelberg, 2007.

[2] Szmacinski, H. L., J. R. Lifetime-based Sensing. In *Topics in Fluorescence Spectroscopy*; Lakowicz, J. R., Ed.; Plenum Press: New York, 1994; Vol. Volume 4.

[3] Tsien, R. Y. *The green fluorescent protein* Annual Review of Biochemistry 1998, *67*, 509.

[4] Davis, D. M.; Birch, D. J. S.; Gellert, P. R.; Kittlety, R. S.; Swart, R. M. *A fluorescence study of Nile red bound to Human Serum Albumin in buffer, denaturant, and reverse micelles* Advances in Fluorescence Sensing Technology Ii 1995, *2388*, 302.

[5] Demchenko, A. P. Fluorescence and Dynamics in Proteins. In *Topics in Fluorescence Spectroscopy*; Lakovwicz, J. R., Ed.; Plenum Press: New York, 1992; Vol. Volume 3.

[6] Sarkar, N.; Das, K.; Nath, D. N.; Bhattacharyya, K. *Twisted Charge-Transfer Process of Nile Red in Homogeneous Solution and in Faujasite Zeolite* Langmuir 1994, *10*, 326.

[7] Daban, J. R.; Samso, M.; Bartolome, S. *Use of Nile Red as a Fluorescent-Probe for the Study of the Hydrophobic Properties of Protein Sodium Dodecyl-Sulfate Complexes in Solution* Analytical Biochemistry 1991, *199*, 162.

[8] Sackett, D. L.; Wolff, J. *Nile Red as a Polarity-Sensitive Fluorescent-Probe of Hydrophobic Protein Surfaces* Analytical Biochemistry 1987, *167*, 228.

[9] Strehmel, B.; Rettig, W. *Photophysical properties of fluorescence probes I: dialkylamino stilbazolium dyes* Journal of Biomedical Optics 1996, *1*, 98.

[10] Jozwik, D.; Miller, E.; Wandelt, B.; Wysocki, S. *The styrylpyridine dye for the silane sol-gel transition studies by time-dependent fluorescence* Spectrochimica Acta Part a-Molecular and Biomolecular Spectroscopy 2006, *64*, 1125.

[11] Strehmel, B.; Seifert, H.; Rettig, W. *Photophysical properties of fluorescence probes .2. A model of multiple fluorescence for stilbazolium dyes studied by*

global analysis and quantum chemical calculations Journal of Physical Chemistry B 1997, *101*, 2232.

[12] Benninger, R. K. P.; Hofmann, O.; McGinty, J.; Requejo-Isidro, J.; Munro, I.; Neil, M. A. A.; deMello, A. J.; French, P. M. W. *Time-resolved fluorescence imaging of solvent interactions in microfluidic devices* Optics Express 2005, *13*, 6275.

[13] Khan, F.; Gnudi, L.; Pickup, J. C. *Fluorescence-based sensing of glucose using engineered glucose/galactose-binding protein: A comparison of fluorescence resonance energy transfer and environmentally sensitive dye labelling strategies* Biochemical and Biophysical Research Communications 2008, *365*, 102.

[14] Adami, R.; Cintio, O.; Trombetta, G.; Choquet, D.; Grazi, E. *On the stiffness of the natural actin filament decorated with alexa fluor tropomyosin* Biophysical Chemistry 2003, *104*, 469.

[15] Lakowicz, J. R.; Malicka, J.; Huang, J.; Gryczynski, Z.; Gryczynski, I. *Ultrabright fluorescein-labeled antibodies near silver metallic surfaces* Biopolymers 2004, *74*, 467.

[16] Li, D. H.; Zhu, Q. Z.; Ye, D.; Fang, Y.; Xu, J. G. *A rapid method for the determination of molar ratio of fluorophore to protein by fluorescence anisotropy detection* Analytica Chimica Acta 1999, *389*, 85.

[17] Levi, V.; Flecha, F. L. G. *Reversible fast-dimerization of bovine serum albumin detected by fluorescence resonance energy transfer* Biochimica Et Biophysica Acta-Proteins and Proteomics 2002, *1599*, 141.

[18] Braeckmans, K.; Remaut, K.; Vandenbroucke, R. E.; Lucas, B.; De Smedt, S. C.; Demeester, J. *Line FRAP with the confocal laser scanning microscope for diffusion measurements in small regions of 3-D samples* Biophysical Journal 2007, *92*, 2172.

[19] Invitrogen *Molecular Probes, The Handbook — A Guide to Fluorescent Probes and Labeling Technologies*, Tenth Edition edition ed.

[20] Reichardt, C. *Solvatochromic Dyes as Solvent Polarity Indicators* Chemical Reviews 1994, *94*, 2319.

[21] Davis, M. M.; Hetzer, H. B. *Titrimetric and Equilibrium Studies Using Indicators Related to Nile Blue A* Analytical Chemistry 1966, *38*, 451.

[22] Zoon, P. D. Fluorescent Probe Molecules with Individual Detection Capability. PhD, University of Amsterdam, 2009.

[23] Rettig, W. Photoinduced Charge Separation Via Twisted Intramolecular Charge-Transfer States. In *Electron Transfer I*, 1994; Vol. 169; pp 253.

[24] Rettig, W. L., R. Fluorescence Probes Based on Twisted Intramolecular Charge Transfer (TICT) States and Other Adiabatic Photoreactions. In *Topics in Fluorescence Spectroscopy*; Lakowicz, J. R., Ed.; Plenum Press: New York, 1994; Vol. Volume 4.

[25] Jonkman, A. M.; vanderMeulen, P.; Zhang, H.; Glasbeek, M. *Subpicosecond solvation relaxation of DASPI in polar liquids* Chemical Physics Letters 1996, *256*, 21.

[26] Kim, J.; Lee, M. *Excited-state photophysics and dynamics of a hemicyanine dye in AOT reverse micelles* Journal of Physical Chemistry A 1999, *103*, 3378.

[27] Haidekker, M. A.; Ling, T. T.; Anglo, M.; Stevens, H. Y.; Frangos, J. A.; Theodorakis, E. A. *New fluorescent probes for the measurement of cell membrane viscosity* Chemistry & Biology 2001, *8*, 123.

[28] Ephardt, H.; Fromherz, P. *Fluorescence and Photoisomerization of an Amphiphilic Aminostilbazolium Dye as Controlled by the Sensitivity of Radiationless Deactivation to Polarity and Viscosity* Journal of Physical Chemistry 1989, *93*, 7717.

[29] Sjoback, R.; Nygren, J.; Kubista, M. *Absorption and Fluorescence Properties of Fluorescein* Spectrochimica Acta Part a-Molecular and Biomolecular Spectroscopy 1995, *51*, L7.

[30] Magde, D.; Wong, R.; Seybold, P. G. *Fluorescence quantum yields and their relation to lifetimes of rhodamine 6G and fluorescein in nine solvents: Improved absolute standards for quantum yields* Photochemistry and Photobiology 2002, *75*, 327.

[31] Panchuk-Voloshina, N.; Haugland, R. P.; Bishop-Stewart, J.; Bhalgat, M. K.; Millard, P. J.; Mao, F.; Leung, W. Y.; Haugland, R. P. *Alexa dyes, a series of new*

fluorescent dyes that yield exceptionally bright, photostable conjugates Journal of Histochemistry & Cytochemistry 1999, *47*, 1179.

[32] Imhof, A.; Megens, M.; Engelberts, J. J.; de Lang, D. T. N.; Sprik, R.; Vos, W. L. *Spectroscopy of fluorescein (FITC) dyed colloidal silica spheres* Journal of Physical Chemistry B 1999, *103*, 1408.

[33] Ramadass, R.; Bereiter-Hahn, J. *Photophysical properties of DASPMI as revealed by spectrally resolved fluorescence decays* Journal of Physical Chemistry B 2007, *111*, 7681.

[34] Yaffe, M. P.; Harata, D.; Verde, F.; Eddison, M.; Toda, T.; Nurse, P. *Microtubules mediate mitochondrial distribution in fission yeast* Proceedings of the National Academy of Sciences of the United States of America 1996, *93*, 11664.

[35] Goss, G. G.; Adamia, S.; Galvez, F. *Peanut lectin binds to a subpopulation of mitochondria-rich cells in the rainbow trout gill epithelium* American Journal of Physiology-Regulatory Integrative and Comparative Physiology 2001, *281*, R1718.

[36] Miller, E.; Wandelt, B.; Wysocki, S.; Jozwik, D.; Mielniczak, A. *The fluorescence studies of the sol-gel transition by styrylpyridine derivative* Biosensors & Bioelectronics 2004, *20*, 1196.

[37] Demas, J. N.; Crosby, G. A. *Measurement of Photoluminescence Quantum Yields - Review* Journal of Physical Chemistry 1971, *75*, 991.

[38] Dashnau, J. L.; Nucci, N. V.; Sharp, K. A.; Vanderkooi, J. M. *Hydrogen bonding and the cryoprotective properties of glycerol/water mixtures* Journal of Physical Chemistry B 2006, *110*, 13670.

[39] *Handbook of Chemistry and Physics*, 57th edition ed.; CRC Press: Boca Raton, FL.

[40] Loutfy, R. O.; Arnold, B. A. *Effect of Viscosity and Temperature on Torsional Relaxation of Molecular Rotors* Journal of Physical Chemistry 1982, *86*, 4205.

[41] Hungerford, G.; Ferreira, J. A. *The effect of the nature of retained solvent on the fluorescence of Nile Red incorporated in sol-gel-derived matrices* Journal of Luminescence 2001, *93*, 155.

[42] Hungerford, G.; Pereira, M. R.; Ferreira, J. A.; Viseu, T. M. R.; Coelho, A. F.; Isabel, M.; Ferreira, C.; Suhling, K. *Probing Si and Ti based sol-gel matrices by fluorescence techniques* Journal of Fluorescence 2002, *12*, 397.

[43] Ruvinov, S. B.; Yang, X. J.; Parris, K. D.; Banik, U.; Ahmed, S. A.; Miles, E. W.; Sackett, D. L. *Ligand-Mediated Changes in the Tryptophan Synthase Indole Tunnel Probed by Nile-Red Fluorescence with Wild-Type, Mutant, and Chemically-Modified Enzymes* Journal of Biological Chemistry 1995, *270*, 6357.

[44] McMillian, M. K.; Grant, E. R.; Zhong, Z.; Parker, J. B.; Li, L.; Zivin, R. A.; Burczynski, M. E.; Johnson, M. D. *Nile Red binding to HepG2 cells: An improved assay for in vitro studies of hepatosteatosis* In Vitro & Molecular Toxicology-a Journal of Basic and Applied Research 2001, *14*, 177.

[45] Hendriks, J.; Gensch, T.; Hviid, L.; van der Horst, M. A.; Hellingwerf, K. J.; van Thor, J. J. *Transient exposure of hydrophobic surface in the photoactive yellow protein monitored with Nile red* Biophysical Journal 2002, *82*, 1632.

[46] Nath, A.; Fernandez, C.; Lampe, J. N.; Atkins, W. M. *Spectral resolution of a second binding site for Nile Red on cytochrome P4503A4* Archives of Biochemistry and Biophysics 2008, *474*, 198.

[47] Lampe, J. N.; Fernandez, C.; Nath, A.; Atkins, W. M. *Nile red is a fluorescent allosteric substrate of cytochrome P450 3A4* Biochemistry 2008, *47*, 509.

[48] Coutinho, P. J. G.; Castanheira, E. M. S.; Rei, M. C.; Oliveira, M. *Nile red and DCM fluorescence Anisotropy studies in C12E7/DPPC mixed systems* Journal of Physical Chemistry B 2002, *106*, 12841.

[49] Dutta, A. K.; Kamada, K.; Ohta, K. *Spectroscopic studies of nile red in organic solvents and polymers* Journal of Photochemistry and Photobiology a-Chemistry 1996, *93*, 57.

[50] Srivatsavoy, V. J. P. *Enhancement of excited state nonradiative deactivation of Nile Red in gamma-cyclodextrin: evidence for multiple inclusion complexes* Journal of Luminescence 1999, *82*, 17.

[51] Tajalli, H.; Gilani, A. G.; Zakerhamidi, M. S.; Tajalli, P. *The photophysical properties of Nile red and Nile blue in ordered anisotropic media* Dyes and Pigments 2008, *78*, 15.

[52] Kawski, A.; Bojarski, P.; Kuklinski, B. *Estimation of ground- and excited-state dipole moments of Nile Red dye from solvatochromic effect on absorption and fluorescence spectra* Chemical Physics Letters 2008, *463*, 410.

[53] Cser, A.; Nagy, K.; Biczok, L. *Fluorescence lifetime of Nile Red as a probe for the hydrogen bonding strength with its microenvironment* Chemical Physics Letters 2002, *360*, 473.

[54] Dutt, G. B.; Doraiswamy, S.; Periasamy, N.; Venkataraman, B. *Rotational Reorientation Dynamics of Polar Dye Molecular Probes by Picosecond Laser Spectroscopic Technique* Journal of Chemical Physics 1990, *93*, 8498.

[55] Golini, C. M.; Williams, B. W.; Foresman, J. B. *Further solvatochromic, thermochromic, and theoretical studies on Nile Red* Journal of Fluorescence 1998, *8*, 395.

[56] Oliveira, M.; Hungerford, G.; Miguel, M. D.; Burrows, H. D. *Solvatochromic fluorescent probes in bicontinuous microemulsions* Journal of Molecular Structure 2001, *563*, 443.

[57] Greenspan, P.; Fowler, S. D. *Spectrofluorometric Studies of the Lipid Probe, Nile Red* Journal of Lipid Research 1985, *26*, 781.

[58] Brown, M. B.; Edmonds, T. E.; Miller, J. N.; Riley, D. P.; Seare, N. J. *Novel Instrumentation and Biomedical Applications of Very near-Infrared Fluorescence* Analyst 1993, *118*, 407.

[59] Hungerford, G.; Rei, A.; Ferreira, M. I. C. *Use of fluorescence to monitor the incorporation of horseradish peroxidase into a sol-gel derived medium* Biophysical Chemistry 2006, *120*, 81.

[60] Hungerford, G.; Rei, A.; Ferreira, M. I. C. *Studies on the interaction of Nile red with horseradish peroxidase in solution* FEBS Journal 2005, *272*, 6161.

[61] Viseu, T. M. R.; Hungerford, G.; Coelho, A. F.; Ferreira, M. I. C. *Dye-host interactions for local effects recognition in homogeneous and nanostructured media* Journal of Physical Chemistry B 2003, *107*, 13300.

[62] Deye, J. F.; Berger, T. A.; Anderson, A. G. *Nile Red as a Solvatochromic Dye for Measuring Solvent Strength in Normal Liquids and Mixtures of Normal Liquids with Supercritical and near Critical Fluids* Analytical Chemistry 1990, *62*, 615.

[63] Ghoneim, N. *Photophysics of Nile red in solution - Steady state spectroscopy* Spectrochimica Acta Part a-Molecular and Biomolecular Spectroscopy 2000, *56*, 1003.

Chapter 5

HYBRID MATRIX MANUFACTURE AND CHARACTERISATION

5.1. Introduction

The encapsulation of enzymes in sol-gel-derived media provides a form of immobilization (important for reuse, cost, and environmental factors) while allowing accessibility so that the enzyme can continue to function as a biocatalyst. This procedure can be followed using spectroscopic means and the incorporated protein monitored by either making use of intrinsic protein fluorescence or extrinsic probes. The latter are advantageous as they can be chosen for their selectivity. Previous work has shown that encapsulation within a sol-gel-derived medium can restrict protein mobility, although the doping biomolecules can serve as a template for silicate [1-3]. It is therefore important to gain an understanding of guest-host interactions to enable the encapsulated biomolecule to exhibit its natural form and behaviour.

Time-resolved fluorescence anisotropy [4] and fluorescence recovery after photobleaching (FRAP) [5] are appropriate techniques with which to obtain information concerning the mobility of the encapsulated biomolecule. FRAP probes the translational diffusion, whereas time-resolved fluorescence anisotropy measurements probe rotational diffusion. The discrimination between translational and rotational diffusion has yielded an insight into protein association in viscous media [6] and, the particular combination of FRAP and time-resolved fluorescence anisotropy measurements have

previously been employed, for example, in the study of the rheological properties of cell cytoplasm using green fluorescent protein [7]. However, to our knowledge, FRAP has been scantily applied to the study of sol-gel-derived media. In this chapter experimental results which have helped to clarify the diffusion process within sol-gel derived media will be presented, employing these techniques with selected fluorescent probes and biomolecules.

In order to assess molecular mobility within the host two biomolecules, horseradish peroxidase (HRP) and bovine serum albumin (BSA), both labelled with the fluorescent probe fluorescein isothiocyanate (FITC) which has known photobleaching properties, were encapsulated in sol-gel matrices. The fluorophore itself was used unbound as representative of an enzymatic substrate. The enzyme HRP was also covalently labelled with the highly photostable probe Alexa Fluor 488 (AF) to ascertain, both the distribution of the biomolecules and their rotational diffusion within the matrices. This was accomplished using a confocal microscope [8,9]. The mobility of the biomolecules during the aging process was monitored via fluorescence lifetime, time-resolved anisotropy and fluorescence recovery after photobleaching (FRAP) measurements [10].

Furthermore, adjustment of the original sol-gel recipe was attempted in order to obtain a more efficient system where the encapsulated biomolecule could express its biological function in full. This resulted in the manufacture of organically modified silica matrices (ORMOSILS) and interpenetrating polymer network matrices (IPN), achieved through the incorporation of either the silanes (3-Aminopropyl)triethoxysilane (APTES), trimethoxypropylsilane (TMPS) or (glycidyloxypropyl)triethoxysilane (GPTES), or the polymers poly(ethylene glycol) (PEG20k, PEG300) and Gelrite® (GR). The chosen silanes have hydrophobic functionalities and were added to promote the biocompatibility, as the enhanced hydrophobic character of the matrices should preserve the protein folding [11,12]. The polymers were added because of the proven capability of pore templating which should help to control the flow of materials through the sol-gel composites [3,13]. The effect of these modifiers upon the gelation and aging processes was examined via time-resolved and steady-state fluorescence measurements of the of the probes 4-(4-(dimethylamino)styryl)-*N*-methylpyridiniumiodine (DASPMI) and Nile red. DASPMI was used to elucidate changes in viscosity and Nile red to report on changes in polarity.

5.2. Monitoring gelation and initial aging phases

5.2.1. Materials and methods

The matrices were prepared based on the method presented by Flora and Brennan [14] in the form of a monolith using a standard 10 mm path length plastic cuvette for a mould. The sol was made by mixing 9 ml of tetraethyl orthosilicate (TEOS) (Aldrich) with 3 ml of water containing 0.2 ml of 0.01 M HCl. This mixture was placed in an ultrasonic bath for 1 h before being placed in a freezer (-18 °C) for about a month. The matrices were produced by taking 2 ml of the sol and mixing it with 2 ml of pH 6, 7 or 8 phosphate buffer solutions containing the fluorophore DASPMI. No additional silanes or polymers were used here, so the monoliths produced are purely inorganic.

Fluorescence measurements and data analysis were described in chapter 3.

5.2.2. Results and Discussion

Since the objective of producing these matrices is the incorporation of proteins, buffer solutions with different pH values (pH 6, 7, and 8) were used in order to ascertain the effect of this factor on the gelation process (figure 5.1). The emission spectra of DASPMI, in all three buffer solutions were identical to the spectrum of DASPMI in water, measured under the same instrumental conditions. In fact, all spectra were structureless, highly symmetrical, and centred at 600 nm. The pH values were also restricted to a range so as not to protonate DASPMI, since this can lead to spectral changes [15,16]. Figure 5.1 shows the relative fluorescence intensity of DASPMI as a function of time, during the gelation and initial aging processes. The intensity of the DASPMI emission (under the same conditions) for different glycerol-water mixtures (percent glycerol shown) is indicated as dashed lines. These results show that samples produced using higher pHs are more viscous. Moreover, the relative intensity of the emission suffers a drastic increase during the gelation process, for pH=7 and pH=8 solutions.

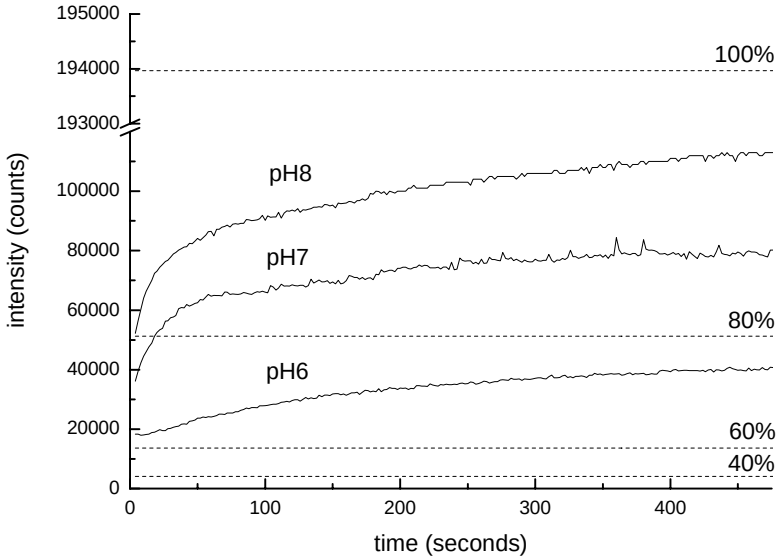

Figure 5.1. Effect of pH on gelation and initial aging of TEOS matrices probed through DASPMI steady state emission. Excitation was at 490nm with emission monitored at 600nm. The intensity of DASPMI emission (under the same conditions) for different glycerol-water mixtures (% glycerol shown) are indicated by the dashed lines.

The observed enhancement of the fluorescence quantum yield is in agreement with the results obtained with water-glycerol mixtures and also with the work of Strehmel and Rettig [17]. These authors have reported a significant increase in fluorescence intensity and emission lifetime of *o*-DASPMI upon an increase in solvent viscosity. More recently, Ramadass and Bereiter-Hahn [18] observed a drastic increase in the emission lifetimes of *o*-DASPMI with an increase of solvent viscosity.

In all subsequent studies pH 7 was adopted in conformity with the requisites of the encapsulated biomolecules.

5.3. Guest-host interactions

5.3.1. Materials and methods

Enzyme Labelling.

For the first set of measurements, horseradish peroxidase (HRP) [CE 1.11.1.7][10] from Sigma, MW = 44,000 [19] was labelled with Alexa Fluor 488 (AF) and then

purified following the provided protocol using a Molecular Probes Alexa Fluor 488 protein labelling kit (A-10235) from Invitrogen S.A. The molecular weight of Alexa Fluor 488 is *ca.*885. Fluorescein (MW 332) was from Sigma-Aldrich.

In a second phase, HRP and bovine serum albumin (BSA) (MW *ca.*67000) were labelled with fluorescein isothiocianate (FITC) (MW = 389.38) and then purified to exclude any uncoupled dye, following the provided protocol and using a Fluoro Tag FITC conjunction kit (Sigma). The labelling ratio was approximately 1:1. The size of FITC is similar to fluorescein which has a radius of 0.54 nm [10], whereas HRP has a radius of 1.5 nm and BSA a radius of 3.5 nm [20,21]. Sol–gel derived media to incorporate the proteins were produced by taking 2 ml of sol (prepared as described in the previous section) and mixing it with 2 ml of buffer solution containing the labelled BSA or HRP or fluorophore. The gels were stored in a refrigerator (at 4 °C) and after approximately 12 h it was possible to remove them from their moulds (standard 10mm pathlength plastic cuvette). They were then rinsed with distilled water and allowed to warm up to room temperature before the measurements.

Measurements and Analysis

Absorption and fluorescence spectra were recorded using the equipment mentioned in chapter 3. Time-resolved fluorescence anisotropy measurements of FITC labelled biomolecules, were made using a 470 nm laser diode excitation source (PLP-10 470, Hamamatsu, optical pulse width 90 ps) pulsed at 20MHz and coupled with a fluorescence lifetime imaging system (Becker & Hickl TCSPC system using a SPC 830 card). The laser beam was passed through a prism to spatially separate the 470 nm from a weak green laser emission around 500 nm and subsequently coupled into the scanhead using a 485 nm dichroic beamsplitter. The fluorescence decays were measured sequentially at polarisations parallel and perpendicular to that of the excitation beam. The fluorescence was collected through a 525 nm interference filter (50 nm bandpass) for 20 s in each polarization in 256 time channels. These measurements were performed at the Physics Department, King's College London.

Time-resolved fluorescence anisotropy measurements of Alexa Fluor 488, were made using equipment mentioned in chapter 3. For the analysis, the "wobble in cone" model was employed and the cone angle θ calculated using equation 3.16, which has been successfully applied in polymer systems [22]. The rotational correlation time was calculated through the Stokes-Einstein relation expressed in equation 3.13. Theoretical

calculations of the volumes were obtained from the qualitative structure activity relationships (QSAR) computation using Hyperchem 7 software on geometrically optimised molecular structures (using a PM3 model for the dyes or AMBER for HRP) [23].

FRAP measurements of fluorescein in sol-gel medium were performed using an inverted confocal microscope (Leica TCS SP2) with a x63 water immersion objective and 488 nm excitation from an argon ion laser. To obtain FRAP curves, five initial intensity images were taken over an area of 288 μm^2, at 2 s intervals. The laser power was then increased and an area of approximately 1002 μm^2 was photobleached. The fluorescence recovery of this area was monitored by reducing the laser power and recording images every 5 s for 200 s (512 x 512 pixels, 400 Hz line scan rate). Regarding the matrices doped with biomolecules (labelled with FITC), confocal microscopy was performed using the confocal microscope with a x20 objective (numerical aperture NA=0.5), with the pinhole set to 1 airy unit (102 μm) yielding an optical section of approximately 2 μm. The excitation source was the same, coupled into the scanhead using a RSP500 dichroic beamsplitter. In order to obtain the FRAP measurements initial intensity images were taken over an area of 750 μm^2 for 1.6 s. The laser power was then increased and a spot approximately 40 μm in diameter was photobleached for 1.6 s. The fluorescence recovery of this area was monitored by reducing the laser power (20% that of the bleach intensity) and recording images every 1.6 s for about 1 minute. In both cases, the recovery curves obtained were corrected by selecting a sample region away from the bleached region of interest and thus obtaining fluorescence intensity *vs.* time curve (control curve) and dividing the raw recovery curve by it. The time taken for the recovery to reach half of the final intensity, $\tau_{1/2}$, was calculated from fitting the recovery to a curve of the form expressed in equation 3.18 using Microcal Origin software. The translational diffusion coefficient D_t was calculated from equation 3.19. All FRAP measurements were performed at the Physics Department, King's College London.

5.3.2. Results and discussion

Dye-Enzyme Interaction in solution

After the coupling reaction and purification, fractions containing the dye-enzyme conjugate (AF-HRP) and the uncoupled dye (AF), were obtained. Both steady state and time-resolved measurements were performed for both AF-HRP and AF in solution prior to incorporation into the sol-gel-derived media. The spectra of the species are shown in figure 5.2.

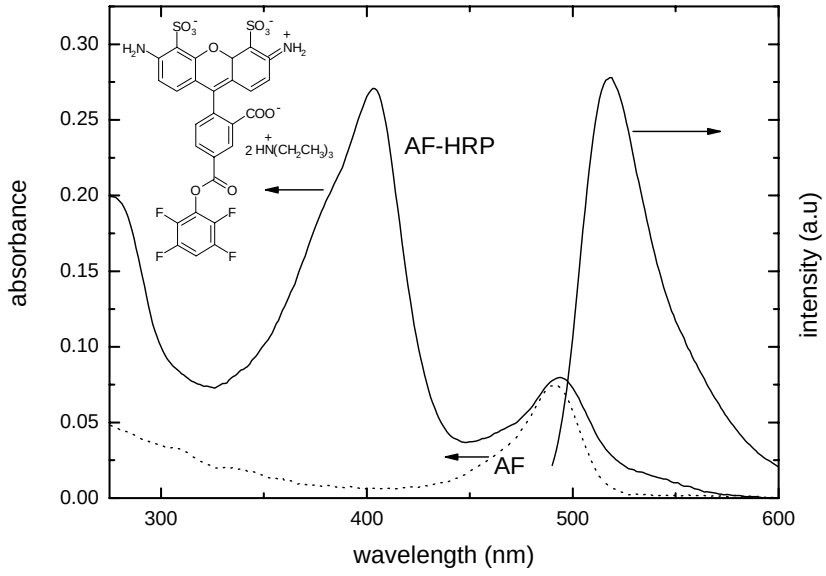

Figure 5.2. Absorption and emission spectra of AF-HRP, along with the absorption spectrum of uncoupled AF (dotted line) for comparison. Inset is the structure of AF.

On coupling, a slight red shift is observed in both the absorption and fluorescence spectra of AF, as shown in table 5.1. The time-resolved data showed a more discernible change going from monoexponential decay to biexponential decay for the AF-HRP conjugate. Here the difference was the emergence of a small contribution of a shorter-lived component. The origin of this component may relate to the covalent linkage and possibly to the local amino acid residues.

measurement		AF	AF-HRP
steady state	absorption Max. (nm)	491	494
	fluorescence max. (nm)	516	518
lifetime	τ_1 (ns)	4.04 ± 0.01	4.11 ± 0.03
	τ_2 (ns)		2.03 ± 0.15
	α_1	1	0.84
	α_2		0.16
	χ^2	1.08	1.05
anisotropy	τ_{r1} (ns)	0.25 ± 0.09	0.51 ± 0.21
	τ_{r2} (ns)		7.87 ± 2.40
	α_1	1	0.63
	α_2		0.37
	r_0	0.260	0.285
	r_∞	0	0.009
	θ		74º
	χ^2	1.02	1.01

Table 5.1. Absorption and fluorescence data for unbound Alexa Fluor (AF) and Alexa Fluor bound to HRP (AF-HRP) in buffer solution.

Another difference was noted in the time-resolved anisotropy data; for uncoupled AF, as expected, a very fast rotational time (0.25 ns), close to the resolution of our equipment, was observed. This is similar to that obtained using equation 3.13 with V calculated from the QSAR properties for AF (assuming a viscosity of 0.89 cP and temperature of 300 K), which returned 0.30 ns. The anisotropy decay obtained for the AF-HRP conjugate required two rotational correlation times to provide an acceptable fit. The shorter one we attribute to the dye rotation, while the longer one reflects the motion of the whole of the enzyme. A similar trend has been previously reported [24]. Our calculation of this rotational time returned a close value of 6.5 ns. As the r_∞ value does not go to zero, this implies a small degree of hindrance (cone angle of 74° according to equation 3.16), which is not surprising as the AF is covalently bound to the enzyme. As the hindrance is small, it is indicative that AF most likely binds to the exterior of the protein. To verify this, a quenching study using potassium iodide (KI) was performed. The effect of the quencher on the steady-state fluorescence is shown in figure 5.3.

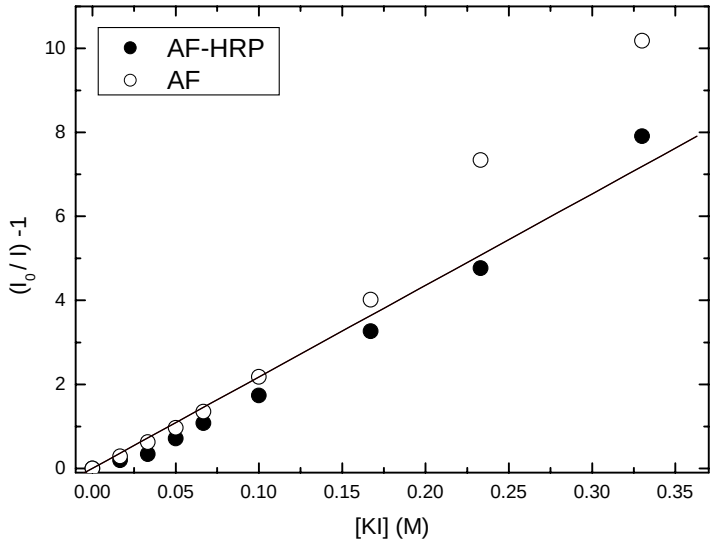

Figure 5.3. Change in steady state fluorescence intensities (I) of AF and AF-HRP in solution on addition of potassium iodide (KI). The line depicts a simple fit to the Stern-Volmer equation for the AF-HRP data.

The plot shows that at lower quencher concentrations there is little difference between the unbound and bound AF. A Stern-Volmer quenching constant of 21.7 M^{-1} was obtained from the slope of the line represented in the figure [25]. At higher concentrations of KI there is an upward trend in the data, which may signify the presence of processes other than a straightforward dynamic quenching mechanism. This is not surprising considering the charged nature of the quencher. However, the similarity of the curves at low quencher concentration supports the of the probe attached to the exterior of the enzyme.

Diffusion within sol-gel derived media

Time-resolved anisotropy measurements were performed on the AF-HRP conjugate encapsulated into a sol-gel matrix over a period of time in which the sample changed from a solid gel to a glassy robust matrix, occupying about 1/8 of the volume of the initial gel. Confocal microscopy showed the distribution of the encapsulated enzyme within the matrix to be uniform. Time-resolved fluorescence anisotropy measurements were made to provide a means by which to monitor the enzyme's rotational mobility. Figure 5.4 illustrates the change in rotational correlation time, $\tau_{r,}$ with aging time.

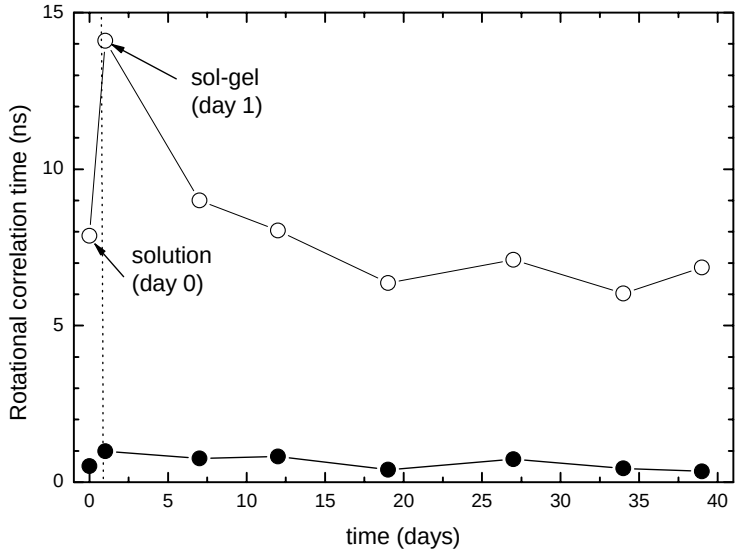

Figure 5.4. Rotational correlation times for AF bound to HRP, both before and after incorporation into a sol-gel derived monolith. The open symbols relate to the rotation of the entire enzyme, while the closed symbols are ascribed to the probe's own rotation.

On incorporation there is an initial increase in the rotational correlation time probably because of a raised viscosity as the matrix gels. After that, as the pore structure starts to form, the value returns close to that of the conjugate in solution. These data indicate that, although the matrix network is contracting, the local environment of the enzyme is comparatively stable, unlike that encountered in another study [1]. It should be noted that a slight decrease in the cone angle was observed, dropping to ca. 53° after 7 days and dropping by another few degrees over the remaining period. This may indicate slight changes in the enzyme conformation, in agreement with previous studies reported by our group [26] or that the enzyme is experiencing a viscosity close to that in solution, but with some mobility restriction imposed by the host. Over the same time period the fluorescence lifetime data exhibited little variation from the corresponding data in solution, thus reinforcing the suitability of this system.

Although the enzyme appears free to rotate within the pore, it is important to ascertain if it is also free to relocate within the matrix and importantly, if it is to be catalytically active, accessible to its substrate. In order to verify this, FRAP measurements using a confocal microscope were performed with fluorescein (Fs) incorporated in the same type of sol-gel-derived monolith. FRAP has previously been used to characterize sol-gel-produced matrices, where dyes were found to diffuse only if

the matrices were hydrated [27]. The results from the FRAP measurements are given in table 5.2.

Time (days)	k (s^{-1})	$\tau_{1/2}$ (s)
2	0.048 ± 0.012	14 ± 4
6	0.015 ±0.002	45 ± 6
8	0.0143 ± 0.0005	49 ± 2
10	0.0067 ± 0.0005	100 ± 7
13	0.0057 ± 0.0006	121 ± 13
15	0.0052 ± 0.0006	132 ± 30
20	0.0036 ± 0.0003	191 ± 17
27	0.0041 ± 0.0004	169 ± 14
35	0.0040 ± 0.0005	174 ± 20

Table 5.2. Recovery rates, k (s^{-1}), and times, $\tau_{1/2}$ (s), obtained using equation 3.18 for the intensity of Fs fluorescence from the FRAP measurements with matrix aging time.

From these measurements the translational diffusion coefficient with aging time was calculated and is depicted in figure 5.5. In terms of diffusion, this is the inverse of what is seen from the rotational information, as shown in figure 5.6.

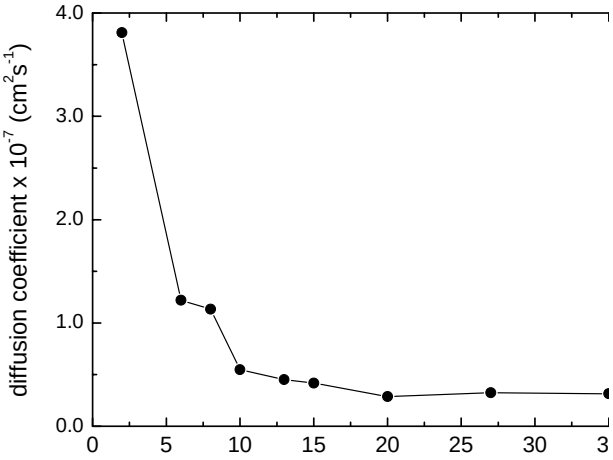

Figure 5.5. Translational diffusion coefficient for Fs in a sol-gel derived monolith with aging time, calculated from the data in table 5.2, according to equation 3.19.

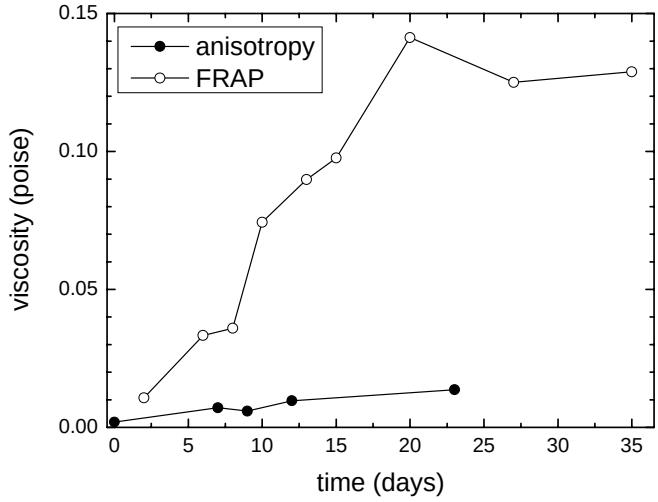

Figure 5.6. Comparison of the sensed viscosity obtained using FRAP measurements of Fs and anisotropy measurements of unbound AF.

An explanation for this is that the rotational diffusion provides information concerning the pore environment, while the translation diffusion gives information relating to interconnections between pores; the enhancement in viscosity sensed by AF means that the network shrinks with time (see figure 5.7). Thus, the two sets of measurements (FRAP and time resolved anisotropy) are complementary in following the changes in matrix morphology.

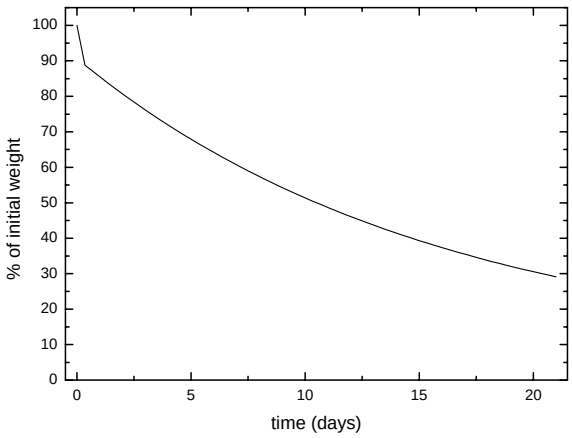

Figure 5.7. Depiction of the percentage change in weight of a sol-gel derived matrix with time, when kept at 4ºC.

It should be emphasised that we are looking at the average behaviour of many Fs molecules. Work at the single molecule level has elucidated that the pore size is important on the diffusion within sol-gel derived monoliths, once two different components relating to mobility were found; one in gels with a pore diameter of about 3 nm, and the other in gels with pores of about 22 nm [28,29]. In comparison to that work,

the diffusion coefficients presented above are several orders of magnitude greater than those found for a silica gel with pores *ca*. 22 nm in diameter and using a larger probe molecule. Nevertheless, the rotational diffusion of the enzyme hints that there is no significant interaction with the pore. Most probably HRP efficiently templates the pore size of its host, hence, the pores inhabited by the biomolecule should be significantly larger than its own dimensions [22].

The photostability of Alexa Fluor 488 limits its usefulness in FRAP measurements, where a fluorescein derivative, fluorescein isothiocyanate (FITC), proved advantageous. Three sol–gel derived hosts were monitored with aging time by means of FRAP and fluorescence anisotropy measurements with the aim of examining lateral and rotational diffusional of macromolecules, respectively. The samples were produced as follows: one monolith containing fluorescein isothiocyanate (FITC), a second one doped with bovine serum albumine (BSA) labelled with FITC (FITC-BSA) and a third one doped with HRP labelled with FITC (FITC-HRP). The FRAP measurements are given in figure 5.8. Typical confocal images for the prebleach, bleach and one minute after bleaching of each sample are also displayed, as are the relative sizes of the dopant molecules.

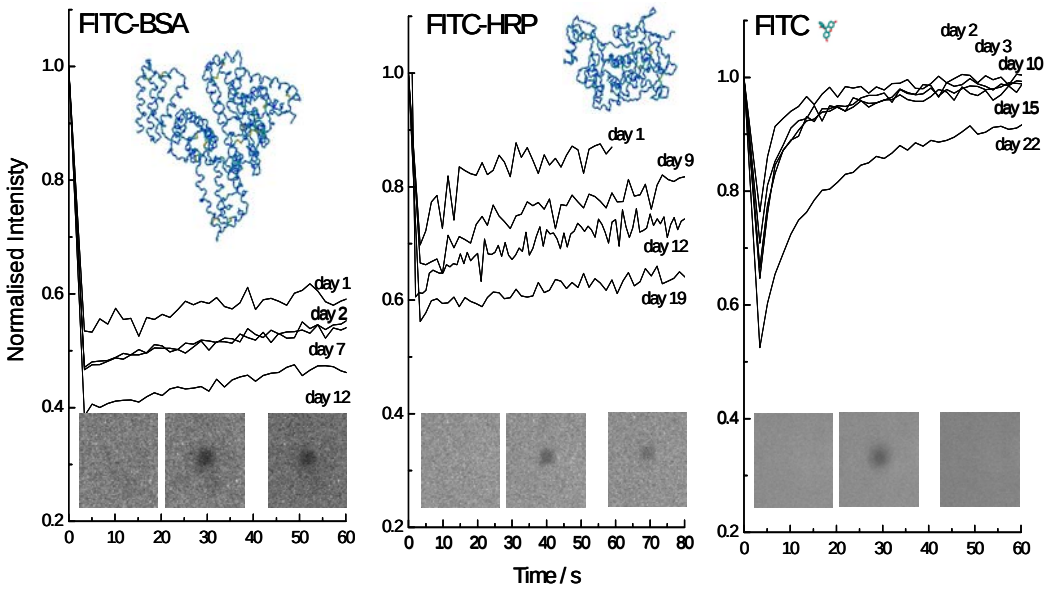

Figure 5.8. FRAP curves for the three samples with aging time. Also given are representative confocal microscope sections from images for prebleach, straight after bleaching and 60 seconds after bleaching. These are given for day 12 for BSA and HRP, with the FITC alone images shown from day 10. The diameter of the bleached area is ca. 40µm throughout. The relative sizes of the molecules incorporated within the sol-gel derived host are also shown (for clarity only the backbone structure is given).

Regarding FITC-BSA sample, negligible recovery was observed after bleaching, indicating that the pore interconnections were already smaller than the dimensions of the protein, one day after encapsulation. Subsequent measurements confirmed that rotational motion had, in fact, ceased and that the pore size was at least comparable to that of BSA. The corresponding time-resolved fluorescence anisotropy measurements showed that the protein was barely able to rotate (figure 5.9).

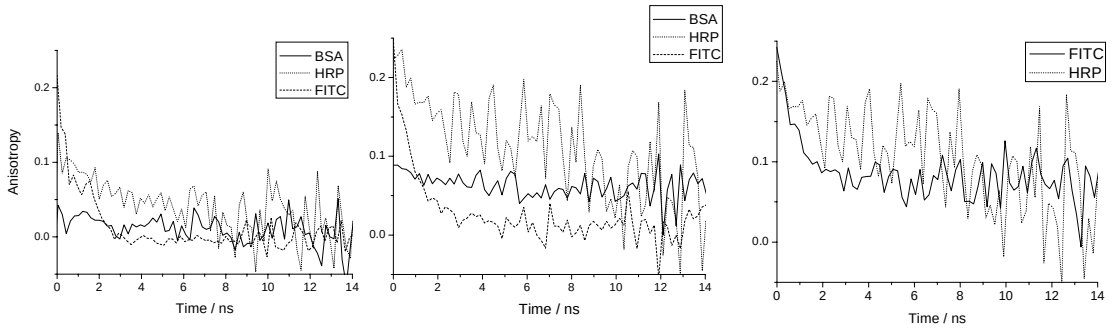

Figure 5.9. Anisotropy decays for day 2, 9 and 12 days respectively, after making sol-gel for all 3 samples.

In the case of FITC-HRP sample, the amount of photobleaching observed was comparatively less and a partial recovery in the fluorescence was seen. Ten days later the recovery was no longer observed, indicating that the interconnections between the pores were probably with a size such as to limit the lateral diffusion of this enzyme. No noticeable lateral diffusion was observed after 12 days. Time-resolved fluorescence anisotropy results show significant rotational freedom which decreases with time (figure 5.9). This is in good agreement with prior measurements using Alexa Fluor 488 labelled HRP, which showed an average rotation correlation time of 3.2 ns after 12 days, with only a minor degree of hindering over a period of over five weeks in the same type of matrix. Thus, we reinforce the idea that, although the connections between the pores may somewhat hinder lateral diffusion, the matrix does appear to template about the enzyme and the pore size must be greater than that of the HRP molecule, although smaller than that of BSA.

Finally, the diffusion of FITC between the pores is relatively free, as can be seen in figure 5.8. The full recovery back to 1 indicates that initially there is no significant immobile fraction, *i.e.* it appears to be no adhesion of FITC to the pore walls (the results using fluorescein show a similar behaviour). However, an immobile FITC fraction appears with time, as indicated by the lack of a full recovery from around day 15. The

corresponding time-resolved fluorescence anisotropy, which initially show a free rotation, begin to exhibit $r_\infty > 0$, indicative of a hindered rotation (figure 5.9). It is worth to mention here, that time-resolved anisotropy data of unbound AF (figure 5.6) are consistent with this observation which hints to an increase of the pore viscosity with time.

In summary, the adopted methodology of combining FRAP and time-resolved fluorescence anisotropy measurements allowed the determination of diffusion properties of biomolecules entrapped within sol-gel derived hosts. Although the matrix can template around an incorporated biomolecule, there is a size limit to this. Only small molecules display high mobility and are relatively free to circulate within the matrix, while a molecule the size of HRP will be retained within the internal pore structure, as summarised in figure 5.10. These are important considerations regarding the use of these materials for biosensor applications.

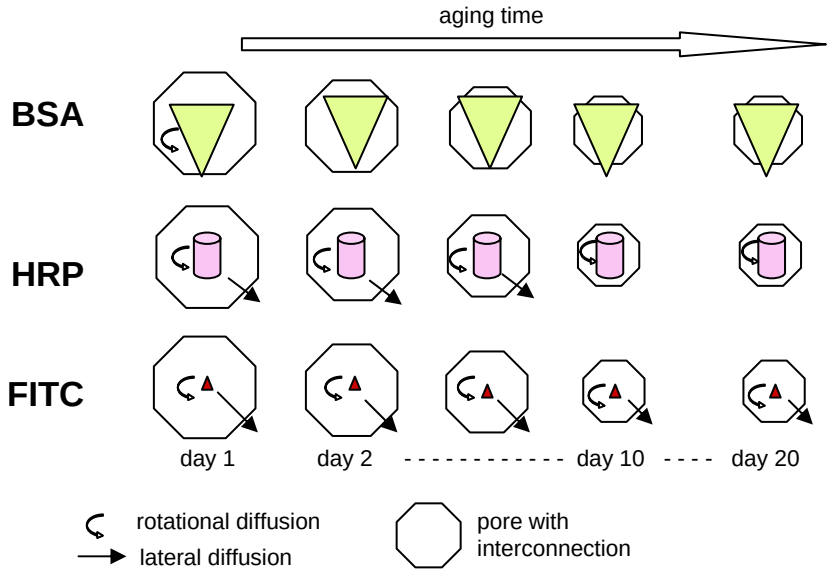

Figure 5.10. Schematic showing evolution of the molecules' behaviour and confinement of FITC labelled HRP and BSA, as well as uncoupled FITC within the sol-gel matrix as it ages.

5.4. Modified matrices (ORMOSIL and IPN monoliths)

5.4.1. Materials and methods

The silanes (3-Aminopropyl)triethoxysilane (APTES), trimethoxypropylsilane (TMPS) and the polymers poly(ethylene glycol) (PEG 20*k*, PEG 300) and Gelrite® (GR), a commercial form of gellan gum, were acquired from Aldrich. (3-Glycidyloxypropyl) triethoxysilane (GPTES) was from Fluka. All chemicals were used as received. The structure of these silanes, and polymers used to manufacture organically modified matrices (ORMOSIL) and interpenetrating polymer network matrices (IPN) are shown in figure 5.11. The structure of TEOS is also shown for completeness.

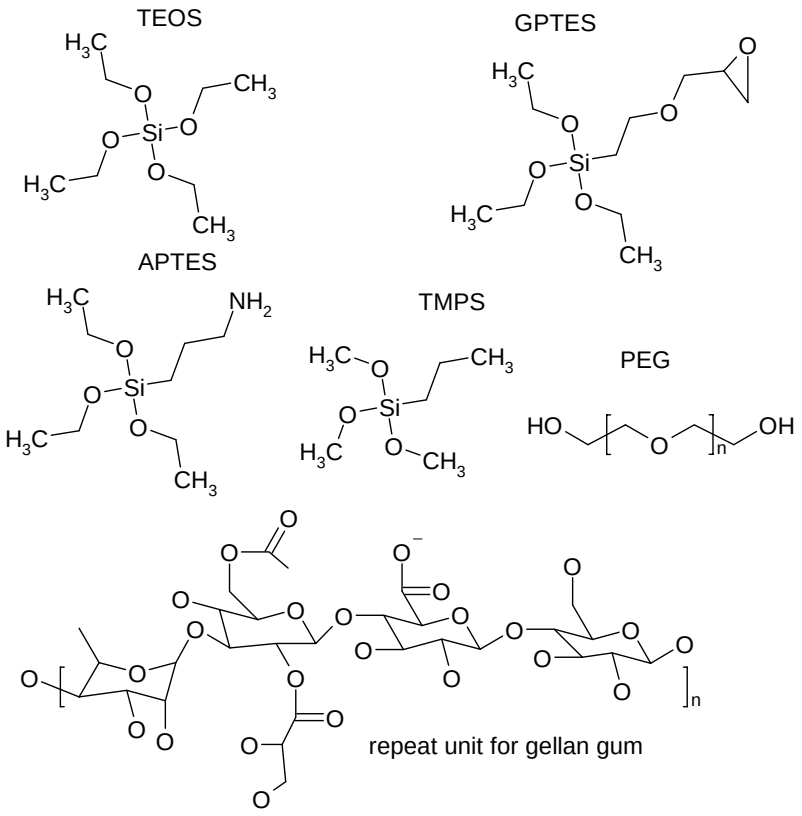

Figure 5.11. Chemical structure of the additives employed with tetraethyl ortosilicate (TEOS) based sol-gel matrices. (TMPS) trimethoxypropylsilane, (APTES) (3-aminopropyl)-triethoxysilane, (GPTES) glycidyloxypropyl triethoxysilane, (poly) ethylene glycol (PEG) and Gelrite® (gellan gum).

The samples were manufactured as previously stated, using 10 mm polystyrene cuvettes (*ca*. 4.5 ml) by taking 2 ml of sol and adding the modifier, DASPMI (in water) or Nile red (in DMSO), and phosphate buffer (pH7, 2 ml). The quantity of each additive was the highest possible to preserve good optical quality, that is, 3.75% (v/v) TMPS or GTPES, 0.5% (v/v) APTES, 2.5% (v/v) PEG300, 0.04 wt % PEG20*k*, and 0.02 wt % GR.

Fluorescence measurements (steady-state and time-resolved) and data analysis were described in chapter 3.

The X-ray diffraction (XRD) measurements were performed on a Bruker D8 Discover diffractometer working with $CuK\alpha_{1,2}$ radiation and equipped with a Goebel mirror. The diffraction patterns were collected by detector scan in the range 1-40º 2θ at angle of incidence 0.5º, using step size of 0.04º and time per step of 1s. The measurements were performed on one surface of each of the monoliths prepared as described above.

The textural characterisation of the matrices was done in an analyser from Quantachrome Instruments, Nova 4200, on the base of nitrogen adsorption-desorption isotherms, at -196 ºC, following the well known BET technique. The samples were previously degassed at 160 ºC. These measurements were performed at the Laboratory of Catalysis and Materials at Faculdade de Engenharia da Universidade do Porto, under the supervision of Professor José Luís Figueiredo.

5.4.2. Results and Discussion

5.4.2.1. Gelation and initial aging

The study on the gelation and initial aging phases was completed by examining the emission of the dye DASPMI in the modified matrices during these processes (figure 5.12).

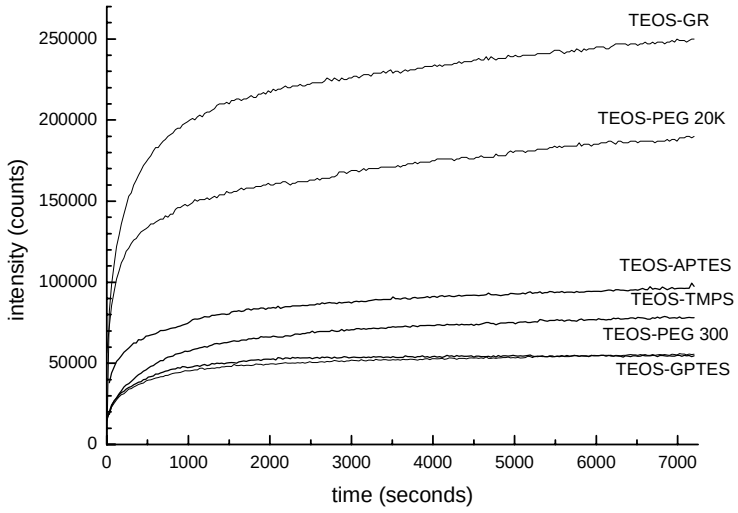

Figure 5.12. Intensity of DASPMI steady state emission during the gelation and initial aging of modified samples. Excitation was at 490 nm with emission maxima at 600 nm.

This figure shows that the reaction is more extensive when GR or PEG20*k* is present. GR is a polysaccharide with self-gelling properties composed of glucose, glucoronic acid, and rhamnose moieties [30]. It is probable that, when mixed with the sol it favours the silica polymerization along its branches, thus explaining the highest intensity of DASPMI emission in its presence. The length of the polymer chain is apparently important, since figure 5.12 shows that PEG300 has considerably less effect than PEG20*k* in the building of the matrix network. The results are in agreement with the work of Shchipunov *et al.* confirming that polysaccharides and polymers enhance the polymerization of the SiO_2 network by creation of hydrogen bonds between hydroxyl groups of the macromolecules and the silanol products of TEOS hydrolysis [13,31]. The remaining modifiers (APTES, TMPS, and GPTES) do not significantly alter the gelation and initial aging rates, as can be seen by comparison between the curves in figure 5.12 and the gelation curve at pH 7 in figure 5.1.

5.4.2.2. Long-term monitoring of the aging process

In order to characterise the *sol-gel* derived media both DASPMI and Nile red were employed. DASPMI was used to elucidate changes in viscosity by monitoring changes in its fluorescence emission and lifetime. Nile red should, because of its hydrophobic nature, locate at the interface between the bulk oxide material and the internal pore structure. Therefore it can report on changes in polarity in this region.

a) Steady state monitoring: DASPMI emission

The aging process was monitored during a period of over 40 days, in which the steady-state emission of DASPMI was measured periodically. Figure 5.13 shows the changes observed in the fluorescence intensity of the dye with aging time. Difference spectra were calculated using Microcal Origin 7 software by normalising the emission spectra at the maximum and subtracting from a reference spectrum taken just after gelation (day 0). As the aging progresses, a solvatochromic shift is reported by about 5% of the excited dye molecules in the TEOS-TMPS and TEOS-APTES samples, 10% in TEOS-GPTES, TEOS-PEG20*k*, and TEOS-GR samples, and 20% in TEOS-PEG300 samples. This blue shift indicates that a significant fraction (5-20%) of the dye molecules probes a slight decrease in the polarity of the host medium, favoured by aging. This behaviour is not surprising since the chemical composition of the liquid phase changes throughout the aging process. It is expected that not only water (the main component), but also some vestigial ethanol may remain in the liquid phase retained in the pores, formed as a by-product of the polymerization of the silica network. Moreover, the modifiers, a few remaining TEOS monomers, and other possible oligomers add to the complexity of the liquid-phase chemical composition.

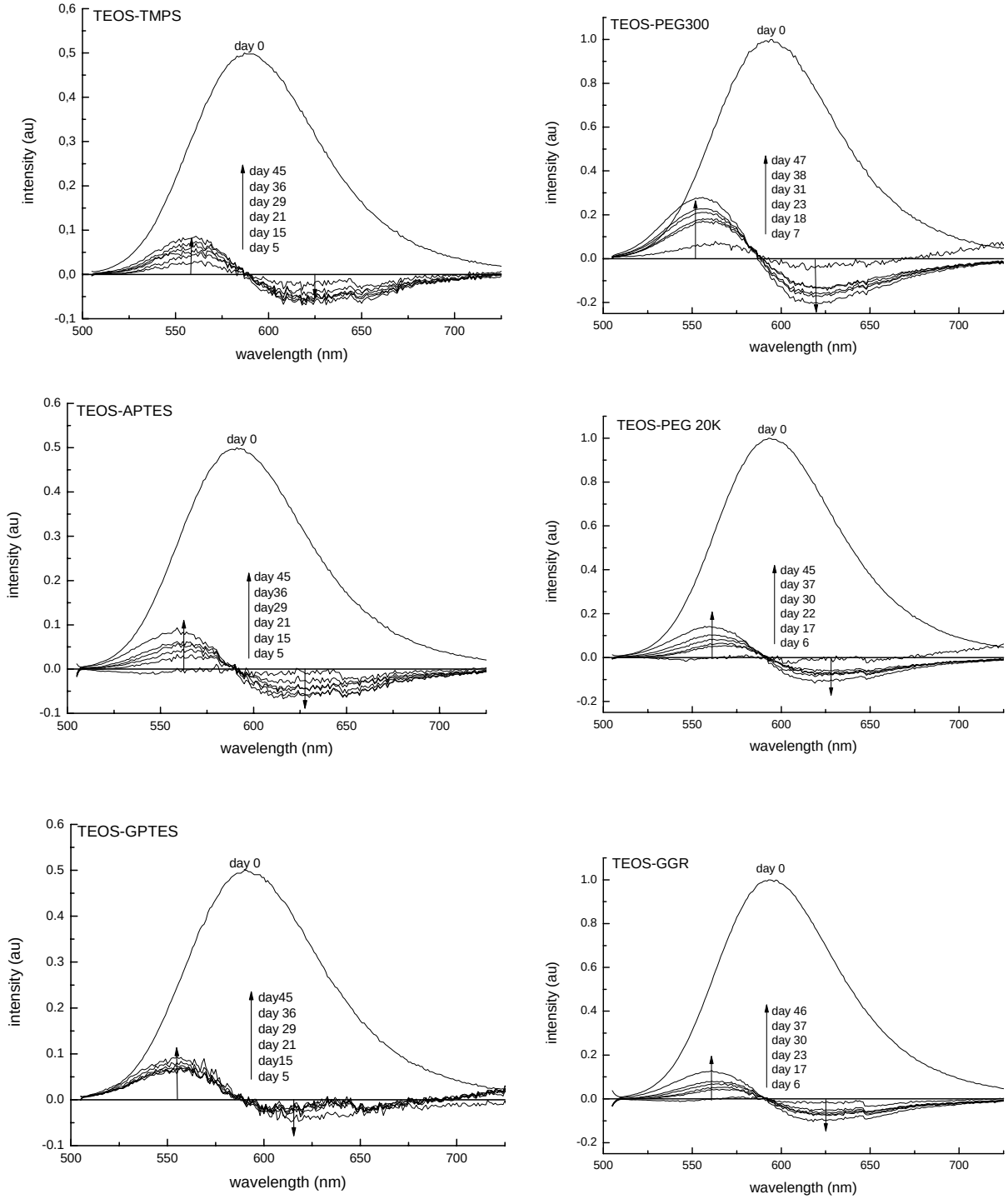

Figure 5.13. DASPMI steady state emission at day 0 and difference spectra with aging time. Spectra were obtained by normalizing to unity at 600 nm and subtracting the spectrum for day 0. This spectrum is also shown reduced to half height, for clarity, in the case of the samples TEOS-TMPS, TEOS-APTES and TEOS-GPTES.

b) Steady state monitoring: Nile red SFS

The changes in local polarity were monitored over the same time period by making use of Nile red combined with synchronous scan fluorescence spectroscopy (SFS). Figure 5.14 shows the Nile red SFS spectra just after gelation of the host media. The spectra are shown normalised at each maximum, to emphasise environmental changes, expressed by band position. Such methodology was adopted to overcome slight increases in the concentration of the entrapped species caused by matrix shrinkage over time. It is clear that Nile red is probing a very polar medium (with an "equivalent" dielectric constant in the order of 60, according to figure 4.7), most probably influenced by the high dielectric constant of the aqueous buffer solution, as expected at this early stage of the aging process, when the matrix network is still embedded in the initial solvent medium.

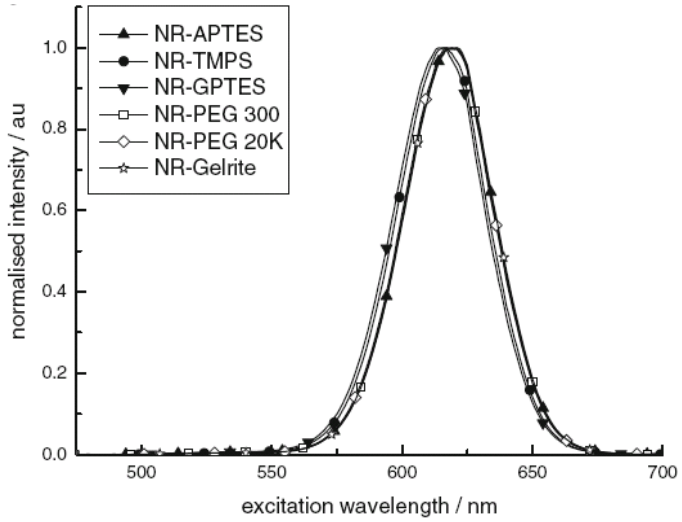

Figure 5.14. Normalised Nile red SFS data obtained with an offset of 20 nm, in the different host media.

Nile red SFS for each of the hosts was measured at regular intervals over an aging period of more than forty days. Figure 5.15 illustrates the shifts in the Nile red maximum wavelength for each matrix as the aging progresses. In all cases, with the exception of the TMPS containing host, a red shift in the Nile red SFS occurs. It is interesting to notice, that the change in the peak wavelength is consistent with matrix stabilisation occurring after twenty days. Using the Nile red SFS guide (figure 4.7) it is possible to make an estimate that Nile red is in a relatively polar hydrogen bond influenced environment (value 60-70), which is unsurprising if it is at the bulk oxide pore interface within the sol-gel derived media.

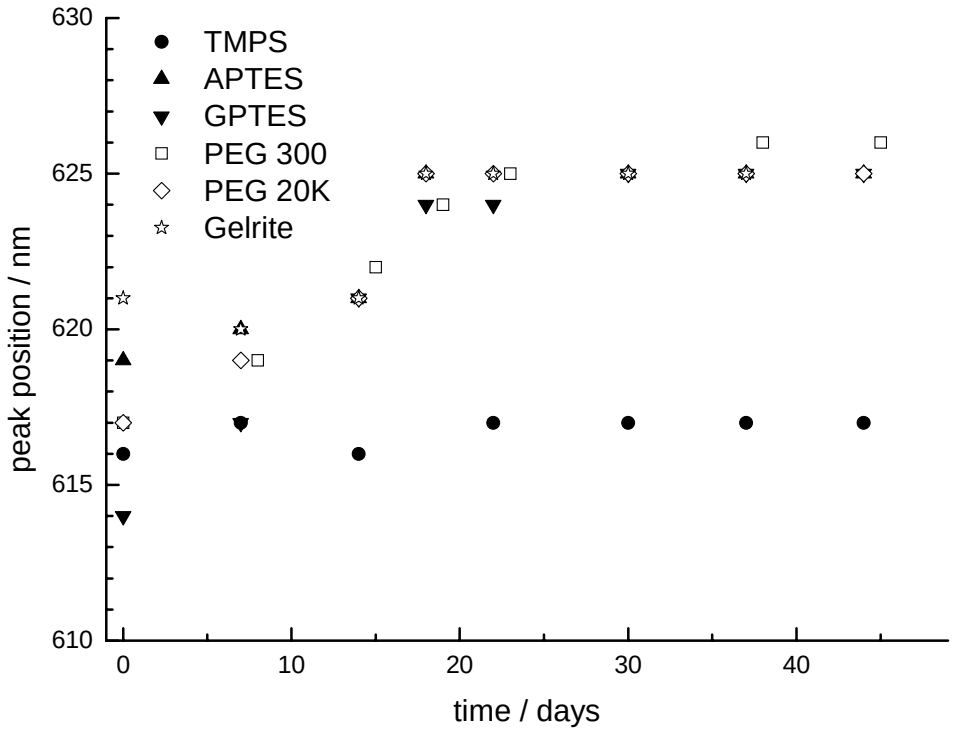

Figure 5.15. Position of the emission peak with aging time, for the different modified matrices. From Nile red synchronous scan data (20nm offset).

c) Time-resolved measurements: DASPMI lifetime

The aging process was further examined through extensive fluorescence lifetime measurements, as shown in tables 5.3 – 5.9 The following general trends were found: (a) all decays can be adjusted to a three-component kinetics, (b) significant scatter in the values of the lifetimes can be found up to the 20th day, (c) the aging process appears to be more stable after the 20th day, (d) the longer lived component, a minor contribution in the early days, becomes more prominent as the aging process develops, and (e) all recovered lifetimes (τ_1, τ_2, and τ_3) increase with aging time. Moreover, it is generally observed that the relative contributions of τ_2 and τ_3 components become more important as the aging progresses.

day	τ_1 (ns)	τ_2 (ns)	τ_3 (ns)	α_1	α_2	α_3	χ^2
0	0.09 ± 0.06	0.96 ± 0.10	2.55 ± 0.03	0.78	0.17	0.05	1.09
1	0.10 ± 0.06	1.14 ± 0.09	2.79 ± 0.02	0.74	0.14	0.12	1.13
2	0.10 ± 0.09	1.13 ± 0.09	2.81 ± 0.02	0.69	0.15	0.15	1.05
3	0.19 ± 0.10	1.28 ± 0.11	2.90 ± 0.02	0.51	0.26	0.23	1.02
4	0.31 ± 0.20	1.43 ± 0.17	2.93 ± 0.03	0.41	0.28	0.32	1.10
6	0.19 ± 0.16	1.38 ± 0.15	2.94 ± 0.03	0.50	0.22	0.28	1.09
8	0.51 ± 0.23	1.80 ± 0.38	3.02 ± 0.05	0.35	0.27	0.38	1.08
11	0.56 ± 0.24	1.85 ± 0.31	3.08 ± 0.04	0.28	0.31	0.41	0.97
14	0.77 ± 0.46	1.89 ± 0.54	3.08 ± 0.05	0.24	0.29	0.47	1.08
17	0.41 ± 0.15	1.87 ± 0.36	3.14 ± 0.04	0.34	0.29	0.38	0.91
24	0.34 ± 0.24	1.73 ± 0.43	3.10 ± 0.03	0.22	0.26	0.52	1.06
29	0.64 ± 0.54	1.97 ± 0.12	3.16 ± 0.17	0.15	0.30	0.55	1.08
32	0.46 ± 0.14	1.99 ± 0.60	3.14 ± 0.05	0.22	0.26	0.52	1.09

Table 5.3. Time-resolved fluorescence data for DASPMI in the TEOS matrix with pH7 buffer, through aging.

day	τ_1 (ns)	τ_2 (ns)	τ_3 (ns)	α_1	α_2	α_3	χ^2
0	0.21 ± 0.08	1.23 ± 0.08	1.23 ± 0.03	0.65	0.23	0.12	1.03
1	0.19 ± 0.09	1.14 ± 0.08	2.66 ± 0.03	0.61	0.23	0.15	1.10
2	0.25 ± 0.10	1.32 ± 0.10	2.77 ± 0.03	0.58	0.26	0.16	1.06
5	0.15 ± 0.09	1.25 ± 0.09	2.75 ± 0.03	0.67	0.19	0.14	1.06
6	0.45 ± 0.18	1.45 ± 0.19	2.80 ± 0.04	0.43	0.31	0.26	1.09
7	0.30 ± 0.13	1.35 ± 0.11	2.79 ± 0.03	0.49	0.29	0.22	1.03
8	0.31 ± 0.15	1.35 ± 0.12	2.80 ± 0.03	0.49	0.28	0.23	1.06
9	0.14 ± 0.11	1.32 ± 0.09	2.80 ± 0.02	0.58	0.23	0.19	1.04
12	0.14 ± 0.11	1.32 ± 0.11	2.80 ± 0.03	0.67	0.18	0.15	1.08
13	0.24 ± 0.18	1.31 ± 0.11	2.82 ± 0.03	0.49	0.27	0.24	1.04
16	0.22 ± 0.13	1.34 ± 0.11	2.85 ± 0.03	0.5	0.27	0.23	1.13
21	0.59 ± 0.16	1.87 ± 0.37	2.97 ± 0.07	0.41	0.33	0.26	1.07
29	0.52 ± 0.18	1.61 ± 0.22	2.90 ± 0.04	0.38	0.3	0.32	1.09
35	0.49 ± 0.05	1.65 ± 0.06	2.96 ± 0.01	0.33	0.36	0.31	1.05
45	0.50 ± 0.17	1.66 ± 0.20	2.94 ± 0.04	0.36	0.32	0.32	1.07

Table 5.4. Time-resolved fluorescence data for DASPMI in TEOS-TMPS matrix, through aging.

day	τ_1 (ns)	τ_2 (ns)	τ_3 (ns)	α_1	α_2	α_3	χ^2
0	0.19 ± 0.05	1.34 ± 0.12	2.88 ± 0.03	0.62	0.21	0.16	1.06
1	0.23 ± 0.07	1.40 ± 0.20	2.91 ± 0.03	0.54	0.22	0.24	1.05
2	0.13 ± 0.09	1.31 ± 0.11	2.92 ± 0.02	0.64	0.17	0.19	1.10
5	0.50 ± 0.36	1.60 ± 0.30	3.00 ± 0.04	0.25	0.31	0.44	1.10
6	0.49 ± 0.25	1.76 ± 0.36	3.02 ± 0.04	0.29	0.28	0.43	1.08
7	0.05 ± 0.07	1.43 ± 0.15	2.98 ± 0.02	0.86	0.05	0.08	1.19
8	0.21 ± 0.18	1.39 ± 0.19	2.94 ± 0.02	0.45	0.19	0.36	1.09
9	0.51 ± 0.14	2.27 ± 0.27	3.30 ± 0.08	0.35	0.41	0.24	1.04
12	0.16 ± 0.27	1.62 ± 0.22	3.03 ± 0.03	0.57	0.16	0.28	1.10
13	0.58 ± 0.14	2.33 ± 0.30	3.31 ± 0.08	0.32	0.42	0.27	1.00
16	0.12 ± 0.10	1.50 ± 0.18	3.04 ± 0.02	0.55	0.15	0.29	1.08
21	0.71 ± 0.28	1.43 ± 0.14	3.00 ± 0.04	0.17	0.2	0.63	1.06
29	0.55 ± 0.28	2.00 ± 0.35	3.16 ± 0.04	0.21	0.3	0.49	1.07
35	0.71 ± 0.27	2.32 ± 0.47	3.25 ± 0.07	0.2	0.4	0.4	1.10
45	0.70 ± 0.42	2.07 ± 0.54	3.14 ± 0.05	0.19	0.28	0.53	1.06

Table 5.5. Time-resolved fluorescence data for DASPMI in the TEOS-APTES matrix, through aging.

day	τ_1 (ns)	τ_2 (ns)	τ_3 (ns)	α_1	α_2	α_3	χ^2
0	0.25 ± 0.05	1.35 ± 0.23	2.81 ± 0.03	0.23	0.6	0.17	1.06
1	0.23 ± 0.07	1.40 ± 0.20	2.91 ± 0.03	0.54	0.22	0.24	1.05
2	0.72 ± 0.14	2.33 ± 0.16	3.78 ± 0.18	0.41	0.52	0.07	1.11
5	0.54 ± 0.22	2.12 ± 0.16	3.44 ± 0.09	0.37	0.49	0.14	1.05
6	0.50 ± 0.08	1.87 ± 0.40	3.06 ± 0.06	0.32	0.39	0.29	1.09
7	0.15 ± 0.09	1.46 ± 0.12	2.93 ± 0.03	0.54	0.24	0.23	1.02
8	0.62 ± 0.14	2.21 ± 0.17	3.47 ± 0.11	0.37	0.5	0.13	1.08
9	0.61 ± 0.16	2.21 ± 0.17	3.46 ± 0.11	0.36	0.5	0.13	1.07
12	0.49 ± 0.17	1.91 ± 0.20	3.10 ± 0.05	0.37	0.38	0.25	1.08
13	0.55 ± 0.13	2.14 ± 0.16	3.41 ± 0.09	0.37	0.48	0.15	1.03
16	0.60 ± 0.18	2.13 ± 0.20	3.32 ± 0.09	0.35	0.47	0.18	1.09
21	0.40 ± 0.18	1.78 ± 0.19	3.05 ± 0.04	0.37	0.35	0.28	1.17
29	0.67 ± 0.14	2.28 ± 0.19	3.48 ± 0.12	0.36	0.5	0.14	1.03
35	0.71 ± 0.22	2.07 ± 0.28	3.17 ± 0.07	0.3	0.43	0.28	1.06
45	0.60 ±0.23	1.91 ± 0.26	3.07 ± 0.05	0.28	0.38	0.34	1.03

Table 5.6. Time-resolved fluorescence data for DASPMI in the TEOS-GPTES matrix, through aging

day	τ_1 (ns)	τ_2 (ns)	τ_3 (ns)	α_1	α_2	α_3	χ^2
0	0.15±0.07	1.05±0.07	2.66±0.03	0.70	0.19	0.11	1.07
1	0.11±0.08	1.12±0.08	2.74±0.02	0.78	0.13	0.09	1.04
2	0.23±0.07	1.39±0.12	2.86±0.03	0.66	0.19	0.15	1.06
3	0.23±0.20	1.34±0.12	2.84±0.03	0.60	0.21	0.19	1.05
4	0.30±0.04	1.47±0.06	2.89±0.01	0.55	0.23	0.22	1.11
7	0.52±0.15	1.83±0.29	3.03±0.06	0.41	0.31	0.28	1.10
8	0.13±0.09	1.33±0.13	2.89±0.02	0.66	0.15	0.19	1.06
9	0.39±0.13	1.69±0.21	2.99±0.04	0.41	0.29	0.29	1.10
10	0.11±0.09	1.26±0.14	2.86±0.02	0.69	0.13	0.18	1.08
11	0.31±0.16	1.62±0.18	2.99±0.03	0.43	0.26	0.30	1.04
14	0.14±0.09	1.34±0.10	2.82±0.02	0.57	0.21	0.22	1.04
15	0.58±0.16	1.96±0.26	3.04±0.06	0.35	0.38	0.27	1.11
18	0.38±0.16	1.78±0.26	3.01±0.04	0.37	0.26	0.38	1.10
23	0.19±0.14	1.61±0.20	2.98±0.03	0.50	0.19	0.31	1.05
31	0.56±0.21	2.10±0.29	3.15±0.05	0.24	0.39	0.37	0.97
37	0.66±0.36	2.14±0.44	3.12±0.06	0.23	0.36	0.41	1.10
47	0.65±0.32	2.10±0.45	3.08±0.05	0.19	0.33	0.47	1.05

Table 5.7. Time-resolved fluorescence data for DASPMI in the TEOS-PEG 300 matrix, through aging.

day	τ_1 (ns)	τ_2 (ns)	τ_3 (ns)	α_1	α_2	α_3	χ^2
0	0.24±0.12	1.12±0.10	2.67±0.03	0.63	0.23	0.14	1.12
1	0.22±0.09	1.26±0.10	2.81±0.03	0.62	0.22	0.16	1.12
2	0.15±0.10	1.18±0.09	2.81±0.02	0.66	0.18	0.16	1.04
3	0.11±0.08	1.31±0.10	2.88±0.03	0.74	0.13	0.12	1.04
6	0.13±0.10	1.44±0.11	2.95±0.03	0.67	0.16	0.17	0.94
7	0.21±0.31	1.42±0.09	2.92±0.03	0.22	0.51	0.28	1.06
8	0.69±0.18	2.06±0.46	3.11±0.09	0.37	0.36	0.27	1.08
9	0.39±0.13	1.69±0.21	2.99±0.04	0.41	0.29	0.29	1.10
10	0.21±0.08	1.43±0.16	2.93±0.03	0.48	0.21	0.31	1.09
13	0.14±0.14	1.28±0.15	2.92±0.02	0.57	0.16	0.27	1.08
14	0.47±0.18	1.95±0.25	3.14±0.04	0.32	0.33	0.34	1.06
17	0.39±0.20	1.91±0.23	3.13±0.04	0.32	0.32	0.36	0.98
22	0.44±0.16	2.13±0.27	3.22±0.06	0.34	0.35	0.31	1.03
30	0.54±0.23	1.97±0.34	3.10±0.04	0.23	0.31	0.46	1.01
36	0.86±0.37	2.50±0.55	3.32±0.11	0.24	0.49	0.28	1.07
46	0.67±0.32	2.04±0.50	3.12±0.05	0.19	0.28	0.53	1.11

Table 5.8. Time-resolved fluorescence data for DASPMI in the TEOS-PEG 20k matrix, through aging.

day	τ_1 (ns)	τ_2 (ns)	τ_3 (ns)	α_1	α_2	α_3	χ^2
0	0.13±0.05	1.06±0.11	2.70±0.03	0.73	0.16	0.10	1.10
1	0.22±0.05	1.26±0.16	2.81±0.03	0.62	0.22	0.16	1.12
2	0.17±0.07	1.32±0.18	2.87±0.03	0.64	0.19	0.17	1.13
3	0.11±0.06	1.28±0.13	2.87±0.02	0.74	0.13	0.13	1.06
6	0.17±0.12	1.43±0.12	2.94±0.03	0.58	0.20	0.22	1.09
7	0.17±0.14	1.39±0.13	2.93±0.02	0.56	0.20	0.25	1.02
8	0.10±0.07	1.39±0.12	2.93±0.02	0.73	0.12	0.15	1.07
9	0.15±0.18	1.40±0.14	2.93±0.02	0.60	0.17	0.23	1.05
10	0.26±0.43	1.36±0.17	2.92±0.02	0.39	0.24	0.37	1.08
13	0.26±0.43	1.36±0.17	2.92±0.02	0.39	0.24	0.37	1.08
14	0.05±0.07	1.24±0.14	2.91±0.02	0.82	0.07	0.11	1.11
17	0.48±0.19	1.97±0.26	3.15±0.05	0.32	0.34	0.34	1.08
22	0.21±0.15	1.50±0.20	3.01±0.02	0.43	0.20	0.37	1.08
30	0.62±0.25	2.04±0.37	3.14±0.05	0.23	0.32	0.45	1.05
36	0.72±0.28	2.21±0.47	3.19±0.07	0.23	0.35	0.42	1.09
46	0.65±0.30	2.32±0.42	3.27±0.08	0.23	0.42	0.35	1.09

Table 5.9. Time-resolved fluorescence data for DASPMI in the TEOS-GGR matrix, through aging.

For the effect of following the trend, the use of an average lifetime is sufficient. The outcome is given in figures 5.16 and 5.17. From twenty days onwards all the polymer modified hosts (figure 5.16) apparently have equivalent average lifetimes, which is indicative that the viscosity sensed by DASPMI is similar within these media. This is in contrast to the intensity data for the initial gelation step, thus indicating that the main influence of the polymers occurs during the matrix forming phase, after which they exhibit similar control. In the case of the silane modified systems there is more of a spread in the average lifetimes, showing that limited control can be exerted over the viscosity on longer timescales by selecting the appropriate silane. It is worth remember that the fluorescence lifetimes obtained are about two orders of magnitude longer than those obtained in non viscous solution [17].

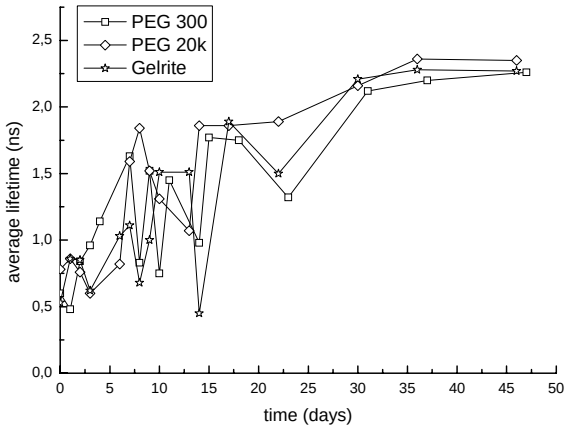

Figure 5.16. The average lifetime of DASPMI in polymer modified hosts with aging time.

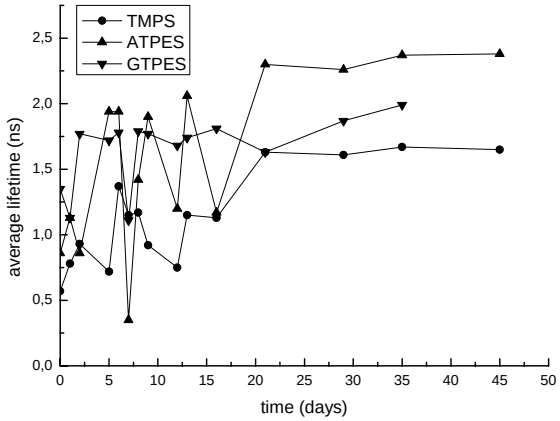

Figure 5.17. The average lifetime of DASPMI in silane modified hosts with aging time.

5.4.2.3. Matrix characterization at the end of aging

In this section the results obtained on the structural and morphological characterization of the matrices are presented. Firstly, figure 5.18 shows the X-ray diffraction (XRD) patterns of the samples. These data indicate that the silica matrix is formed as an amorphous silicate hydrate usually referred to as opal, in all samples except the GPTES sample. Most probably the short range disorder of the silica network is higher in presence of this modifier as compared to the others thus precluding the detection of the opal characteristic peak. These results suggest that, although in presence

of a diversity of modifiers, the building of the network is mainly controlled by the sol-gel synthesis of the silica matrix.

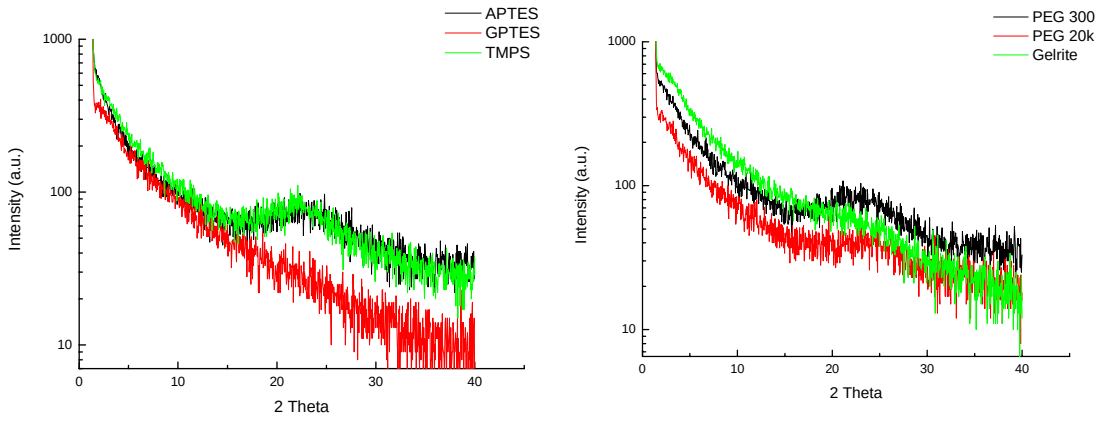

Figure 5.18. XRD patterns of the sol-gel matrices. At left side, matrices doped with silanes; at the right side, matrices doped with polymers.

The textural characterization of the matrices was done by the application of the BET method, which gave isotherms classified as type IV (typical from mesoporous materials) with type H_2 hysteresis which associated to porous of irregular shape (ink-bottle-like). Figure 5.19 shows the nitrogen adsorption isotherms (at 77 K) of the porous silica matrices.

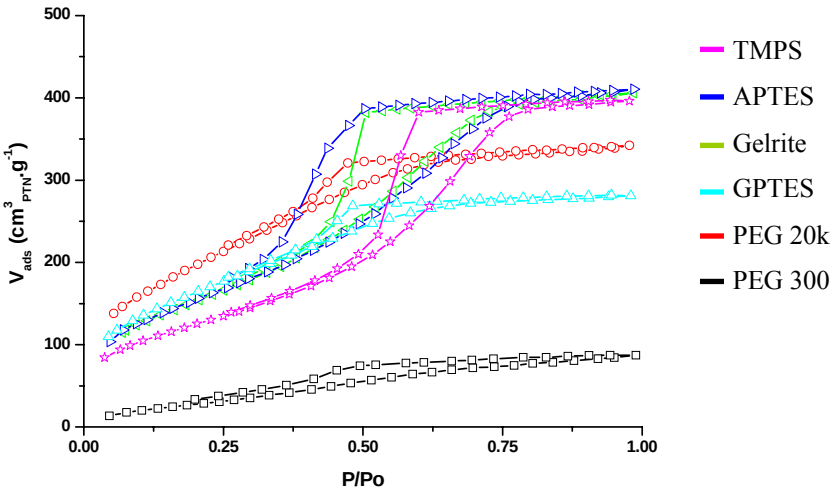

Figure 5.19. Nitrogen adsorption isotherms (at 77 K) of mesoporous silica.

Table 5.10 lists the following parameters: the specific surface area, S_{BET}, the total volume of pores, V_p (calculated at relative pressure P/P0_0.98), and average pore diameter, mouth diameter (r_m) and pore body diameter (r_b) respectively, estimated by the Kelvin equation [32]. The BET technique was also applied, for comparison purposes, to two additional samples of the matrix without any modifier, e.g., SiO_2 samples — one as aged as the modified samples and the other a fresher sample (wet gel).

Sample	S_{BET} ($m^2.g^{-1}$)	V_p ($cm^3.g^{-1}$)	r_m (nm)	r_b (nm)
PEG300	127	0.13	1.6	2.0
PEG 20k	731	0.53	1.6	1.9
Gelrite	570	0.62	1.7	2.1
APTES	575	0.62	1.3	2.1
GPTES	604	0.43	1.6	1.9
TMPS	458	0.61	2.0	2.6
SiO_2 (aged gel)	590	0.40	1.3	1.3
SiO_2 (wet gel)	832	0.63	1.5	1.5

Table 5.10. Physical properties of the samples. S_{BET} -specific surface area; total volume of pores - V_p (calculated at relative pressure $P/P_0 \approx 0.98$); pore mouth diameter – r_m and pore body diameter - r_b.

In order to interpret these results it is important to keep in mind that the preparation of the matrices involves two major steps, gelation and aging [33]. The first step is characterized by extensive and profound chemical and physical changes, namely the hydrolysis and the condensation of the silica network. During the aging process, polycondensation progresses with concomitant local solubilisation and re-precipitation events, thereby causing a significant decrease in porosity and increase in mechanical strength. The connectivity of the silica network increases substantially during this step. As the syneresis (shrinkage) occurs, an important fraction of liquid is expelled from the pores. Comparison between the two SiO_2 samples confirms that aging induces a decrease in the specific surface area (S_{BET}), in the total volume of the pores (V_p) and also in pore size (r_m, and r_b). Moreover the values found for r_m and r_b suggest these

matrices possess tubular/cylindrical pores that tend to shrink with aging as expected. It is important to note that the results on the modified matrices, shown in table 5.10, were obtained after the aging step, therefore on samples considered to be dry gels. Comparison between the values of r_m, and r_b for SiO_2 (aged) and the ensemble of the modified samples show the general effect of the modifiers: not only the pores' size increase but the shape of the pores becomes "ink-bottle-like". Moreover, the specific surface area (S_{BET}), and the total volume of the pores (Vp) tend to increase upon addition of the modifier, except for PEG 300 where the opposite effect was unexpectedly observed. It is interesting to note that PEG 20k behaves in a similar way to the other modifiers. This specific effect observed with PEG 300 is ascribed to a more effective interaction of the hydroxyl groups of this polymer with the silica network, as compared with the longer chained PEG 20k.

5.5. Conclusion

Two fluorescent probes, Nile red and DASPMI were used in monitoring the profound changes that occur in sol-gel matrices during the gelation and aging stages. The combination of such fluorescent dyes, made it possible to gain an insight into these dynamic systems.

During the gelation process DASPMI exhibited a drastic enhancement in quantum yield related to the increasing viscosity through the sol to gel transition, caused by a reduction in the non-radiative pathways. During the aging time a high degree of scatter was seen, in both the steady-state and time-resolved data, as DASPMI molecules encounter a range of different environments before the structure of the media becomes more stable. The systems stability is observed from day 20 onward. Changes in the peak steady-state emission most probably relate to alterations in the local polarity of the pore liquid, while the marked increase in intensity and lifetime values relate to decreased nonradiative de-excitation caused by increasing local viscosity. Nile red, in turn, reports on the interface between the bulk oxide material and the internal pore structure. The SFS data showed an enhancement in the polarity through aging, strongly influenced by

hydrogen bonding. In both cases the data revealed that, overall, the aging process stabilises from day 20 onward.

Time-resolved measurements of DASPMI, made clear that the viscosity enhancement of the pore solvent, does not prevent the formation of the TICT state, which is favoured by the aging process. The complementary study on the photophysics of DASPMI in glycerol-water mixtures had provided evidence for the coexistence of hydrodynamic factors, where hydrogen bonding within the solvent cage inhibited the formation of the TICT state in this system. But in sol-gel systems studied, that was not the case.

Complementary FRAP and anisotropy measurements are in agreement and furthermore suggest that the "viscosity" increase is primarily related to pore interconnections. Making use of these techniques also shows the ability of the hosts to retain relatively large biomolecules (while allowing them restricted mobility) and allows the free diffusion of smaller molecules.

Finally, the results obtained from the BET measurements, although not directly related to the FRAP and time resolved measurements, nevertheless, corroborate the hypothesis present in this section.

These important considerations are fundamental in the usage of sol-gel hybrid media for biosensor applications.

5.6. References

[1] Gottfried, D. S.; Kagan, A.; Hoffman, B. M.; Friedman, J. M. *Impeded rotation of a protein in a sol-gel matrix* Journal of Physical Chemistry B 1999, *103*, 2803.

[2] Holthoff, E. L.; Bright, F. V. *Molecularly templated materials in chemical sensing* Analytica Chimica Acta 2007, *594*, 147.

[3] Shchipunov, Y. A.; Kojima, A.; Imae, T. *Polysaccharides as a template for silicate generated by sol-gel processes* Journal of Colloid and Interface Science 2005, *285*, 574.

[4] Steiner, R. F. Fluorescence Anisotropy: Theory and Applications. In *Topics in Fluorescence Spectroscopy*; Lakovwicz, Ed.; Plenum Press: New York, 1991; Vol. Volume 2.

[5] Braeckmans, K.; Peeters, L.; Sanders, N. N.; De Smedt, S. C.; Demeester, J. *Three-dimensional fluorescence recovery after photobleaching with the confocal scanning laser microscope* Biophysical Journal 2003, *85*, 2240.

[6] Kuttner, Y. Y.; Kozer, N.; Segal, E.; Schreiber, G.; Haran, G. *Separating the contribution of translational and rotational diffusion to protein association* Journal of the American Chemical Society 2005, *127*, 15138.

[7] Swaminathan, R.; Hoang, C. P.; Verkman, A. S. *Photobleaching recovery and anisotropy decay of green fluorescent protein GFP-S65T in solution and cells: Cytoplasmic viscosity probed by green fluorescent protein translational and rotational diffusion* Biophysical Journal 1997, *72*, 1900.

[8] Suhling, K.; French, P. M. W.; Phillips, D. *Time-resolved fluorescence microscopy* Photochemical & Photobiological Sciences 2005, *4*, 13.

[9] Suhling, K. Fluorescence lifetime imaging. In *Methods Express, Cell Imaging*; Stephens, D., Ed.; Scion Publishing Ltd: Bloxham, 2006.

[10] Suhling, K.; Siegel, J.; Lanigan, P. M. P.; Leveque-Fort, S.; Webb, S. E. D.; Phillips, D.; Davis, D. M.; French, P. M. W. *Time-resolved fluorescence anisotropy imaging applied to live cells* Optics Letters 2004, *29*, 584.

[11] Menaa, B.; Herrero, M.; Rives, V.; Lavrenko, M.; Eggers, D. K. *Favourable influence of hydrophobic surfaces on protein structure in porous organically-modified silica glasses* Biomaterials 2008, *29*, 2710.

[12] Bottini, M.; Venere, A. d.; Tautz, L.; Desideri, A.; Lugli, P.; Avigliano, L.; Rosato, N. *Structural Stability of Azurin Encapsulated in Sol-Gel Glasses: A Fluorometric Study* Journal of Sol-Gel Science and Technology 2004, *30*, 205–214.

[13] Shchipunov, Y. A.; Karpenko, T. Y. *Hybrid polysaccharide-silica nanocomposites prepared by the sol-gel technique* Langmuir 2004, *20*, 3882.

[14] Flora, K. K.; Brennan, J. D. *Characterization of the microenvironments of PRODAN entrapped in tetraethyl orthosilicate derived glasses* Journal of Physical Chemistry B 2001, *105*, 12003.

[15] Strehmel, B.; Seifert, H.; Rettig, W. *Photophysical properties of fluorescence probes .2. A model of multiple fluorescence for stilbazolium dyes studied by global analysis and quantum chemical calculations* Journal of Physical Chemistry B 1997, *101*, 2232.

[16] Hungerford, G.; Pereira, M. R.; Ferreira, J. A.; Viseu, T. M. R.; Coelho, A. F.; Isabel, M.; Ferreira, C.; Suhling, K. *Probing Si and Ti based sol-gel matrices by fluorescence techniques* Journal of Fluorescence 2002, *12*, 397.

[17] Strehmel, B.; Rettig, W. *Photophysical properties of fluorescence probes I: dialkylamino stilbazolium dyes* Journal of Biomedical Optics 1996, *1*, 98.

[18] Ramadass, R.; Bereiter-Hahn, J. *Photophysical properties of DASPMI as revealed by spectrally resolved fluorescence decays* Journal of Physical Chemistry B 2007, *111*, 7681.

[19] Welinder, K. G. *Amino-Acid Sequence Studies of Horseradish-Peroxidase .4. Amino and Carboxyl Termini, Cyanogen-Bromide and Tryptic Fragments, the Complete Sequence, and Some Structural Characteristics of Horseradish Peroxidase-C* European Journal of Biochemistry 1979, *96*, 483.

[20] Herren, J. I.; Kunzelman, K. S.; Vocelka, C.; Cochran, R. P.; Spiess, B. D. *Horseradish peroxidase as a histological indicator of mechanisms of porcine retinal vascular damage and protection with perfluorocarbons after massive air embolism* Stroke 1997, *28*, 2025.

[21] Bolton, G. R.; Deen, W. M.; Daniels, B. S. *Assessment of the charge selectivity of glomerular basement membrane using Ficoll sulfate* American Journal of Physiology-Renal Physiology 1998, *274*, F889.

[22] Egelhaaf, H. J.; Lehr, B.; Hof, M.; Hafner, A.; Fritz, H.; Schneider, F. W.; Bayer, E.; Oelkrug, D. *Solvation and solvent relaxation in swellable copolymers*

as studied by time-resolved fluorescence spectroscopy Journal of Fluorescence 2000, *10*, 383.

[23] Hungerford, G.; Rei, A.; Ferreira, M. I. C. *Studies on the interaction of Nile red with horseradish peroxidase in solution* FEBS Journal 2005, *272*, 6161.

[24] Alexiev, U.; Rimke, I.; Pohlmann, T. *Elucidation of the nature of the conformational changes of the EF-interhelical loop in bacteriorhodopsin and of the helix VIII on the cytoplasmic surface of bovine rhodopsin: A time-resolved fluorescence depolarization study* Journal of Molecular Biology 2003, *328*, 705.

[25] Eftink, M. R. Fluorescence Quenching: Theory and Applications. In *Topics in Fluorescence Spectroscopy*; Lakowicz, J. R., Ed.; Plenum Press: New York, 1991; Vol. Volume 2 - Principles.

[26] Hungerford, G.; Rei, A.; Ferreira, M. I. C. *Use of fluorescence to monitor the incorporation of horseradish peroxidase into a sol-gel derived medium* Biophysical Chemistry 2006, *120*, 81.

[27] Weiss, A. M.; Saraidarov, T.; Reisfeld, R. *Confocal microscopy for characterization of porous sol-gel glasses incorporating luminescent dyes* Optical Materials 2001, *16*, 15.

[28] Hellriegel, C.; Kirstein, J.; Brauchle, C.; Latour, V.; Pigot, T.; Olivier, R.; Lacombe, S.; Brown, R.; Guieu, V.; Payrastre, C.; Izquierdo, A.; Mocho, P. *Diffusion of single streptocyanine molecules in the nanoporous network of sol-gel glasses* Journal of Physical Chemistry B 2004, *108*, 14699.

[29] Hellriegel, C.; Kirstein, J.; Brauchle, C. *Tracking of single molecules as a powerful method to characterize diffusivity of organic species in mesoporous materials* New Journal of Physics 2005, *7*.

[30] Shungu, D.; Valiant, M.; Tutlane, V.; Weinberg, E.; Weissberger, B.; Koupal, L.; Gadebusch, H.; Stapley, E. *Gelrite as an Agar Substitute in Bacteriological Media* Applied and Environmental Microbiology 1983, *46*, 840.

[31] Shchipunov, Y. A.; Karpenko, T. Y.; Bakunina, L. Y.; Burtseva, Y. V.; Zvyagintseva, T. N. *A new precursor for the immobilization of enzymes inside sol-gel-derived hybrid silica nanocomposites containing polysaccharides* Journal of Biochemical and Biophysical Methods 2004, *58*, 25.

[32] Ribeiro, J. L. F. F. R. *Catálise heterogénea*, segunda edição ed.; Fundação Calouste Gulbenkian, 2007.

[33] Hench, L. L.; West, J. K. *The Sol-Gel Process* Chemical Reviews 1990, *90*, 33.

Chapter 6

PROTEIN ENCAPSULATION AND CATALYTIC ACTIVITY

6.1. Introduction

The previous chapter presented the methods and techniques utilised to monitor silica matrices through the *sol* to *gel* transition and the aging process. The present chapter will focus on assessing the conformational stability and activity of two different catalytically active proteins encapsulated within these hosts. Hybrid sol-gel media, with either polymers or silanes to moderate the internal pore environment, were produced containing subtilisin *Carlsberg* or cytochrome *c*. Subtilisin *Carlsberg* is a member of the superfamily of subtilisin-like serine proteases (subtilases) occurring in Archaea, Bacteria, Fungi and higher eukariotes [1]. It has been systematically characterised and the complete aminoacid sequence of the mature protein is known since 1968 [2]. Applications of proteolitic enzymes include drug delivery [3,4], food industry, laundry detergents [5] and organic synthesis [6]. C-type cytochromes are found in almost all organisms, and are involved in electron transport [7]. In eukariotes, it is synthesised in the cytoplasm, but is in the inner-membrane space of the mitochondria organelle that it gains its haem moiety. Its most carefully studied function is as an electron carrier of the eukaryotic respiratory chain, but it is also important in both apoptosis and oxidative stress. The peroxidase activity of this electron carrier is associated with the iron of the haem group [8].

The encapsulated proteins exhibited activity over a forty day period, during which host aging occurred. The modifiers were characterised in chapter 5 and their structure is presented in figure 5.11.

The highly solvatochromic dye Nile red was used in conjunction with synchronous scan fluorescence spectroscopy (SFS) to elucidate changes in the tertiary structure of the proteins, upon incorporation into sol–gel derived media. By examining this and the catalytic reaction (initial velocity and amount of substrate transformed into product) it was possible to ascertain the influence of the different hosts on the catalytic rate. It is clear that, although some unfolding of the proteins occurred, the major effect on the catalytic reaction is that of mass transport within the host.

6.2. Encapsulation and activity of subtilisin *Carlsberg*

6.2.1. Materials and methods

All spectra (absorption and synchronous scan fluorescence) were measured with the instruments mentioned in chapter 3. Difference spectra were calculated by normalising the spectra and subtracting from the reference spectrum.

Sols were manufactured as reported in section 5.2.1. Subtilisin *Carlsberg* (EC 3.4.21.62) from Sigma, was dissolved in phosphate buffer solution pH7 to a concentration of 1.5×10^{-5} M and was labelled with Nile red by continuous stirring at room temperature for 2 hours. This gave a molar ratio of 1 dye molecule to 15 molecules of enzyme. The hybrid hosts were then manufactured using 10 mm pathlength polystyrene cuvettes (*ca*. 4.5 ml volume) by taking 2 ml of sol and adding silane or polymer, and 2 ml of the enzyme solution. The modifiers were presented in the previous chapter. After combining the selected *sol* and enzyme solution, the resultant gel was stored at 4 ºC between measurements with the top of the cuvette covered. Under these conditions an average shrinkage of *ca*. 40% occurred over the period of the experiment.

Catalytic experiments used the enzyme substrate Ala-Ala-Phe-7-amido-4-methyl coumarin (AAF-AMC) (Aldrich) and the product formation, amido-4-methyl coumarin (AMC) was followed spectrophotometrically [9].

6.2.2. Results and discussion

An important aim of the entrapment of biologically active molecules is that the host can provide a protective environment for the biomolecules under conditions such that their activity is preserved. In the present section the studies on the enzyme conformation are reported, through the analysis of the fluorescence spectroscopy of Nile Red as the aging of the matrices proceeds. The enzymatic activity of subtilisin *Carlsberg* incorporated into different sol-gel derived media is also reported. In order to provide a reference, the catalytic reaction was also studied in aqueous solution (pH7). This reference study was carried out under conditions (i.e. concentration of substrate) similar to the study of subtilisin *Carlsberg* activity when incorporated into the chosen matrices. It should be stressed that all the catalytic and spectroscopic measurements were done during the period of wet aging. In fact, in chapter 4 it was shown that the actual pore size of the wet-gels is such that the enzyme has ample space to rotate, thus providing adequate conditions to probe the enzyme's activity, a major purpose of the present work.

6.2.2.1. Catalytic activity of subtilisin *Carlsberg* in homogeneous solution (reference system)

The reaction mechanism of subtilisin *Carlsberg* is well established, as serine proteases belong to the most comprehensively studied class of proteolytic enzymes [10]. The catalytic activity of subtilisin *Carlsberg* was examined using the substrate Ala-Ala-Phe-7-amido-4-methyl coumarin (AAF-AMC) and monitoring the formation of the product 7-amido-4-methyl coumarin (AMC).

According to Kamal et al. [9] the enzymatic reaction is described by the following mechanism:

$$AAF-AMC+SC \underset{k_{-1}}{\overset{k_1}{\longleftrightarrow}} AAF-AMC-SC \xrightarrow{k_2} SC+AMC \qquad (6.1)$$

where AAF-AMC—SC is the enzyme-substrate complex. Under steady–state conditions, the reaction rate will be:

$$v = -\frac{d[AAF-AMC]}{dt} = \frac{d[AMC]}{dt} = \frac{k_2[SC]_T[AAF-AMC]}{K_M + [AAF-AMC]} \tag{6.2}$$

in agreement with the well kown Michaelis – Menten formalism, with $K_M = 9\times10^{-4}$ M and $k_2 = 1.9\times10^{-2}$ s^{-1}. In equation 6.2, $[SC]_T$ refers to the total concentration of enzyme, K_M is the Michaelis constant and k_2 is the rate of decomposition of the enzyme-substrate complex into product and enzyme.

The concentration of both the substrate Ala-Ala-Phe-7-amido-4-methyl coumarin (AAF-AMC) and the product (AMC) was determined spectrophotometricaly at 325 nm and 370 nm, respectively, according to the absorption spectra of both species, shown in figure 6.1.

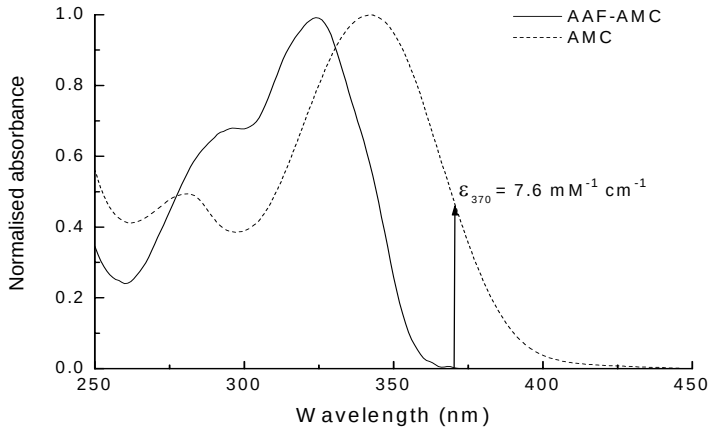

Figure 6.1. Spectral characteristics of the absorption spectra of substrate (AAF-AMC) and the product (AMC) of the enzymatic reaction. The arrow indicates the wavelength at which the product formation was monitored during the reaction. The extinction coefficient of AAF-AMC at 325 nm is ε_{325} = 16 mM^{-1} cm^{-1} whereas the extinction coefficient of AMC at 370 nm is ε_{370} = 7.6 mM^{-1} cm^{-1} [9].

In the present work, the activity of subtilisin *Carlsberg* at various concentrations was examined by monitoring the formation of the reaction product, 7-amido-4-methyl coumarin (AMC), with a fixed substrate concentration of 1.3x10^{-4} M, in aqueous solution (pH7), as shown in figure 6.2.

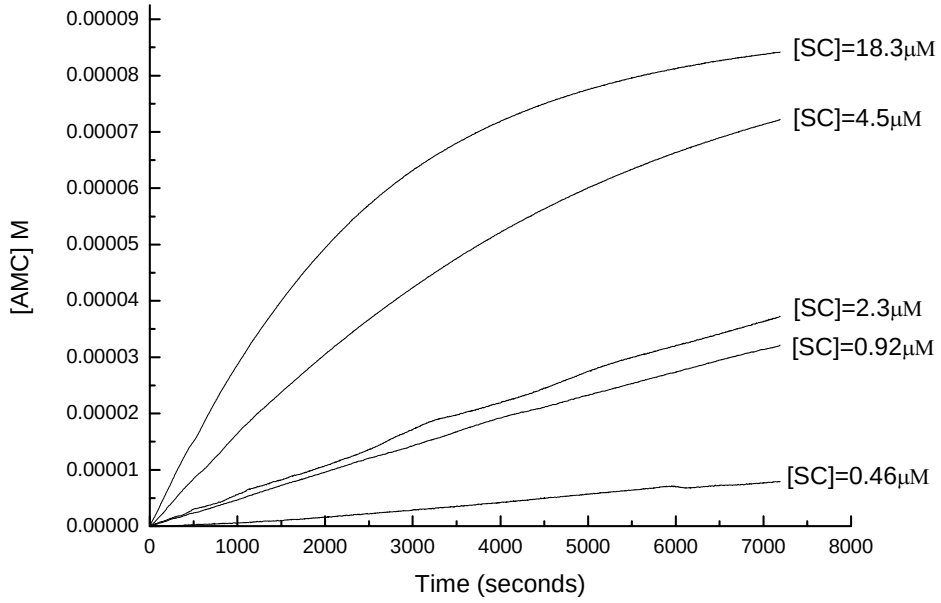

Figure 6.2. Monitoring the formation of the reaction product, AMC, at 370 nm, with a fixed substrate concentration of 1.3 x 10^{-4} M, at various concentrations of subtilisin *Carlsberg*.

The initial rate (v_0) of the reaction was determined using the derivative of the concentration of the product at the beginning of the reaction t = 0 (equation 6.3) and, in practical terms, calculated before ~10% of the substrate was converted to product [11],

$$v_0 = \left(\frac{d[AMC]}{dt} \right)_{t=0} \tag{6.3}$$

The values of the initial reaction rate, plotted against the concentration of enzyme in solution, are shown in figure 6.3. The figure shows that, under these experimental conditions, the initial velocity is linearly dependent upon $[SC]_T$, the total enzyme concentration.

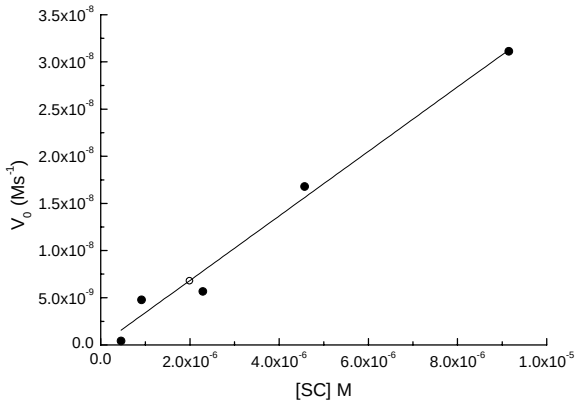

Figure 6.3. Initial velocity of the reaction at various enzyme concentrations. The slope of the linear fitting to the data is 3.42×10^{-3}. The open symbol, not an experimental point, indicates the rate that corresponds to the enzyme load to be used in the sol-gel matrices.

This result confirms that not only the enzymatic reaction follows the expected reaction mechanism, but also [AAF-AMC] is always in excess relatively to $[SC]$. In fact, whenever $[AAF-AMC] << K_M$, equation (6.2) simplifies to

$$v \approx \frac{k_2}{K_M}[SC]_T[AAF-AMC] \approx k'[SC]_T \tag{6.4}$$

Therefore, at the very early stages of conversion it is appropriate to assume that $[AAF-AMC]$=1.3×10^{-4} M is constant throughout the first stages of the catalytic process, e.g., $t \rightarrow 0$. The slope obtained from figure 6.3, 3.4×10^{-3} s^{-1} is in agreement with the corresponding value k'=2.4×10^{-3} s^{-1} predicted from Kamal's data when $[AAF-AMC] = 1.3 \times 10^{-4}$ M.

6.2.2.2. Catalytic activity of entrapped subtilisin *Carlsberg*

The catalytic activity of subtilisin *Carlsberg* in sol-gel derived matrices was monitored under experimental conditions equivalent to the ones used in the solution study, by cutting a slice of ca. 200 mg of matrix and putting it into a cuvette with substrate solution. This means that, in each reaction vessel, a total amount of ca. 0.1 mg of enzyme was present. The low enzyme loading, *ca.* 0.05 wt%, was deliberate so that $[AAF-AMC]$was always in excess relative to $[SC]$. From figure 6.3 it is possible to

estimate the reaction rate, in homogeneous medium, that corresponds to the enzyme load used in the matrices in the present case is $5.24 \times 10^{-5}\ s^{-1}$.

As previously pointed out, all the catalytic measurements were done during the period of wet aging, so that the actual pore size of the wet-gels is such that the enzyme has ample space to rotate, thus providing adequate conditions to probe the enzyme's activity. Moreover, it has been shown in the previous chapter that the stabilization of these sol-gel matrices occurs only after 20 days. As a result, the activity of subtilisin *Carlsberg* was monitored in wet gels after an aging period of two months. The $[AMC]$ versus time curves shown in figure 6.4, when compared to the corresponding curves measured for the reference system (figure 6.2), indicate that the enzymatic process, although occurring, is much slower when subtilisin *Carlsberg* is entrapped. Moreover significant activity occurs only after an "induction period", of duration quite dependent upon the modifier. It is shorter for Gelrite and PEG 20 K and longer for TMPS and APTES matrices.

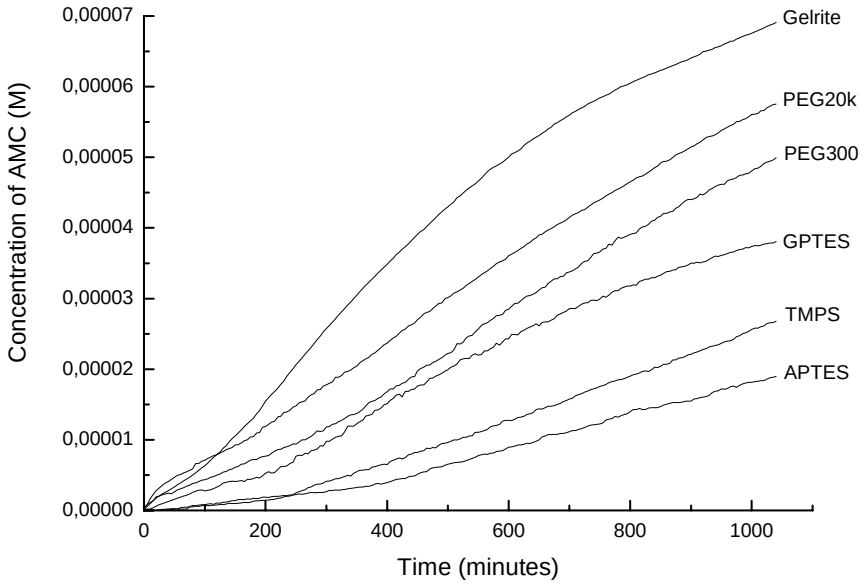

Figure 6.4. Catalytic activity of subtilisin *Carlsberg* within sol-gel media after an aging period of 2 months.

Several approaches have been developed to the study of the kinetics of enzymatic reactions when incorporated into complex systems such as living cells or heterogeneous media such as nanostructures [12-15]. Considerable attention was paid to enzymatic processes that follow the Michaelis – Menten mechanism [14,15]

$$S + E \underset{k_{-1}}{\overset{k_1}{\longleftrightarrow}} E - S \xrightarrow{k_2} P \tag{6.5}$$

According to these authors [14] their simulation studies indicate that, under these circumstances, k_1 shows a time dependence whereas k_{-1} and k_2 are time independent. These results confirm that in spatially constrained media k_1 is unequivocally affected, e.g., k_1 becomes time dependent.

According to Kopelman [16,17] the time dependence of the rate constant can be adequately described by the fractal like kinetics:

$$k(t) = k_0 t^{-h} \quad \text{for } t \to \infty \tag{6.6}$$

where k_0 is the rate constant in absence of constraints, and h is the fractal dimension.

In the present study, since the enzyme is trapped into the matrix, the accessibility of the substrate to the pores that retain the enzyme is somewhat inhibited. Therefore it is expected that the access to the enzyme will control the kinetics with obvious time dependent effects on k_1. Under these circumstances it was assumed that the enzymatic process becomes a pseudo–first order process

$$AAF - AMC \xrightarrow{k} AMC \tag{6.7}$$

Where $k = k(t)$ obeys equation (6.6). Under these circumstances

$$-\frac{d[AAF - AMC]}{dt} = k(t)[AAF - AMC] = k_0 t^{-h}[AAF - AMC] \tag{6.8}$$

Integration of equation 6.8 leads to:

$$\ln \frac{[AAF - AMC]_0}{[AAF - AMC]_t} = \frac{k_0}{(1-h)} t^{1-h} \qquad (6.9)$$

From the experimental curves shown in figure 6.4, plots of $\ln\left[\ln \frac{[AAF - AMC]_0}{[AAF - AMC]_t} \right]$ versus ln *t* were obtained. Such plots were adjusted to equation 6.9 and the respective fits are shown in figure 6.5. Table 6.1 shows the results thus obtained.

SAMPLE	% of product after 17hours [AMC]/[AAF-AMC] x 100	h	k_0(min^{-1})	k_0(s^{-1})
APTES	14.6%	-0.58	4.54E-06	7.56673E-08
GPTES	29.2%	-0.21	9.91E-05	1.65167E-06
TMPS	20.0%	-0.65	4.12E-06	6.86964E-08
PEG300	38.4%	-0.05	0.000306	5.10365E-06
PEG20k	44.2%	0.03	0.000623	1.03886E-05
Gelrite	53.1%	-0.17	0.0003	4.99366E-06

Table 6.1. Kinetic data obtained from the plots shown in figure 6.5 for the different sol-gel samples.

The table confirms that all values of the rate constant, k_0, are significantly lower than the corresponding homogeneous value of 5.24×10^{-5} s^{-1}, as expected. This value was obtained from the kinetic data in homogeneous solution, when the enzyme load is identical to the load in the matrices. It is also important to notice that negative values of the fractal dimension were obtained. This means that the true morphology of the matrix is complex, with a variability of patterns at different scales. These results suggest the need to develop in future new models and simulations that approach these materials in a more realist way, albeit at the expenses of added complexity [18].

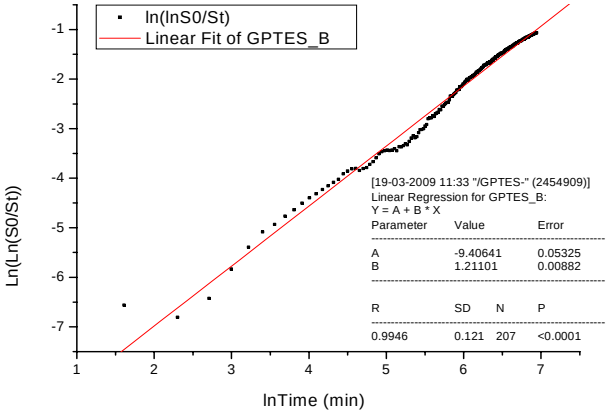

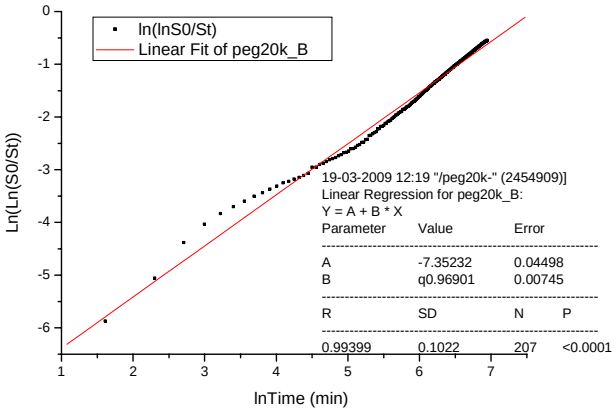

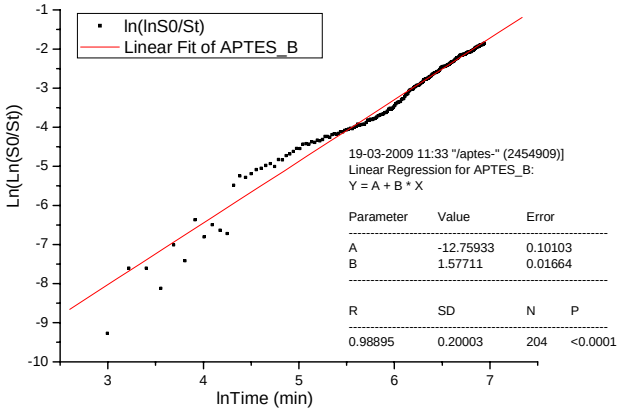

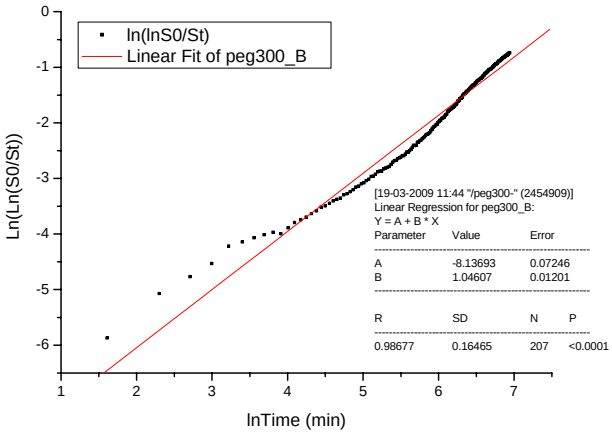

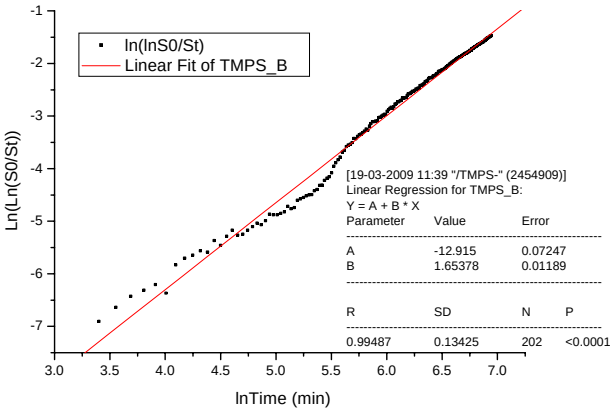

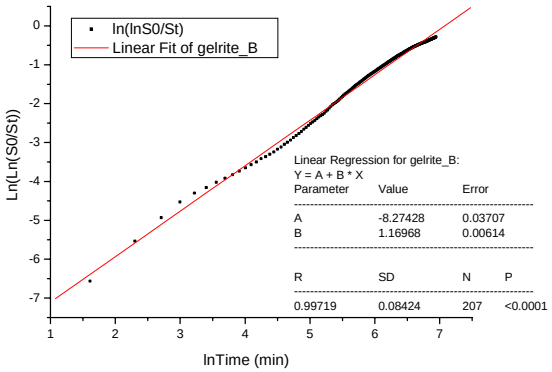

Figure 6.5. Plots of $\ln\left[\ln\frac{[AAF\ -\ AMC\ ]_0}{[AAF\ -\ AMC\ ]_t}\right]$ versus ln t adjusted to equation 6.9 and the respective linear fits.

6.2.2.3. Enzyme conformation during aging

The enzyme's conformation was monitored by analysing the synchronous fluorescence scan spectra (SFS) of the extrinsic fluorescent probe Nile red, as explained previously. As a preliminary study, subtilisin *Carlsberg* (SC) was deliberately denatured with urea to elucidate the SFS spectrum of Nile red in presence of the unfolded species. The enzyme and Nile red were mixed in buffer solution (pH 7) and the incubation proceeded for 2 hours with continuous gentle stirring prior to measurement (figure 6.6, solid line). Urea was then added to the enzyme solution and, after dissolving, the spectrum was re-measured (figure 6.6, dotted line). It is evident from figure 6.6, that treatment with urea causes an enhancement of the fluorescence intensity at 625 nm. Emission at this wavelength corresponds to Nile red sensing a more aqueous (polar) environment, which is attributed to unfolding of the protein. The concentration of urea used, 4 M, is not enough to completely denature SC (it retains *ca.* 35% relative hydrolysis activity)[19], although a certain degree of unfolding is expected due to solvation of the hydrophobic core [20].The synchronous scan fluorescence spectra clearly reveal that, after urea treatment, the probe senses a more polar environment, with the Nile red band intensity at 625 nm increasing dramatically, accompanied by a red shift of 4 nm. The same technique was utilised to monitor the conformation of SC encapsulated in the sol-gel modified monoliths.

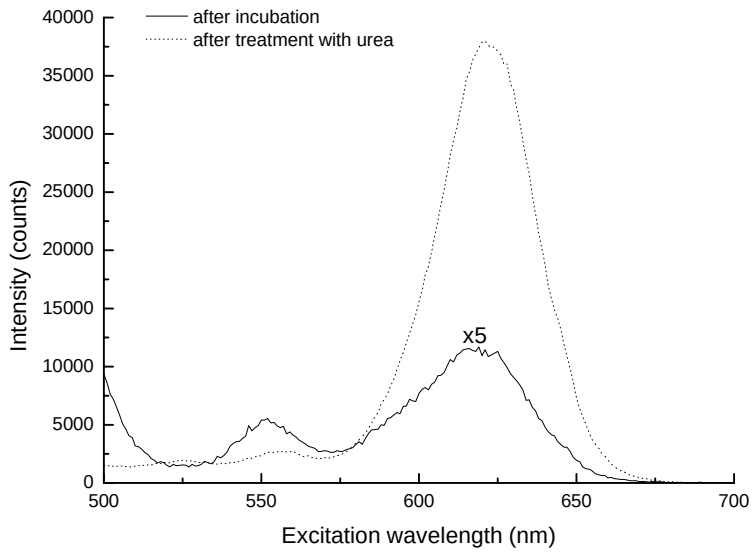

Figure 6.6. Nile red synchronous scan fluorescence spectra in solution immediately after incubation with SC (solid line) and after treatment with urea (dotted line). A massive increase in the intensity along with a 4 nm red shift of the spectrum after urea treatment should be noted.

After the encapsulation in sol-gel derived media, the SFS technique was used to follow changes in the enzyme's conformation during the aging period. The difference spectra were generated by normalising the spectra and subtracting the reference (day 0) spectrum using Microcal Origin 7 software (figure 6.8).

It is assumed throughout that, after encapsulation, Nile red does not leach to any appreciable extent from the enzyme and that the enhancement of the band at 630nm is attributed to protein unfolding, exposing the probe to a more aqueous environment. This happens at the expenses of the band at 600nm. The enhancement in each sample varies between 35% and 40%, except for TMPS sample where it reaches 10%, indicating that this host is the one that better preserves the enzyme integrity. This then leads to the question of what is the meaning of the band at 550nm or lower wavelengths that appears in both the APTES and TMPS samples. As Nile red is a very hydrophobic probe, changes in its surroundings could force some molecules to relocate to less polar positions. Also, the quantum yield of Nile red in non polar environments is higher than in polar ones, so the fluorescence intensity of the relocated molecules is relatively enhanced. Favourable effect of TMPS addition to silica matrices has previously been reported on myoglobin conformation [21].

Overall, these results show that the confinement in sol-gel derived media does not lead to any significant denaturing of SC; moreover the results suggest a favourable effect of TMPS addition on SC conformation.

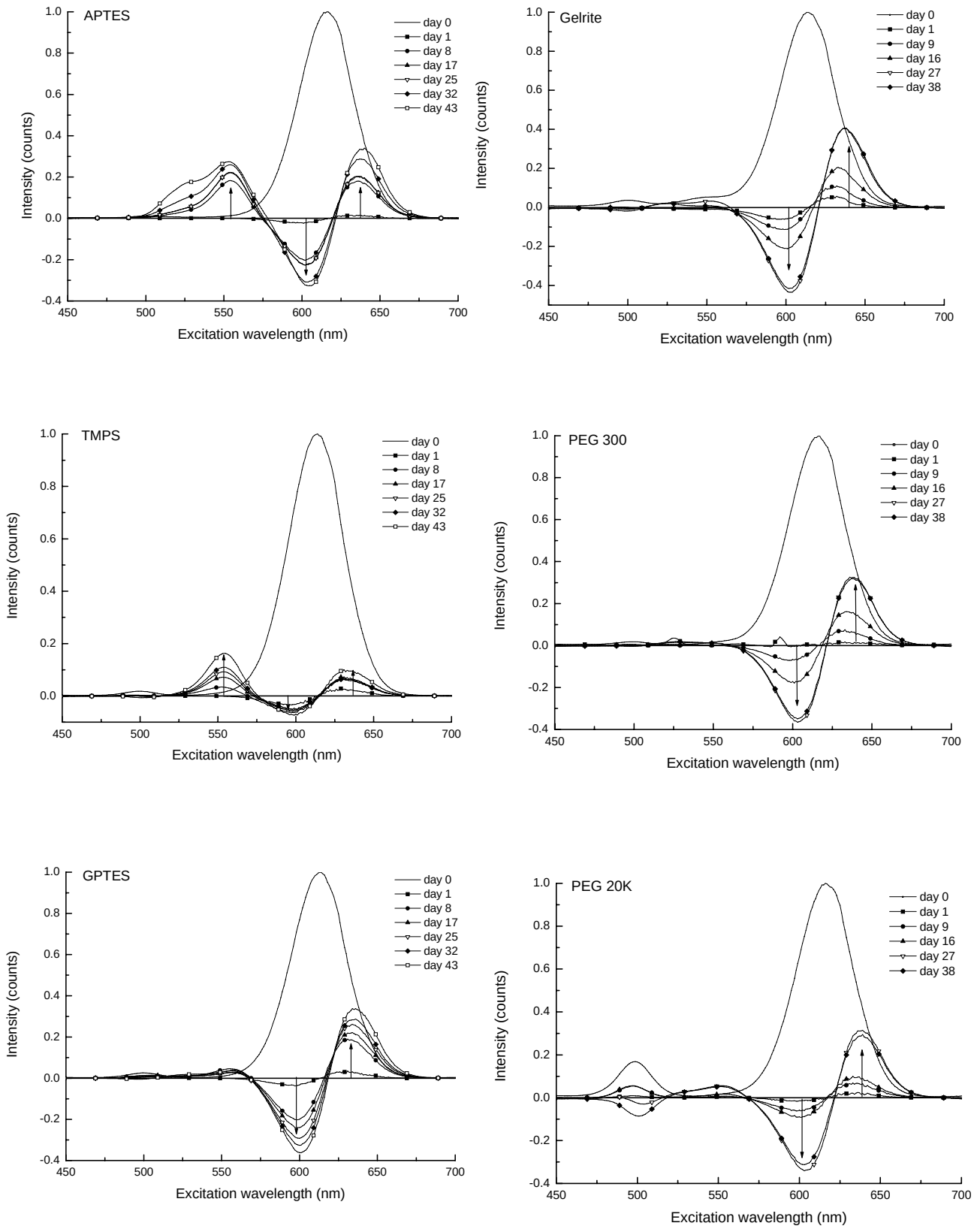

Figure 6.8. Comparison of Nile red difference SFS in subtilisin *Carlsberg* with sol-gel aging time when incorporated into both silane and polymer modified hosts.

6.3. Encapsulation and activity of cytochrome c

6.3.1. Materials and methods

Cytochrome *c* (horse heart, Aldrich) was either used as received or labelled with Nile red by taking 0.3 mg of protein in 2 ml of phosphate buffer solution (pH7) and incubating with 2 μl of 10^{-3} M Nile red solution in dimethylsulfoxide for one hour. The cytochrome c activity was obtained from the oxidation of ABTS (2,2-Azino-bis(3-ethylbenzothiazoline-6-sulfonic acid) diammonium salt, (from Sigma) by hydrogen peroxide (H_2O_2, 37% Aldrich) [8]. The sol-gel derived media manufacturing process was described previously (section 6.2.1). All measurements (described in chapter 3) were performed at ambient temperature and taken over a 40 day period to check for longer term changes during sol–gel aging.

6.3.2. Results and discussion

Activity measurements in aqueous solution served as reference to the measurements involving the sol–gel matrices and were performed using differing quantities of cytochrome with a fixed substrate concentration. For the studies on the sol–gel derived systems, 100 mg of matrix (a slice cut from the monolith) was taken and added to a cuvette containing 2 ml of 2.5×10−5 M ABTS and 8 μl H_2O_2 in buffer solution. The absorption spectrum was recorded in the range 250–500 nm, both before the addition of the matrix and after the kinetic study was complete. The progress curves were built either on the addition of the cytochrome c or protein containing matrix and followed the formation of the $ABTS^{\bullet+}$ radical by monitoring absorption changes at 414 nm [22]. The peroxidase activity of cytochrome c shows a typical Michaelis–Menten kinetics for H_2O_2 [8].

6.3.2.1. Catalytic activity of cytochrome c in homogeneous solution (reference system)

The reaction of H_2O_2 with cytochrome c, produces a highly reactive ferryl-haem species, the intermediate compound I which, by reduction with ABTS, regenerates the original cytochrome c molecule [8]. In agreement to Deere *et al.* [23] cytochrome c mediates the oxidation of ABTS, with one mole of H_2O_2 reacting with two moles of ABTS, according to equations 6.10 and 6.11.

$$cytochrome\ c\ \ Fe(III) + H_2O_2 \rightarrow compound\ \ I + H_2O \qquad (6.10)$$

$$compound\ \ I + 2ABTS \rightarrow cytochrome\ \ c\ \ Fe(III) + 2ABTS^{\bullet+} \qquad (6.11)$$

For the catalytic reaction a fixed concentration of H_2O_2 and ABTS were used, at various protein concentrations, in a range similar to that expected in the hosts. The formation of the $ABTS^{\bullet+}$ radical was monitored at 414 nm with time, using absorption spectroscopy (figure 6.9).

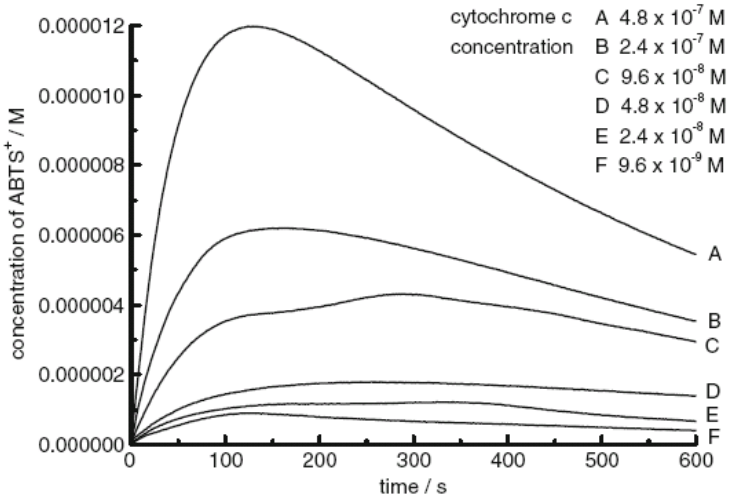

Figure 6.9. Catalytic activity in solution, with fixed substrate and H_2O_2 concentrations and varying amounts of cytochrome c. The product formation was monitored at 415 nm.

From these progress curves, the initial rate (v_0) of the catalytic reaction was calculated by taking the derivative [24]. The values obtained are given in table 6.2 and show that the initial rate of the reaction is proportional to the protein concentration. The initial

reaction rate (v_0) was chosen, as determination of other kinetic parameters can be problematic in sol-gel derived media [24,25]. The reaction forming the $ABTS^{\bullet+}$ radical is reversible, through a complex mechanism [25], so longer time course measurements were precluded. Curve A in figure 6.9, shows an initial rapid increase, followed by a decrease (also observed in some of the other kinetic curves) which relates to the reversibility of this reaction. It was expected that the results would be obtained in a regime where the substrate would be in excess in relation to cytochrome *c*.

[cytochrome *c*] / M	v_0 / Ms^{-1}
9.6×10^{-9}	2.36×10^{-8}
2.4×10^{-8}	3.33×10^{-8}
4.8×10^{-8}	2.63×10^{-8}
9.6×10^{-8}	5.70×10^{-8}
2.4×10^{-7}	1.33×10^{-7}
4.8×10^{-7}	2.53×10^{-7}

Table 6.2. Initial velocities (v_0) for the ABTS, H_2O_2, cytochrome c system for varying concentrations of cytochrome *c*.

6.3.2.2. Catalytic activity of entrapped cytochrome c

Comparing the values for the initial velocity from the *sol-gel* hosts over a period of approximately 40 days (figure 6.10), these media exhibit v_0 values one to two orders of magnitude lower than that seen in the solution data (table 6.2). An example of the kinetic curves for the formation of the $ABTS^{\bullet+}$ radical at various points during the aging process, in this case APTES, is given in figure 6.11. This shows that the amount of radical formed over the period of the experiment is similar in magnitude to the lower concentrations of cytochrome c employed in the solution study.

There is a general trend for the amount of radical formed during the time of the experiment to reduce with aging time. To perform these measurements slices taken from a monolith were used rather than powders, and this could partially explain the low v_0's obtained. Other explanations that need exploring are unfolding of the protein and its accessibility within the host to the substrate. The fact that a charged radical is formed in

the reaction and that it has to exit the matrix before it is detected spectroscopically is also an issue. Considering the whole of the dataset shown in figure 6.10, it is evident that there is a trend for the initial velocity to decrease with aging time.

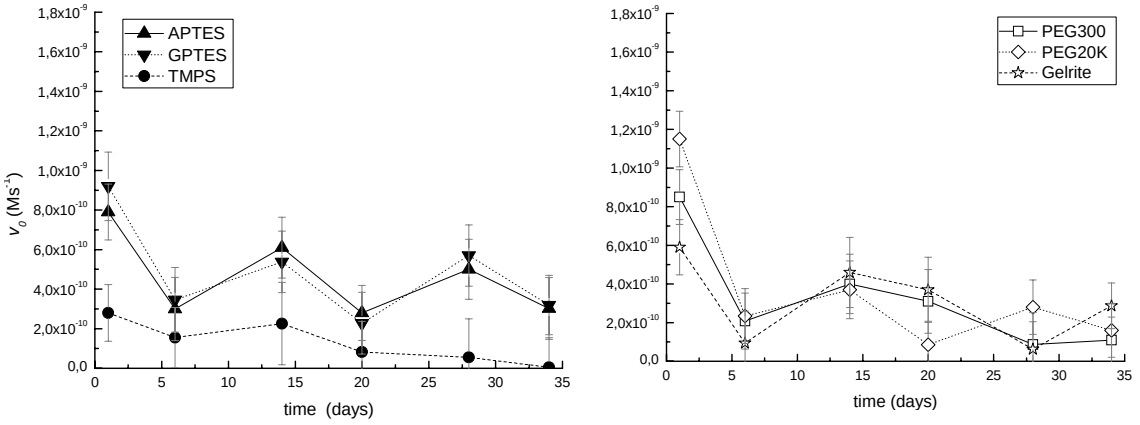

Figure 6.10. Initial velocity of the catalytic peroxidase activity of cytochrome *c* within the modified hosts with aging time. (at the left) with additional silanes, (at the right) with additional polymers.

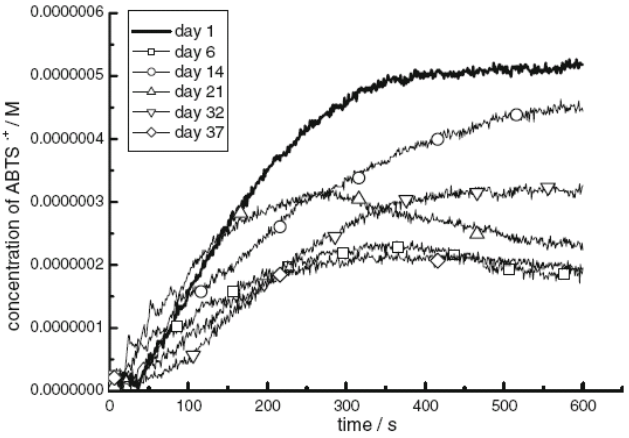

Figure 6.11. Catalytic activity with aging time for cytochrome c in an APTES modified host.

The first set of activity measurements (figure 6.10) shows that cytochrome *c* in the different media exhibits similar initial velocities, the main exception is that of the TMPS containing host, which consistently displays a lower v_0 and eventually drops to 98% of its initial value. The other silane containing hosts fare better, with a comparative decrease between the first and last measurements of about two thirds of the initial v_0 value. A similar behaviour is seen in the Gelrite modified host. Both of the PEG

modified media exhibit the same relative reduction in v_0 (by ~85%). Much of the change occurs within the first week of aging, when major morphological changes occur.

6.3.2.3. Cytochrome c conformation during aging

Continued monitoring of the Nile red emission, via SFS, allowed changes of its environment within cytochrome c to be elucidated (figure 6.11).

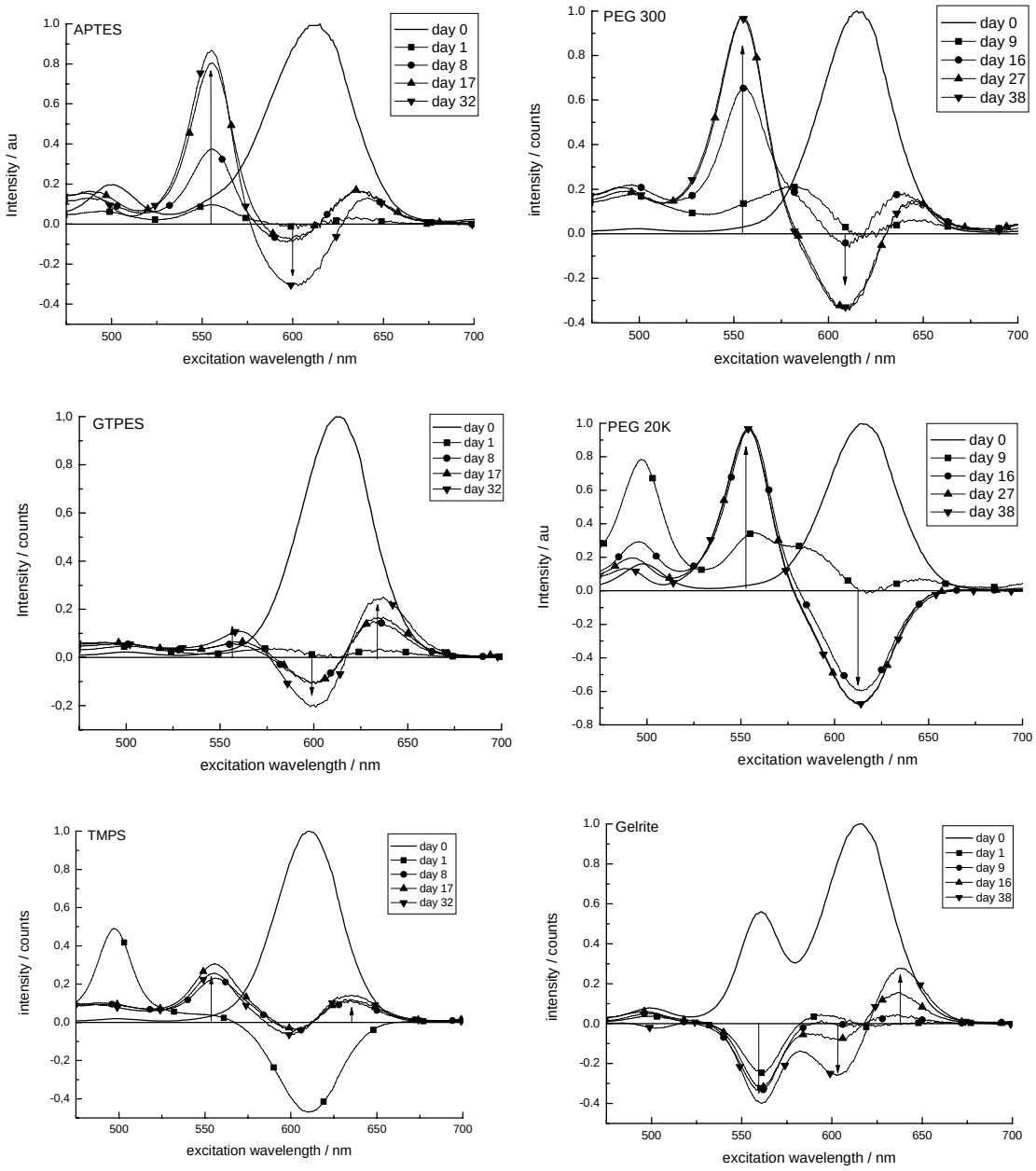

Figure 6.11. Comparison of Nile red difference SFS in cytochrome *c* with sol-gel aging time when incorporated into both silane and polymer modified hosts.

This was assessed using synchronous scan difference spectra, which were generated by normalising the synchronous scan spectra for the different matrices and subtracting from the initial spectrum taken after gelation.

Generally the data in figure 6.11 show that there is a decrease in the main band (in the region 600 nm to 620 nm) and relative increases at both shorter (*ca*. 560 nm and below) and longer (ca. 635 nm) wavelengths. The fact that in the region of the dominant band the difference spectra exhibit both an increase and decrease along with a cross over point is indicative that this band is probably the sum of two or more component spectra, with Nile red located in distinct, reasonably polar microenvironments. The degree of spectral change appears dependent on the modifying agent. Tentatively the longer wavelength increase can indicate an opening of the protein structure exposing the probe to an increased polarity. This may relate to some denaturing of the protein (or even a small degree of probe leaching), however in comparison to the effect of adding urea to cytochrome *c* in solution (data not shown), the degree of denaturing appears low.

It should also be noted that absorption spectra taken at the end of the study period showed the presence of the haem Soret band in all of the samples at 407 nm indicating the retention of protein within the hosts. This wavelength is close to that we observe in solution (408 nm) and indicates that the protein is hydrated [26] and should be functional within the hosts. Also the loading used (0.01 wt %) should be low enough to avoid protein aggregation, although higher loading on silicate materials can be obtained [23].

6.3.2.4. Correlation between spectral and catalytic data

In order to help explain the results in the previous sections we have explored the possibility that there exists a connection between the SFS and initial velocity data. The possible factors that we can envisage to explain the catalytic activity data are changes in the protein structure and access of the substrate to the protein. The former relates to the cytochrome itself, while the latter is more influenced by the host. If it is assumed that increases in the SFS 635 nm band and decreases in the 600–615 nm band are assigned to unfolding of the protein, it should be possible to use the relative importance of the 600–615 nm band as a measure of protein conformation changes. We advance this hypothesis, as previous studies of cytochrome *c* in *sol-gel* derived media, making use of

circular dichroism, have shown the ability of this protein to unfold and refold within the matrix structure [27].

Considering the first (just after gelation) and final measurements, then any difference between these values should reflect the influence of the host. Table 6.3 shows that, overall, the reduction in v_0 is significantly higher than the reduction exhibited by the 600–615 nm band. This difference is most dramatic for the TMPS modified host, which, according to the present hypothesis, means that although this matrix appears suitable for retaining the cytochrome c conformation (relatively small changes in SFS – figure 6.11), it provides poor accessibility for the cytochrome to react with the ABTS and hydrogen peroxide. Both the GTPES and PEG 300 modified hosts show the next biggest difference between our two chosen parameters, with the other modified media exhibiting similar differences.

Additive	**% reduction in v_0**	**average decrease per day in v_0 (x 10^{-12} Ms^{-1})**	**% reduction in SFS band 600-620 nm**
APTES	62	9.4	37
GPTES	65	9.4	20
TMPS	98	7.5	8
PEG 300	87	16.5 (6.9)*	34
PEG 20K	86	20.4 (2.8)*	67
Gelrite	51	6.9	26

Table 6.3. Comparison of the reduction in v_0 (in relation to the first activity measurement) with that of the SFS band situated between 600 and 620 nm (in relation to the spectra measured just after gelation) for the last dataset for the differently modified media. The decrease in v_0 obtained from a linear fit to all the data is also given to provide an indication of the average decrease per day over the study period. (*)The bracketed number was obtained omitting day 1 data points.

When combining all the data, these observations allow us to suggest that the Gelrite modified host appears to exhibit the most promising properties probably related to the templating properties of this polysaccharide [28]. This approach shows that it is possible to make a good comparison, making use of Nile SFS and activity measurements, between the modified sol–gel derived media.

6.4. Conclusion

Sol-gel derived hosts, containing either polymers or silanes to moderate the internal structure and pore environment, were produced containing subtilisin *Carlsberg* and cytochrome c.

By examining protein change conformation *via* Nile red synchronous fluorescence spectroscopy (SFS), it appears that no major unfolding of the proteins happens upon incorporation. However, during the aging time considered, the protein structure alters and this effect is seemingly influenced by the host. For cytochrome c, the sample with TMPS gave the most promising results(see table 6.3 that reports the highest decrease in the reaction rate!), with Nile red SFS difference spectra showing as much as 8% alteration. The opposite effect was obtained with PEG samples with significant changes of about 67%. Nile red SFS difference spectra of the samples with subtilisin *Carlsberg* gave very similar results. Apparently TMPS has beneficial influence on the protein structure as difference spectra show an alteration of only 10%. All other samples showed a difference of about 40%. This could be related to the hydrophobic character of the modifier (through the propyl group) and also to a more stable environment through aging, as probed by Nile red SFS in TMPS sample without protein. It was shown (figure 5.15) that the probe reports on a relatively constant polarity, during aging time.

The incorporated proteins exhibited catalytic activity in all the media over a forty day period, in which host aging occurred. The catalytic activity was inferior to that exhibited in solution one to two orders of magnitude and diminished with time. Polymer doped hosts fare better in terms of catalytic activity, with the best results obtained with Gelrite®. This was confirmed with an activity study over a prolonged timescale using subtilisin *Carlsberg*, which also suggest that the substrate may be in default inside the matrices pores, thus affecting the reaction kinetics. It is possible that although the bulk substrate concentration is in excess relatively to the encapsulated enzyme, the concentration inside the pores may not observe this premise, resulting in atypical progress curves. Complementary theoretical studies applied to enzymatic Michaelis–Menten mechanisms confirm that the true morphology of the sol-gel matrix is complex, with a variability of patterns at different scales.

It is clear that, although some unfolding of the proteins occurs, the major effect on the catalytic reaction is that of mass transport within the host.

6.5. References

[1] Siezen, R. J.; Leunissen, J. A. M. *Subtilases: The superfamily of subtilisin-like serine proteases* Protein Science 1997, *6*, 501.

[2] Smith, E. L.; Delange, R. J.; Evans, W. H.; Landon, M.; Markland, F. S. *Subtilisin Carlsberg .V. Complete Sequence - Comparison with Subtilisin Bpn' - Evolutionary Relationships* Journal of Biological Chemistry 1968, *243*, 2184.

[3] Meldal, M. *Smart combinatorial assays for the determination of protease activity and inhibition* Qsar & Combinatorial Science 2005, *24*, 1141.

[4] Finnie, K. S.; Jacques, D. A.; McGann, M. J.; Blackford, M. G.; Barbe, C. J. *Encapsulation and controlled release of biomolecules from silica microparticles* Journal of Materials Chemistry 2006, *16*, 4494.

[5] Lee, S.; Jang, D. J. *Progressive rearrangement of subtilisin Carlsberg into orderly and inflexible conformation with Ca2+ binding* Biophysical Journal 2001, *81*, 2972.

[6] Bordusa, F. *Proteases in organic synthesis* Chemical Reviews 2002, *102*, 4817.

[7] Daltrop, O.; Ferguson, S. J. *Cytochrome c maturation - The in vitro reactions of horse heart apocytochrome c and Paracoccus denitrificans apocytochrome c(550) with heme* Journal of Biological Chemistry 2003, *278*, 4404.

[8] Kim, N. H.; Jeong, M. S.; Choi, S. Y.; Kang, J. H. *Peroxidase activity of cytochrome c* Bulletin of the Korean Chemical Society 2004, *25*, 1889.

[9] Kamal, J. K. A.; Xia, T. B.; Pal, S. K.; Zhao, L.; Zewail, A. H. *Enzyme functionality and solvation of Subtilisin Carlsberg: from hours to femtoseconds* Chemical Physics Letters 2004, *387*, 209.

[10] Dunn, b. M. Determination of protease mechanism. In *Proteolytic Enzymes* Beynon, R. B., J. S., Ed.; Oxford University Press: New York, 2001.

[11] Devlin, T. M. *Textbook of Biochemistry with Clinical Correlations*, Fifth edition ed.; Willey-Liss: New York, 2002.

[12] Grima, R.; Schnell, S. *A mesoscopic simulation approach for modeling intracellular reactions* Journal of Statistical Physics 2007, *128*, 139.

[13] Grima, R.; Schnell, S. *A systematic investigation of the rate laws valid in intracellular environments* Biophysical Chemistry 2006, *124*, 1.

[14] Schnell, S.; Turner, T. E. *Reaction kinetics in intracellular environments with macromolecular crowding: simulations and rate laws* Progress in Biophysics & Molecular Biology 2004, *85*, 235.

[15] Berry, H. *Monte Carlo simulations of enzyme reactions in two dimensions: Fractal kinetics and spatial segregation* Biophysical Journal 2002, *83*, 1891.

[16] Kopelman, R. *Fractal Reaction-Kinetics* Science 1988, *241*, 1620.

[17] Kopelman, R. *Rate-Processes on Fractals - Theory, Simulations, and Experiments* Journal of Statistical Physics 1986, *42*, 185.

[18] Mandelbrot, B. B. *Negative Fractal Dimensions and Multifractals* Physica A 1990, *163*, 306.

[19] Guo, Y. Z.; Clark, D. S. *Activation of enzymes for nonaqueous biocatalysis by denaturing concentrations of urea* Biochimica Et Biophysica Acta-Protein Structure and Molecular Enzymology 2001, *1546*, 406.

[20] Bennion, B. J.; Daggett, V. *The molecular basis for the chemical denaturation of proteins by urea* Proceedings of the National Academy of Sciences of the United States of America 2003, *100*, 5142.

[21] Rocha, V. A.; Eggers, D. K. *Hydrophobic, organically-modified silica gels enhance the secondary structure of encapsulated apomyoglobin* Chemical Communications 2007, 1266.

[22] Childs, R. E.; Bardsley, W. G. *Steady-State Kinetics of Peroxidase with 2,2'-Azino-Di-(3-Ethylbenzthiazoline-6-Sulphonic Acid) as Chromogen* Biochemical Journal 1975, *145*, 93.

[23] Deere, J.; Magner, E.; Wall, J. G.; Hodnett, B. K. *Oxidation of ABTS by silicate-immobilized cytochrome c in nonaqueous solutions* Biotechnology Progress 2003, *19*, 1238.

[24] Pierre, A. C. *The sol-gel encapsulation of enzymes* Biocatalysis and Biotransformation 2004, *22*, 145.

[25] Kadnikova, E. N.; Kostic, N. M. *Oxidation of ABTS by hydrogen peroxide catalyzed by horseradish peroxidase encapsulated into sol-gel glass. Effects of glass matrix on reactivity* Journal of Molecular Catalysis B-Enzymatic 2002, *18*, 39.

[26] Dunn, B.; Zink, J. I. *Probes of pore environment and molecule-matrix interactions in sol-gel materials* Chemistry of Materials 1997, *9*, 2280.

[27] Savini, I.; Santucci, R.; Di Venere, A.; Rosato, N.; Strukul, G.; Pinna, F.; Avigliano, L. *Catalytic and spectroscopic properties of cytochrome-c, horseradish peroxidase, and ascorbate oxidase embedded in a sol-gel silica matrix as a function of gelation time* Applied Biochemistry and Biotechnology 1999, *82*, 227.

[28] Shchipunov, Y. A.; Karpenko, T. Y. *Hybrid polysaccharide-silica nanocomposites prepared by the sol-gel technique* Langmuir 2004, *20*, 3882.

Chapter 7

CONCLUSION AND FUTURE WORK

This work supports the use of fluorescence in following the whole of the sol-gel manufacturing process for protein encapsulation; the gelation and aging steps, the biomolecule incorporation, and protein conformation during aging. It also demonstrates that it is possible to retain an enzyme's catalytic activity for several weeks which is an important achievement for use in biosensor applications.

Even though *sol-gel* derived media based on producing a pure SiO_2 bulk oxide matrix have been employed for protein encapsulation, recent research has shown that it can be advantageous to modify the reaction procedure to make the resulting host more amenable. With this in mind, we focused on manufacturing organically modified silanes and polymer doped matrices to host different proteins with catalytic activity. The chosen additives not only contribute to template the pores, but also provide biocompatibility, by controlling the internal pore environment and/or by modifying the waterpool-bulk oxide interface of the host. Cytochrome c and subtilisin *Carlsberg* were successfully incorporated into modified sol–gel derived hosts in absence of major structural changes. The protein conformation was indirectly monitored via the use of Nile red synchronous fluorescence spectra (SFS) a technique that allowed changes in micropolarity to be sensed, and thus to follow changes in the integrity of the biomolecule structure. This hydrophobic dye probes different environments within the protein and does not leach to any appreciable extent into the matrix pores. Combining the two sets of data (Nile red SFS and catalytic rates), made it possible to discriminate

between changes attributed to alterations in the protein conformation and effects from the mass transport restrictions ascribed to the aging of the host. The matrices exhibited good optical quality thus allowing for the spectroscopic monitoring.

In general the initial reaction rate becomes about one to two orders of magnitude lower upon encapsulation as compared with solution measurements. The access to the enzyme appears to become more restricted with aging time, possibly related to closure of the pores and decreased interconnectivity.

The modifiers used in the present work enabled the adjustment of the sol-gel reaction to host the enzyme from different standpoints. The polysaccharide Gelrite® widens the three-dimensional network at early stages of the sol-gel process and PEG allows better diffusion of reactants. The silanes APTES, GPTES and TMPS modulate chemically the interior of the pore and do not substantially alter its diameter. Our data point to the following:

- The silane additive TMPS has a more favourable effect on the conformation of subtilisin *Carlsberg*, and GPTES is more beneficial to cytochrome c integrity. This can be related with the hydrophobic/hydrophilic balance of the pore induced by the modifier. The protein conformation was accessed by monitoring Nile red synchronous fluorescence spectra. Regarding the catalytic measurements, TMPS and GPTES matrices gave poor results for both proteins. It is apparent that, although the structure of the biomolecules is intact, the diffusion within TMPS and GPTES hosts is severely affected.
- Detailed studies on the enzymatic process of subtilisin *Carlsberg* (Michaelis–Menten mechanism) in aged matrices confirm that the true morphology of the sol-gel matrix is complex, with a variability of patterns at different scales. It is clear that, although some unfolding of the proteins occurs, the major effect on the catalytic reaction is that of mass transport within the host.
- Measurements of the catalytic activity, as reflected by the initial velocity, showed a reduction during the aging process, in cytochrome c matrices. This effect was ascribed mainly to mass transport increased restrictions, as the building of the silica matrix progresses. In general, the polymers PEG and Gelrite permit better diffusion of reactants inside the sol-gel hosts. The charge of the reactants could also be influential; in the present case, the reaction product of cytochrome c catalysed reaction is a positively charged radical ($ABTS^{\bullet+}$) that could be delayed or trapped due to the negatively charged walls of the pores.

This is an area in which further effort may provide help in understanding the interaction between the different entities introduced in this study. The ideal host has to conciliate both the shrinkage resistance during aging and the pore hydrophobicity to preserve the protein folding, while permitting the free passage of reactants.

The choice of fluorescent probes is of great importance if the system is to be monitored via fluorescence techniques. Here we made use of the viscosity and polarity sensitive fluorescence probes DASPMI and Nile red respectively, to monitor the host gelation and aging processes of the modified matrices. Time-correlated single-photon counting fluorescence spectroscopy of DASPMI was used to study the alterations in the pore viscosity with aging time.

The gelation (as probed by DASPMI emission) was found to be a two step process, which, by silane or polymer addition slows down by an order of magnitude as compared to non-doped media. The main influence of the polymers occurs during the matrix forming phase, after which they exhibit similar control. The lifetimes obtained for silane-doped hosts showed that these additives exert limited control over the viscosity on longer timescales. During aging, the microviscosity increases, but the pore environment stabilises only after a period of 20 days. Nile red reported on the polarity within the pores via synchronous fluorescence spectroscopy (SFS). Overall, the polarity increases as aging progresses and the results suggest the occurrence of hydrogen bonds at the bulk oxide pore interface.

The fact that Nile red is not covalently linked with the proteins means that the global movements of the biomolecule are difficult to assess. A fixed linkage between probe and protein is preferable in elucidating the motion of biomolecules within the host, with aging time. This was achieved with the covalent dyes Alexa Fluor 488 and fluorescein isothyocyanate (FITC), using fluorescence recovery after photobleaching experiments (FRAP) and fluorescence lifetime anisotropy measurements. These techniques proved complementary in monitoring the dynamics of sol-gel hybrid systems, namely the proteins' rotation and ability to diffuse within the matrix. Rotational diffusion is related to the environment inside the pore, while translational diffusion is related to the pore interconnections. In terms of the effective viscosity sensed by the probes Alexa Fluor and fluorescein, the values correlate with the formation and stabilisation of the pore's structure. It appears from our data, using silica

monoliths, that the pores retain a liquid phase through aging. However, as the interconnections between the pores constrict with time, the effective viscosity increases. This methodology enabled us to understand that although the matrix can template around an incorporated biomolecule or modifier, there is a size limit to that, and only small molecules display high mobility and are relatively free to circulate within the host.

This study concentrated on what could be described as the "active part" of the biosensor – the interaction of the enzyme and an immobilisation medium. An advance would be the fabrication of a flow based system. This could help in the study of the catalytic process under well controlled mass flows, to be used in future devices.

Also the use of thin films, rather than the use of monoliths, could be advantageous for sensing purposes as it reduces the distance that the reactants have to diffuse before encountering the entrapped enzyme. A stack of thin films containing different sensing moieties would even increase the area of the biosensor and the possibility of detecting multiple analytes.

The ability to include sol-gel hybrids at the end of an optical fibre would be the ultimate step towards a functional optical biosensor. In this case, the light from a convenient source would travel through the fiber passing through the sol-gel biocatalyst sensor. The fluorescence response produced after the biochemical reaction would travel through the same fibre to a detector, giving the measure of the concentration of the analyte.

One very challenging group of enzymes to investigate is the cytochrome P450 superfamily (CYP). CYPs are involved in the synthesis of steroid and bile acids, hydroxylation of fatty acids, and elimination of xenobiotics and steroids from the body. The interest comes from their role in drug interactions, drug toxicity and creation of carcinogenic by-products; the isoform aromatase, for example, is a key enzyme of intratumoral production of estrogen in breast cancer. The immobilisation of this system is therefore very attractive to analyse drug metabolism. Arrays of multiple CYP isoforms could be designed to characterise the different metabolic pathways and predict drug-drug interactions.

A new generation of biosensors can be expected within the next few decades!